Proceedings of the International Conference

Numerical Methods for Scientific Computations and Advanced Applications (NMSCAA'14)

May 19-22, 2014, Bansko, Bulgaria

Krassimir Georgiev (Editor)

Institute of Information and Communication Technologies
Bulgarian Academy of Sciences

In cooperation with

Sofia, 2014

Numerical Methods for Scientific Computations and Advanced Applications
(NMSCAA'14)

Proceedings of the International Conference

ISBN: 978-954-91700-7-8

Printed in Sofia, Bulgaria
Cover design: Boris Staikov
Printing and binding: Demetra Ltd.

PREFACE

This book contains extended abstracts (short communications) of some of the presented papers during the International Conference on "Numerical Methods for Scientific Computations and Advanced Applications" (NMSCAA'14), May 19-22, 2014, Bansko, Bulgaria. The conference was organized by the Institute of Information and Communication Technologies, Bulgarian Academy of Sciences in cooperation with Society for Industrial and Applied Mathematics (SIAM) and devoted to the 60th anniversary of Svetozar Margenov.

His main fields of research include: Large-Scale Scientific Computing and Parallel Algorithms; Numerical Methods for Partial Differential Equations (Finite Difference Schemes and Finite Element Method); Computational Linear Algebra (Iterative Methods and Algorithms, Preconditioning, Sparse Matrices); Large-Scale Computing of Environmental Problems; Biomedical and Engineering Problems; Supercomputing applications, etc. Svetozar Margenov receive his PhD in 1984 and the degree of Doctor of Science in 2002. From 2003 he was promoted to Full Professor in 2003. Currently, prof. Margenov is Director of the Institute of Information and Communication Technologies of the Bulgarian academy of sciences and Head of the Department of Scientific computing in the the same institute. He is an eminent scientists and university lecturer. Svetozar Margenov is an author of two monographs and more than 140 papers published in high ranked international journals and proceedings of conferences. He is a member of the Editorial Boards of

- *Numerical Linear Algebra with Applications* (NLAA),
- *Scalable Computing: Practice and Experience* (SCPE),
- *International Journal of Numerical Analysis and Modelling*, Series B.

During his very successful carrier he was a scientific advisor and mentor of many Ph.D. and MSc students.

The Conference Specific topics of interest are as follows:

- Multiscale and multiphysics problems;
- Robust preconditioning;
- Monte Carlo methods;
- Optimization and control systems;
- Scalable parallel algorithms;
- Advanced computing for innovations.

The list of plenary invited speakers includes: Peter Arbenz (ETH Zurich, CH); Owe Axelsson (Institute of Geonics, ASCR, CR); Radim Blaheta (Institute of Geonics, ASCR, CR); Oleg Iliev (ITWM, Kaiserslautern, Germany); Johannes Kraus (RICAM, Linz, AT); Raytcho Lazarov (TA&MU, College Station, USA); Peter Minev (University of Alberta, CA); Panayot Vassilevski (LLNL, Livermore, USA); Vladimir Veliov (TU-Vienna, AT and IMI BAS, BG) and Lyudmil Zikatanov (The Pennsylvania State University, USA).

Krassimir Georgiev

May 2014

Contents

Part A: Extended abstracts (short communications) **9**

Laura-Iulia Aniţa, Sebastian Aniţa, Costică Moroşanu
A Periodic Optimal Control Problem in Biology **11**

Emanouil Atanassov, Todor Gurov, and Aneta Karaivanova
Energy Aware Performance Study for a Class of MC Algorithms **15**

R. Blaheta, O. Axelsson, M. Hasal, Z. Michalec
Preconditioners for Linear and Nonlinear Poroelasticity Problems **19**

Gabriel Dimitriu, Răzvan Ştefănescu, Ionel M. Navon
Reduced Order POD-DEIM Application of a Haptotaxis Model Describing a Process of Tumor Invasion **23**

Nina Dobrinkova
Methods For Flood Hazard Mapping On The Test Area Of Svilengrad **27**

Stefka Fidanova and Pencho Marinov
Wind Model in a Wild Fire Spread **31**

Georgi Gadzhev, Kostadin Ganev, Maria Prodanova,
Dimiter Syrakov, Nikolai Miloshev
Computer Simulations of the Atmospheric Composition Climate of Bulgaria - Some Basic Results **35**

Ivelina Georgieva
Air Quality Index Evaluations for Bulgaria **39**

Todor Gurov, Emanouil Atanassov, Aneta Karaivanova,
Ruslan Serbezov, and Nikolai Spassov
Statistical Estimation of Brown Bears Population in Rhodope Mountains **43**

Nevena Ilieva, Damyan Grancharov, Peicho Petkov,
Michael Kenn, Reiner Ribarics, and Wolfgang Schreiner
Structure Analysis of HLA Complexes in the Presence of Co-Receptors **47**

Mariya Ishteva, Konstantin Usevich, Ivan Markovsky
Structured Low-Rank Approximation by Factorization **49**

Kab Seok Kang
LScalable implementation of the parallel multigrid method on massively parallel computer **53**

Adem Kaya, Dr. Ali Şendur
Finite element based finite difference method for multidimensional convection-diffusion-reaction equations **57**

Johnwill Keating and Peter D. Minev
A Fast Parallel Algorithm for Direct Simulation of Particulate Flows Using Conforming Grids **61**

J. Kraus, R. Lazarov, M. Lymbery, S. Margenov, L. Zikatanov
Robust preconditioning of Darcy problem for highly heterogeneous media **65**

Angelos Liolios, George Hatzigeorgiou, Konstantinos Liolios, Stefan Radev, Krassimir Georgiev, Ivan Georgiev
A Computational Approach for the Seismic Damage Response of Adjacent Tall RC Structures Environmentally Degradated and Strengthened by Ties **71**

Maria Lymbery
Robust Balanced Semi-Coarsening Multilevel Preconditioning for Bicubic FEM Discretizations **75**

Emil Manoach and Jerzy Warminski
Large amplitude vibrations of heated Timoshenko beams with delamination **79**

Ivan Markovsky
Data-Driven Signal Processing: A Low-Rank Approximations Approach **83**

Aydın Özbey, Erol Uzal, Aşkın Mutlu, Hüseyin Yıldız
Fuzzy Logic Nonlinear Control of an Inverted Pendulum on a Chart **85**

Aydın Özbey, Erol Uzal, Hüseyin Yıldız, Aşkın Mutlu
Control of a Robot Arm Using Magnetic Forces **89**

Peicho Petkov, Elena Lilkova, Damyan Grancharov, Stoyan Markov, Nevena Ilieva, Leandar Litov
Libraries for treatment of electrostatic interactions for Intel Xeon Phi **93**

Vicenta Sanchez, Fernando Sanchez, Chumin Wang
Electronic Transport in Generalized Fibonacci Lattices: A Real-Space Renormalization Approach to the Kubo-Greenwood Formula **95**

Kiril S. Shterev
Acceleration of iterative algorithm for calculation of unsteady, viscous, compressible and heat-conductive gas flows on GPU **99**

Stanislav Stoykov
The influence of geometrical nonlinearity on the dynamics of elastic structures **103**

Rosangela Sviercoski and Svetozar Margenov
A Multiscale Multigrid Algorithm Applied to Bone Tissue Modeling **107**

D. Syrakov, M. Prodanova, E. Georgieva, K. Slavov
Estimation of WRF-CMAQ Modeling System Performance Using AQMEII Infrastructure **111**

Tasho D. Tashev, Vladimir V. Monov
A Numerical Procedure for Computation of the Upper Bound of the Throughput of a Crossbar Switch Node **115**

Chumin Wang, Vicenta Sanchez
Renormalization Plus Convolution Method Applied to the Analysis of AC Resonant States in Aperiodic Nanowires **119**

Katarzyna Wasielewska, Maria Ganzha, Marcin Paprzycki, Ivan Lirkov
Multicriteria Analysis of Ontologically Represented Information **123**

Zahari Zlatev, Krassimir Georgiev, Ivan Dimov
Non-linear systems of PDEs arising in large-scale environmental models **127**

Part B: List of participants **133**

Part A

Extended abstracts[1] (Short communications)

[1] Arranged alphabetically according to the family name of the first author.

A Periodic Optimal Control Problem in Biology

Laura-Iulia Aniţa, Sebastian Aniţa, Costică Moroşanu

The model to be investigated here describes the dynamics of a population species:

$$\begin{cases} h'(t) = rh(t)\left(1 - \dfrac{h(t)}{K}\right) + f(t), & t > 0 \\ h(0) = h_0, \end{cases}$$

where $h(t)$ is the number of individuals at the moment t, $r > 0$ is the natural growth rate of this species, K is the carying capacity of the region, and $h_0 > 0$ is the initial number of individuals; $f(t)$ represents a certain infusion of population, which is time periodic (the period is $T > 0$). Actually, this model describes for example the dynamics of the horse chestnut leafminer moth and $f(t)$ represents the individuals brought in the domain by wind, car wheels, etc. and T is one year. Since we wish to diminish this population acting in the region (we are not able to act everywhere), then a natural problem would be to introduce a certain periodic control with period T (represented in this case by traps) such that the cost of this control to be small and to get a long-term diminishment of the population. The particularity of the trap is that it acts on a certain time interval and that its action diminish exponentially. Actually, considering the traps, the problem becomes

$$\begin{cases} h'(t) = rh(t)\left(1 - \dfrac{h(t)}{K}\right) + f(t) - \left(\displaystyle\int_0^t w^u(a,t)da\right) h(t), & t > 0 \\ h(0) = h_0, \end{cases} \tag{1}$$

where w^u is the solution to

$$\begin{cases} w_t(a,t) + w_a(a,t) = -\alpha w(a,t), & a \in (0,T),\ t > 0 \\ w(0,t) = u(t), & t > 0 \\ w(a,0) = 0, & a \in (0,T). \end{cases} \tag{2}$$

Here $\alpha > 0$ and

$$u \in \mathcal{U} = \{v \in L^\infty(0,\infty);\ 0 \le u(t) \le L \text{ a.e. },\ v(t+T) = v(t) \text{ a.e. }\}.$$

Hence, w^u satisfies an age structured problem.
Assume that

$$f \in L^\infty(0,+\infty),\ f(t+T) = f(t) \text{ a.e. } t > 0,\ f(t) > 0 \text{ a.e. } t > 0.$$

We denote $\tilde{h}^u$ the solution to (1) corresponding to $u \in \mathcal{U}$. The first thing we shall prove is that

$$\lim_{t \to +\infty} (\tilde{h}^u(t) - h^u(t)) = 0,$$

(for any $h_0 > 0$) where h^u is the unique positive solution to

$$\begin{cases} h'(t) = rh(t)\left(1 - \dfrac{h(t)}{K}\right) + f(t) - \left(\displaystyle\int_0^t w^u(a,t)da\right) h(t), & t > 0 \\ h(t+T) = h(t), & t \geq 0. \end{cases} \tag{3}$$

It means that for any $\gamma > 0$:

$$\int_{nT}^{(n+1)T} \left[\tilde{h}^u(t) + \gamma u(t)\right] dt \to \int_0^T \left[h^u(t) + \gamma u(t)\right] dt,$$

as $n \to +\infty$, for any $u \in \mathcal{U}$.

The optimal control problem to be investigated is the following one

$$(\mathbf{P}) \qquad Minimize \int_0^T \left[h^u(t) + \gamma u(t)\right] dt,$$

where $\gamma > 0$ is a positive constant. It means we are interested to minimize the pest population over one year on long term at a small control cost. We shall prove that problem (P) has at least one optimal control u^*.
The following Pontryagin principle can be derived:

Theorem. *If u^* is an optimal control for problem (P) and if p is the solution to*

$$\begin{cases} p'(t) = -rp(t) + \dfrac{2rh^{u^*}}{K} p(t) + \left(\displaystyle\int_0^t w^{u^*}(a,t)da\right) p(t) - 1, & t > 0 \\ p(t+T) = p(t), & t \geq 0, \end{cases} \tag{4}$$

then

$$u^*(t) = \begin{cases} 0, & \gamma - e^{\alpha t} \displaystyle\int_t^T p(\theta) h^{u^*}(\theta) e^{-\alpha\theta} d\theta > 0 \\ L, & \gamma - e^{\alpha t} \displaystyle\int_t^T p(\theta) h^{u^*}(\theta) e^{-\alpha\theta} d\theta < 0. \end{cases} \tag{5}$$

Using (3), (4) and (5) we shall derive and a numerical algorithm to approximate the optimal control u^*. Numerical results will be obtained.
We shall extend the investigation to a model containing diffusion and migration terms.

References

[1] S. Aniţa, Analysis and Control of Age-Dependent Population Dynamics, Kluwer Academic Publishers, 2000.

[2] S. Aniţa, V. Arnăutu, V. Capasso, An Introduction to Optimal Control Problems in Life Sciences and Economics. From Mathematical Models to Numerical Simulation with MATLAB, Birkhäuser, 2010.

[3] S. Aniţa, J. Casas, C. Suppo, Impulsive spatial control of an invading pests by a generalist predators, Mathematical Medicine and Biology,
DOI: 10.1093/imammb/dqt011.

Energy Aware Performance Study for a Class of MC Algorithms

Emanouil Atanassov, Todor Gurov, and Aneta Karaivanova

Performance per watt is a measure of the energy efficiency of a particular computer system. It measures the rate of computation that can be delivered by a computer for every watt of power consumed. In this sense, there is an improvement by over a trillion times in last 50 years. Development of energy efficient algorithms becomes more and more important with the growing size of the applied problems that need solution and the power of modern computer systems. The development of exascale systems made it clear that current technologies, algorithmic practices and performance metrics need significant improvement. The FLOPS/WATT (F/W) metric was introduced and successfully used as the de facto standard in measuring the energy efficiency of a computing system, see www.green500.org. The scientific community continues to investigate metrics and approaches that address the effective use of computer systems in terms of energy efficiency. The importance of fault tolerance in algorithmic design has also been raised due to increased probability of hardware failure. Considering the significant probability of error during a run, some authors [1, 2] proposed the time to solution metric for algorithm performance. Small time to solution means reduced chances of a hardware error happening. On the other hand, fast restart from intermediate results will lead to decreased time to solution. They propose to use $f(timetosolution).energy(FTTSE)$ as the performance metric, where $f(.)$ is an application-dependent function of time [1].

In this work we propose and study a performance metric that includes not only time to solution and energy, but also price of equipment, divided over its efficient lifetime, with the aim to define a metric that optimizes the overall output from the computer system.

In our work we concentrated on use-cases that we observed during the establishment of a regional high-performance computing infrastructure for the South-Eastern Europe, taking into account the specific requirements that arise due to the economical and social conditions in the region. Considering the current deployments (several high-performance clusters and two Blue Gene P supercomputers) and extrapolating the future deployment plans, we concentrate on the study of heterogeneous high-performance computing clusters, since the other type of resource is extensively studied by IBM research groups (see, e.g., the publication [1]). Here we point out two important features: (i) the extensive use of computational accelerators like GPU-computing cards and Intel Xeon Phi processors; (ii) the rapid evolution of hardware in HPC clusters, which leads to frequent necessity to upgrade in order to meet the challenges of contemporary research.

These points motivate the inclusion of substantial factor to account for the purchasing price of the equipment, so that the individual optimization efforts at the level of algorithms should lead to global optimum in the sense of computational results achieved for a given yearly budget. Our experience shows that although the hardware can

GPU cards (n)	ΔW_n	GPGPU Time (s)	KWh	Equipment cost	Energy cost	Total cost
1	442	246	0.3020	0.75	2.42	3.17
2	609	145	0.2453	0.89	1.96	2.85
4	790	89	0.1953	1.09	1.56	2.65
8	1066	67	0.1984	1.64	1.59	3.22

Table 1: Test results using GPU devices.

be operational for longer period, there is an *efficient lifetime* for a cluster that lasts between 3 to 4 years. On the other hand the x86-based HPC clusters can be upgraded in a more gradual way, presenting the possibility to use savings of energy costs for hardware upgrading. We propose to enhance the formula in [1] in the following way:

$$F(T).(E + nCT),$$

where C is the price of core-hour, excluding energy, n is the number of cores used by the algorithm, T is the time to solution and E is the cost of energy consumed. The price C should be based mainly on purchasing price of the equipment, divided by number of cores and number of hours in the efficient lifetime. Based on the substantial improvements in the computational power of accelerators over time we can postulate the efficient lifetime to be equal to 4 years, because experience shows that after 4 years the same computational results can be achieved by several times less expensive equipment that also uses much less energy. We point out that cloud providers offer access to their equipment based on single price-per-core number. However, a national computational infrastructure provider has more flexibility and can stimulate the development of algorithms that minimize the above function instead. Our formula is not more difficult to compute because the purchasing price is readily available.
The initial experiments in our study were performed on the heterogeneous cluster HPCG in the Grid Computing Centre of the Institute of Information and Communication Technologues, Bulgarian Academy of Sciences (IICT-BAS) [5].This cluster combines CPU-based computing blades with servers with high-end GPU computing devices. Let us remind that GPUs have continued to increase in energy usage, while CPUs designers have recently focused on improving performance per watt. High performance GPUs may now be the largest power consumer in a system. Peak performance of any system is essentially limited by the amount of power it can draw and the amount of heat it can dissipate. Consequently, performance per watt of a GPU design translates directly into peak performance of a system that uses that design.
Our study is based on the purchasing price of our equipment, which lead us to consider the cost of CPU-core hour to be 1.248 €cents per 1 hour for a CPU core and 11 €cents per 1 hour for 1 GPU card NVIDIA M2090. The price of energy is taken as 8 €cents per $1KWh$. The energy consumption when using n CPU cores or GPU devices is denoted by W_0 while W_n means the consumption when using n processing elements. The difference $\triangle W_n = W_n - \triangle W_0$ is attributed to the computational workload being run.
The Table 1 shows the energy consumption, cost and equipment costs for a particular

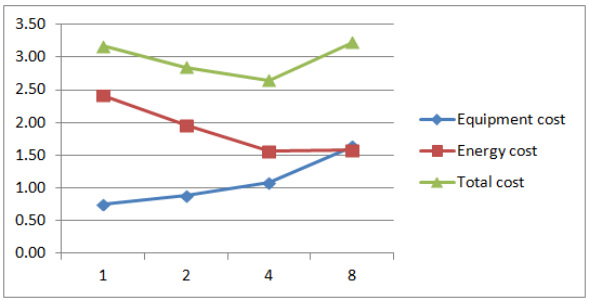

Figure 1: Cost per GPU device (€ cents).

CPU Cores (n)	ΔW_n	CPU Time (s)	KWh	Equipment cost	Energy cost	Total cost
1	51	84.2	0.0119	0.02898	0.0954	0.1244
2	60	42.2	0.0070	0.02905	0.0563	0.0853
4	77	21.6	0.0046	0.02974	0.0370	0.0667
8	144	11.06	0.0044	0.03045	0.0354	0.0658
16	316	6.06	0.0053	0.03337	0.0426	0.0759
32	704	2.94	0.0057	0.03238	0.0460	0.0784
64	1201	1.56	0.0052	0.03436	0.0416	0.0760
128	1951	1.02	0.0055	0.04493	0.0442	0.0892

Table 2: Test results using CPU cores.

Monte Carlo algorithm that uses Metropolis-Hastings sampling in order to fit the parameters of a Heston process modeling price evolution. The total cost is obtained in € cents.

We can observe from the table and the following graph (Figure 1) how there is an optimum in energy price when using the highest possible number of cards, while the optimum in total usage according to our formula $E + nCT$ is achieved at lower number of GPU devices, suggesting that sharing the computational facilities with other computational jobs or finding other strategy for course-grain parallelization should be performed.

Similarly in the case of CPU-based computations we see how the shapes of the curves describing energy use and total cost are different. They both suggest that optimal usage will be achieved when one blade node is used. However, when the problem size becomes larger this will not be feasible.

In any case the use of the rough metrics $E + nCT$ favors usage similar to Grid jobs, where a large number of jobs divide the resources. When we consider the full metrics $F(T).(E + nCT)$, the situation is changed dramatically, because the function $F(T)$ that penalizes algorithms that are slow to reach a solution heavily favors jobs that use the maximum amount of processing elements. In our view more work should be done to establish a function $F(T)$ that leads to more desirable usage patterns instead of those proposed so far. For example, a power low with exponent between 0 and 1 may be more useful.

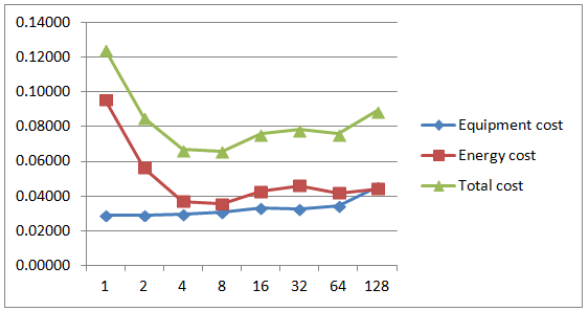

Figure 2: Cost per CPU core (€ cents).

The initial results of our study demonstrate the importance of taking into account not only energy efficiency but also equipment cost. It also shows how the optimal algorithm from point of view of the scientific user may be different from the behavior that is desirable from point of view of an infrastructure operator that attempts to optimize their OPEX and CAPEX expenses. In the future work more precise measurements should be done and the impact of mixing of different computational tasks should be studied.

Acknowledgments

This work was supported by the National Science Fund of Bulgaria under Grant DCVP 02/1 CoE SuperCA++ and by the European Commission under FP7 project EGI-InSPIRE (contract number RI-261323).

References

[1] C. Becas, A. Curioni, A new energy aware performance metric, Springer, Comput. Sci. Res Dev (2010) 25: 187-195, DOI 10.1007/s00450-010-0119-z.

[2] Bekas C, Curioni A, Fedulova I (November 2009) Low cost high performance uncertainty quantification.Workshop on HPC finance, SC09, Portland, OR, USA.

[3] Meswani, M., Carrington, L., Unat, D., Peraza, J., Snavely, A., Baden, S., and Poole, S., Modeling and Predicting Application Performance on Hardware Accelerators, International Journal of High Performance Computing (2012).

[4] J. Demmel, A. Gearhart, B. Lipshitz, O. Schwartz, Perfect Strong Scaling Using No Additional Energy. Proc. of IEEE 27th IPDPS13. IEEE Computer Society, 2013.

[5] E. Atanassov, T. Gurov, A. Karaivanova, Capabilities of the HPC cluster at IICT-BAS, J. Automatika and Informatika, 2/2011, 7-11, ISSN: 0861-7562

Preconditioners for Linear and Nonlinear Poroelasticity Problems

R. Blaheta, O. Axelsson, M. Hasal, Z. Michalec

We shall consider efficient preconditioners for a hierarchy of porous media flow models starting from stationary Darcy flow model and continuing through nonstationary Darcy flow model to Richards model with variable saturation. The stationary Darcy flow is described by the equations

$$\begin{aligned} \nabla \cdot (\rho v) + \rho Q = 0 \\ v = -\frac{k_{sat}}{\mu}(\nabla p + \rho g \nabla G) \quad , \end{aligned}$$

where ρ is the fluid density, μ is the fluid viscosity, v is the Darcy velocity, Q stands for the fluid source/sink, k_{sat} stands for the permeability, p is the pore pressure, g is the gravity acceleration and G is the elevation function. Note that $v = \phi v_f$ where ϕ is the porosity and v_f is the fluid velocity.
If the quantities p, Q depend on time, and $0 \neq \frac{\partial(\rho\phi)}{\partial t} = \frac{\partial(\rho\phi)}{\partial p}\frac{\partial p}{\partial t} \sim \rho C_{stor}\frac{\partial p}{\partial t}$ we get nonstationary Darcy flow described by the equations

$$\begin{aligned} \rho C_{stor}\frac{\partial p}{\partial t} + \nabla \cdot (\rho v) = \rho Q \\ v = -k_{sat}(\nabla p + \rho g \nabla G). \end{aligned}$$

above, C_{stor} is the storativity coefficient.
In the case of variable saturation, we add the saturation function $S \in \langle 0, 1\rangle$ and consider correspondingly modified mass conservation and velocity equations

$$\begin{aligned} \rho(C_{scap}(S) + SC_{stor})\frac{\partial p}{\partial t} + \nabla \cdot (\rho v) = \rho Q \\ v = -\frac{k_{rel}(S)k_{sat}}{\mu}(\nabla p + \rho g \nabla G). \end{aligned}$$

These equations describe variable saturated flow, if we assume that the pore space is variably saturated by fluid and gas and that the gas pressure remain constant. Assuming also that saturation is through the water retention curve a function of pressure, $S = R(p)$, the above equations define so called Richards flow model.
All the above models can be discretized by mixed finite element method with lowest order Thomas-Raviart finite elements. This space discretization can be combined with backward Euler discretization in time for the nonstacionary Darcy and Richards model and Picard linearization for the Richards model.
For the stationary Darcy flow, it leads to the solution of systems in the form

$$\begin{bmatrix} M & B^T \\ B & 0 \end{bmatrix} \begin{bmatrix} \mathbf{v} \\ \mathbf{p} \end{bmatrix} = \begin{bmatrix} \mathbf{f_1} \\ \mathbf{f_2} \end{bmatrix},$$

where M is a positive definite velocity mass matrix, B is a full rank matrix representing the divergence of velocity and B^T the pressure gradient. The systems can be

solved by a suitable Krylov space method with a preconditioner. In [5] we investigated block type preconditioners with a special emphasis on augumented lagrangian type preconditioners in the block diagonal or block triangular form, e.g.

$$\begin{bmatrix} M + r^{-1}B^TW^{-1}B & \\ & rW \end{bmatrix},$$

where r is a parameter, W is a suitable matrix (can be also identity).
For the nonstationary Darcy flow, we have to solve systems in the form

$$\begin{bmatrix} M & B^T \\ B & -\frac{1}{\triangle t}C \end{bmatrix} \begin{bmatrix} \mathbf{v} \\ \mathbf{p} \end{bmatrix}^k = \begin{bmatrix} \mathbf{f_1} \\ \mathbf{f_2}^k - \frac{1}{\triangle t}C\mathbf{p}^{k-1} \end{bmatrix}$$

in each time step k. Here M and B are the same matrices as before, C is a positive definite diagonal mass matrix arising from the time derivative term. The term $\frac{1}{\triangle t}C$ provides a regularization, which strength depends on physical parameters (storativity) and can be employed for the block preconditioners of the same type as before.
For the Richards equations, we get nonlinear systems in each time step

$$\begin{bmatrix} M(\mathbf{p}) & B^T \\ B & -\frac{1}{\triangle t}C(\mathbf{p}) \end{bmatrix}^k \begin{bmatrix} \mathbf{v} \\ \mathbf{p} \end{bmatrix}^k = \begin{bmatrix} \mathbf{f_1} \\ \mathbf{f_2}^k - \frac{1}{\triangle t}C(\mathbf{p^{k-1}})\mathbf{p}^{k-1} \end{bmatrix}.$$

Using the simplest Picard linearization we get the same type of systems as before and therefore we can use the same type of preconditioners as above.
Moreover the nonstationary Darcy flow and Richards flow models can be coupled with elasticity through a source term

$$Q = -\alpha\chi(p)\frac{\partial(tr\varepsilon)}{\partial t}$$

and elasticity model with the effective stress, i.e.

$$\begin{aligned} \nabla \cdot \sigma + f_m &= 0 \\ \sigma &= \sigma' - \alpha\chi(p)pI \\ \sigma' &= \mathbb{C} : \varepsilon(u) \end{aligned}$$

where σ is the total stress, σ' is the effective stress, u is the displacement, $\varepsilon(u)$ is the small strain tensor, $tr\varepsilon$ is the trace of ε, $\mathbb{C}$ is the elasticity tensor, α is the Biot-Willis constant, $\chi(p)$ is the Bishop function, which is identical to identity for the nonsationary Darcy problem and equal to saturation or a function of saturation in the unsaturated case. The arising coupled poroelasticity models with the flow part discretized as shown above and the mechanical part discretized by standard linear finite elements lead to linear systems

$$\begin{bmatrix} A & & B_u^T \\ & M & B^T \\ B_u & B & -\frac{1}{\triangle t}C \end{bmatrix} \begin{bmatrix} u \\ v \\ p \end{bmatrix}^k = \begin{bmatrix} f_1 \\ f_2 \\ \mathbf{f_2}^k - \frac{1}{\triangle t}C\mathbf{p}^{k-1} \end{bmatrix}$$

or, it the case of Richards flow, to nonlinear systems

$$\begin{bmatrix} A & & B_u^T(p) \\ & M(p) & B^T \\ B_u(p) & B & -\frac{1}{\triangle t}C(p) \end{bmatrix}^k \begin{bmatrix} u \\ v \\ p \end{bmatrix}^k = \begin{bmatrix} f_1(p) \\ f_2 \\ \mathbf{f_2}^k - \frac{1}{\triangle t}C(\mathbf{p^{k-1}})\mathbf{p}^{k-1} \end{bmatrix},$$

which provide systems of the above type if we apply the Picard linearization. As it is described in [3], these systems can be again solved by block diagonal or block triangular preconditioners with Schur complements with respect to the lower right C block.

Let us mention that the systems of the above type also appear if the backward Euler time discretization is replaced by the Radau type higher order discretization method, see [2, 4].

The poroelasticity problems with saturated or variably saturated flow have a lot applications in geosciences and other fields. As an example we can mention modelling the test of the rock mass permeability which was done in the Tournemire underground rock laboratory as a part of SEALEX experiments oriented to assessment of long term performance of bentonite plugs within the concept of underground deposition of the spent nuclear fuel, see [6].

Acknowledgments

This work was supported by the European Regional Development Fund in the IT4Innovations Centre of Excellence project (CZ.1.05/1.1.00/02.0070).

References

[1] Axelsson, O., Blaheta, R.: Preconditioning of matrices partitioned in two by two block form: eigenvalue estimates and Schwarz DD for mixed FEM. Numer. Linear Algebra Appl. 17, 787-810 (2010)

[2] Axelsson, O., Blaheta, R., Sysala, S., Ahmad, B.: On the solution of high order stable time integration methods. J. Boundary Value Probl. Springer open 108 (2013).

[3] Axelsson, O., Blaheta, R. Byczanski, P.: Stable discretization of poroelasticity problems and efficient preconditioners for arising saddle point type matrices. Comput Visual Sci. DOI:10.1007/s00791-013-0209-0;
link.springer.com/article/10.1007/s00791-013-0209-0

[4] Axelsson, R. Blaheta, R. Kohut: Preconditioned methods for high order strongly stable time integration methods with an application for a DAE problem, Submitted

[5] Axelsson, O., Blaheta, R. Byczanski, P., Karatson, J. and Ahmad, B.: Preconditioners for regularized saddle point operators with an application for heterogeneous Darcy flow and transport problems. Submitted

[6] Blaheta, R., Hasal, M. and Michalec, Z.: Hydro-Mechanical Modelling of Water Infiltration Test within the SEALEX experimentt. Decovalex workshop, Avignon, April 2014

Reduced Order POD-DEIM Application of a Haptotaxis Model Describing a Process of Tumor Invasion

Gabriel Dimitriu, Răzvan Ştefănescu, Ionel M. Navon

Proper Orthogonal Decomposition (POD) is probably the mostly used and most successful nonlinear model reduction technique and relies on the fact that the desired simulation is well simulated in the input collection. The basis functions contain information from the solutions of the dynamical system at pre-specified time-instances, so-called *snapshots*. Due to a possible linear dependence of the snapshots a singular value decomposition is carried out and the leading generalized eigenfunctions are chosen as a basis, referred to as the POD basis. A considerable reduction in complexity is obtained by DEIM âĂŞ a discrete version of "Empirical Interpolation Method" (EIM), introduced by Barrault et al. in [2]. This method eliminates the POD major disadvantage where the nonlinear reduced terms still have to be evaluated on the original state space making the simulation of the reduced-order system too expensive.
In this study we perform an application of DEIM combined with POD to provide dimension reduction of a model describing a process of tumor invasion into surrounding healthy tissue. The model proposed in [1] is defined by the 2D system of advection-reaction-diffusion equations:

$$\begin{aligned} &u_t + \nabla \cdot (\chi(v) u \nabla v) = d_u \Delta u - \psi(x,y,w)u + \rho(x,y,w)u, \\ &v_t = -\alpha(x,y)hv, \\ &h_t = d_h \Delta h + \delta(x,y)u - \beta(x,y)h, \\ &w_t = d_w \Delta w + \gamma(x,y)v - e(x,y)w - \eta(x,y,u)w. \end{aligned} \tag{1}$$

The dependent variables in (1) have the following significance: $u(x,y,t)$ represents the density of tumor cells, $v(x,y,t)$ is the density of extracellular matrix macromolecules, $h(x,y,t)$ is the concentration of matrix degradative enzyme, and $w(x,y,t)$ denotes the concentration of oxygen. The parameters $\chi(v)$, d_u, $\psi(x,y,w)$, $\rho(x,y,w)$, $\alpha(x,y)$, d_h, $\delta(x,y)$, $\beta(x,y)$, d_w, $\gamma(x,y)$, $\eta(x,y,u)$, and $e(x,y)$, as well as the initial and boundary conditions associated to (1) are specified in the numerical tests. In our numerical approach we only consider ρ and η variable parameters (depending on w and u, respectively), the other ones being constant parameters.
Using the notations $\mathbf{u}$, $\mathbf{v}$, $\mathbf{h}$, $\mathbf{w} \in \mathbb{R}^n$ with $n = n_x n_y$ being the number of mesh points, the system (1) in matrix form after discretization of the space variables becomes

$$\begin{aligned} &\dot{\mathbf{u}}(t) = -\mathbf{N}_1(\mathbf{u}(t), \mathbf{v}(t)) + d_u \mathbf{G}\mathbf{u}(t) + \mathbf{F}_1(\mathbf{u}(t)) + \mathbf{N}_2(\mathbf{u}(t), \mathbf{w}(t)), \\ &\dot{\mathbf{v}}(t) = \mathbf{N}_3(\mathbf{v}(t), \mathbf{h}(t)), \\ &\dot{\mathbf{h}}(t) = d_h \mathbf{G}\mathbf{h}(t) + \mathbf{F}_2(\mathbf{u}(t), \mathbf{h}(t)), \\ &\dot{\mathbf{w}}(t) = d_w \mathbf{G}\mathbf{w}(t) + \mathbf{F}_3(\mathbf{v}(t), \mathbf{w}(t)) + \mathbf{N}_4(\mathbf{u}(t), \mathbf{w}(t)). \end{aligned} \tag{2}$$

In (2), $\mathbf{F}_1 : \mathbb{R}^n \to \mathbb{R}^n$ and $\mathbf{N}_1$, $\mathbf{N}_2$, $\mathbf{N}_3$, $\mathbf{N}_4$, $\mathbf{F}_2$, $\mathbf{F}_3 : \mathbb{R}^n \times \mathbb{R}^n \to \mathbb{R}^n$ are

$$\begin{aligned}
&\mathbf{N}_1(\mathbf{u},\mathbf{v}) = \chi(\mathbf{u}.*\mathbf{G}\mathbf{v} + \mathbf{G}_x\mathbf{u}.*\mathbf{G}_x\mathbf{v} + \mathbf{G}_y\mathbf{u}.*\mathbf{G}_y\mathbf{v}),\\
&\mathbf{N}_2(\mathbf{u},\mathbf{w}) = -\rho(\mathbf{w}).*\mathbf{u}, \quad \mathbf{N}_3(\mathbf{v},\mathbf{h}) = -\alpha\mathbf{h}.*\mathbf{v}, \quad \mathbf{N}_4(\mathbf{u},\mathbf{v},\mathbf{w}) = -\eta(\mathbf{u}).*\mathbf{w},\\
&\mathbf{F}_1(\mathbf{u}) = -\psi\mathbf{u}, \quad \mathbf{F}_2(\mathbf{u},\mathbf{h}) = \delta\mathbf{u} - \beta\mathbf{h}, \quad \mathbf{F}_3(\mathbf{v},\mathbf{w}) = \gamma\mathbf{v} - e\mathbf{w}.
\end{aligned}$$

POD-reduced system. We consider the following snapshot matrices for the construction of POD-reduced system: $\widehat{\mathbf{U}} = [\mathbf{u}^1,\ldots,\mathbf{u}^{n_s}]$, $\widehat{\mathbf{V}} = [\mathbf{v}^1,\ldots,\mathbf{v}^{n_s}]$, $\widehat{\mathbf{H}} = [\mathbf{h}^1,\ldots,\mathbf{h}^{n_s}]$, and $\widehat{\mathbf{W}} = [\mathbf{w}^1,\ldots,\mathbf{w}^{n_s}] \in \mathbb{R}^{n\times n_s}$. Here, $\mathbf{u}^j$, corresponds to the solution of the FD discretized system at time t_j and similarly for $\mathbf{v}^j$, $\mathbf{h}^j$ and $\mathbf{w}^j$. Let $r_u = \mathrm{rank}(\widehat{\mathbf{U}})$, $r_v = \mathrm{rank}(\widehat{\mathbf{V}})$, $r_h = \mathrm{rank}(\widehat{\mathbf{H}})$, $r_w = \mathrm{rank}(\widehat{\mathbf{W}})$. Let $k \le \min\{r_u, r_v, r_h, r_w\}$. The POD basis of dimension k of the snapshots $\{\mathbf{u}^j\}_{j=1}^{n_s}$ is the set of left singular values and likewise for the snapshots $\{\mathbf{v}^j\}_{j=1}^{n_s}$, $\{\mathbf{h}^j\}_{j=1}^{n_s}$, $\{\mathbf{w}^j\}_{j=1}^{n_s}$. Hence, the POD basis of the snapshots $\{\mathbf{u}^j\}_{j=1}^{n_s}$ denoted by $\mathbf{A}$ consists of the leading k orthonormal columns of $\widehat{\mathbf{A}}$, $\mathbf{A} = \widehat{\mathbf{A}}(:, 1:k) \in \mathbb{R}^{n\times k}$ where

$$\widehat{\mathbf{U}} = \widehat{\mathbf{A}}\Sigma^u(\mathbf{Z}^u)^T$$

is the SVD of $\widehat{\mathbf{U}}$ with $\widehat{\mathbf{A}} \in \mathbb{R}^{n\times n}$, $\Sigma^u \in \mathbb{R}^{n\times n_s}$ and $\mathbf{Z}^u \in \mathbb{R}^{n_s\times n_s}$. The diagonal entries of Σ^u are the singular values of $\widehat{\mathbf{U}}$. Similarly, let $\mathbf{B}$, $\mathbf{C}$, $\mathbf{D} \in \mathbb{R}^{n\times k}$ be matrices whose columns corresponding to the POD basis of dimension k of the snapshots $\{\mathbf{v}^j\}_{j=1}^{n_s}$, $\{\mathbf{h}^j\}_{j=1}^{n_s}$, and $\{\mathbf{w}^j\}_{j=1}^{n_s}$.
The POD reduced-order system is constructed by applying Galerkin projection method on the equations in (2). In particular, replacing the discrete state variables by their truncated POD expansions

$$\mathbf{u} \leftarrow \mathbf{A}\tilde{\mathbf{u}}, \qquad \mathbf{v} \leftarrow \mathbf{B}\tilde{\mathbf{v}}, \qquad \mathbf{h} \leftarrow \mathbf{C}\tilde{\mathbf{h}} \qquad \mathbf{w} \leftarrow \mathbf{D}\tilde{\mathbf{w}}$$

with reduced variables $\tilde{\mathbf{u}}$, $\tilde{\mathbf{v}}$, $\tilde{\mathbf{h}}$, $\tilde{\mathbf{w}} \in I\!R^k$, and then forcing the Galerkin orthogonality condition of the residuals by pre-multiplying the four equations in (2) by $\mathbf{A}^T$, $\mathbf{B}^T$, $\mathbf{C}^T$, and $\mathbf{D}^T$, respectively, we obtain the following reduced-order system

$$\begin{aligned}
\dot{\tilde{\mathbf{u}}}(t) &= -\mathbf{A}^T\tilde{\mathbf{N}}_1(\tilde{\mathbf{u}}(t),\tilde{\mathbf{v}}(t)) + d_u\underbrace{\mathbf{A}^T\mathbf{G}\mathbf{A}}_{\mathbf{G}_u}\tilde{\mathbf{u}}(t)\\
&\quad + \mathbf{A}^T\mathbf{F}_1(\mathbf{A}\tilde{\mathbf{u}}(t)) + \mathbf{A}^T\tilde{\mathbf{N}}_2(\tilde{\mathbf{u}}(t),\tilde{\mathbf{w}}(t)),\\
\dot{\tilde{\mathbf{v}}}(t) &= \mathbf{B}^T\tilde{\mathbf{N}}_3(\tilde{\mathbf{v}}(t),\tilde{\mathbf{h}}(t)),\\
\dot{\tilde{\mathbf{h}}}(t) &= d_h\underbrace{\mathbf{C}^T\mathbf{G}\mathbf{C}}_{\mathbf{G}_h}\tilde{\mathbf{h}}(t) + \mathbf{C}^T\mathbf{F}_2(\tilde{\mathbf{u}}(t),\tilde{\mathbf{h}}(t)),\\
\dot{\tilde{\mathbf{w}}}(t) &= d_w\underbrace{\mathbf{D}^T\mathbf{G}\mathbf{D}}_{\mathbf{G}_w}\tilde{\mathbf{w}}(t) + \mathbf{D}^T\mathbf{F}_3(\mathbf{B}\tilde{\mathbf{v}}(t),\mathbf{D}\tilde{\mathbf{w}}(t)) + \mathbf{D}^T\tilde{\mathbf{N}}_4(\tilde{\mathbf{u}}(t),\tilde{\mathbf{w}}(t)),
\end{aligned} \tag{3}$$

where $\tilde{\mathbf{N}}_1$, $\tilde{\mathbf{N}}_2$, $\tilde{\mathbf{N}}_3$, $\tilde{\mathbf{N}}_4 : \mathbb{R}^k \times \mathbb{R}^k \to \mathbb{R}^n$ are

$$\begin{aligned}
\tilde{\mathbf{N}}_1(\tilde{\mathbf{u}},\tilde{\mathbf{v}}) &= \chi(\tilde{\mathbf{u}}.*\mathbf{A}^T\mathbf{G}\mathbf{B}\tilde{\mathbf{v}} + \mathbf{A}^T\mathbf{G}_x\mathbf{A}\tilde{\mathbf{u}}.*\mathbf{A}^T\mathbf{G}_x\mathbf{B}\tilde{\mathbf{v}} + \mathbf{A}^T\mathbf{G}_y\mathbf{A}\tilde{\mathbf{u}}.*\mathbf{A}^T\mathbf{G}_y\mathbf{B}\tilde{\mathbf{v}})\\
\tilde{\mathbf{N}}_2(\tilde{\mathbf{u}},\tilde{\mathbf{w}}) &= -\rho(\tilde{\mathbf{w}}).*\tilde{\mathbf{u}}, \quad \tilde{\mathbf{N}}_3(\tilde{\mathbf{v}},\tilde{\mathbf{h}}) = -\alpha\tilde{\mathbf{h}}.*\tilde{\mathbf{v}}, \quad \tilde{\mathbf{N}}_4(\tilde{\mathbf{u}},\tilde{\mathbf{w}}) = -\eta(\tilde{\mathbf{u}}).*\tilde{\mathbf{w}},
\end{aligned}$$

Let $\mathbf{f}:\mathcal{D}\mapsto\mathbb{R}^n$ be o nonlinear vector-valued function with $\mathcal{D}\subset\mathbb{R}^d$, for some positive integer d. Let $\{\mathbf{S}\}_{\ell=1}^m\subset\mathbb{R}^n$ be a linearly independent set, for $m=1,\ldots,n$. For $\tau\in\mathcal{D}$, the DEIM approximation of order m for $\mathbf{f}(\tau)$ in the space spanned by $\{\mathbf{S}\}_{\ell=1}^m$ is given by ([3])

$$\widehat{\mathbf{f}}(\tau):=\mathbf{S}(\mathbf{P}^T\mathbf{S})^{-1}\mathbf{P}^T\mathbf{f}(\tau),$$

where $\mathbf{S}=[\mathbf{S}_1,\ldots,\mathbf{S}_m]\in\mathbb{R}^{n\times m}$ collects the first m POD basis modes of nonlinear function $\mathbf{f}$ and $\mathbf{P}=[\mathbf{e}_{\varrho_1},\ldots,\mathbf{e}_{\varrho_m}]\in\mathbb{R}^{n\times m}$ is the DEIM interpolation selection matrix. The DEIM procedure employs a greedy technique and iteratively constructs a set of indices $\{\varrho_1,\ \ldots,\ \varrho_m\}$ using the input basis $\{\mathbf{S}_i\}_{i=1}^m$, in such a way that, at each iteration, the current selected index captures the maximum variation of the input basis vectors (see [2], [3]).

POD-DEIM reduced system. Let $\mathbf{S}^{N_1}$, $\mathbf{S}^{N_2}$, $\mathbf{S}^{N_3}$, $\mathbf{S}^{N_4}\in\mathbb{R}^{n\times m}$, $m\leq n$ be the matrices whose columns containing the POD basis of the nonlinear functions $\tilde{\mathbf{N}}_1$, $\tilde{\mathbf{N}}_2$, $\tilde{\mathbf{N}}_3$, and $\tilde{\mathbf{N}}_4$ defined in (3). These POD bases are used to select the sets of m interpolation indices from DEIM algorithm. Let $\mathrm{vec}(\varrho)^{N_1}$, $\mathrm{vec}(\varrho)^{N_2}$, $\mathrm{vec}(\varrho)^{N_3}$, $\mathrm{vec}(\varrho)^{N_4}$, be the DEIM interpolation indices of the nonlinear functions defined in (3). Let $\mathbf{P}_{N_1}\in\mathbb{R}^{n\times m}$ be the matrix whose j-th column is the $\varrho_j^{N_1}$-th column of the identity matrix, i.e., it is the vector $[0,\ldots,0,1,0,\ldots,0]^T\in\mathbb{R}^n$, having all zeros entries except one at the entry $\varrho_j^{N_1}$, for $j=1,\ldots,m$. Define $\mathbf{P}_{N_2}$, $\mathbf{P}_{N_3}$, $\mathbf{P}_{N_4}\in\mathbb{R}^{n\times m}$ in a similar way as $\mathbf{P}_{N_1}$. Then the DEIM approximation of the nonlinear functions in (3) is of the form:

$$\begin{array}{lll}\tilde{\mathbf{N}}_1 & \approx \mathbf{S}^{N_1}(\mathbf{P}_{N_1}^T\mathbf{S}^{N_1})^{-1}\tilde{\mathbf{N}}_1^m, & \tilde{\mathbf{N}}_2\approx\mathbf{S}^{N_2}(\mathbf{P}_{N_2}^T\mathbf{S}^{N_2})^{-1}\tilde{\mathbf{N}}_2^m,\\ \tilde{\mathbf{N}}_3 & \approx \mathbf{S}^{N_3}(\mathbf{P}_{N_3}^T\mathbf{S}^{N_3})^{-1}\tilde{\mathbf{N}}_3^m, & \tilde{\mathbf{N}}_4\approx\mathbf{S}^{N_4}(\mathbf{P}_{N_4}^T\mathbf{S}^{N_4})^{-1}\tilde{\mathbf{N}}_4^m,\end{array}\tag{4}$$

and the nonlinear terms for the POD reduced system can be approximated as

$$\mathbf{A}^T\tilde{\mathbf{N}}_1(\tilde{\mathbf{u}},\tilde{\mathbf{v}})\approx\underbrace{\mathbf{A}^T\mathbf{S}^{N_1}(\mathbf{S}^{N_1}_{\mathrm{vec}(\varrho)})^{-1}}_{E_1}\tilde{\mathbf{N}}_1^m,\quad \mathbf{A}^T\tilde{\mathbf{N}}_2(\tilde{\mathbf{u}},\tilde{\mathbf{w}})\approx\underbrace{\mathbf{A}^T\mathbf{S}^{N_2}(\mathbf{S}^{N_2}_{\mathrm{vec}(\varrho)})^{-1}}_{E_2}\tilde{\mathbf{N}}_2^m,$$

$$\mathbf{B}^T\tilde{\mathbf{N}}_3(\tilde{\mathbf{v}},\tilde{\mathbf{h}})\approx\underbrace{\mathbf{B}^T\mathbf{S}^{N_3}(\mathbf{S}^{N_3}_{\mathrm{vec}(\varrho)})^{-1}}_{E_3}\tilde{\mathbf{N}}_3^m,\quad \mathbf{D}^T\tilde{\mathbf{N}}_4(\tilde{\mathbf{u}},\tilde{\mathbf{w}})\approx\underbrace{\mathbf{D}^T\mathbf{S}^{N_4}(\mathbf{S}^{N_4}_{\mathrm{vec}(\varrho)})^{-1}}_{E_4}\tilde{\mathbf{N}}_4^m,$$

where the nonlinear functions $\tilde{\mathbf{N}}_1^m$, $\tilde{\mathbf{N}}_2^m$, $\tilde{\mathbf{N}}_3^m$, $\tilde{\mathbf{N}}_4^m:\mathbb{R}^k\times\mathbb{R}^k\to\mathbb{R}^m$ are defined as:

$$\begin{array}{ll}\tilde{\mathbf{N}}_1^m(\tilde{\mathbf{u}},\tilde{\mathbf{v}})=\mathbf{P}_{N_1}^T\tilde{\mathbf{N}}_1(\tilde{\mathbf{u}},\tilde{\mathbf{v}}), & \tilde{\mathbf{N}}_2^m(\tilde{\mathbf{u}},\tilde{\mathbf{w}})=\mathbf{P}_{N_2}^T\tilde{\mathbf{N}}_2(\tilde{\mathbf{u}},\tilde{\mathbf{w}}),\\ \tilde{\mathbf{N}}_3^m(\tilde{\mathbf{v}},\tilde{\mathbf{h}})=\mathbf{P}_{N_3}^T\tilde{\mathbf{N}}_3(\tilde{\mathbf{v}},\tilde{\mathbf{h}}), & \tilde{\mathbf{N}}_4^m(\tilde{\mathbf{u}},\tilde{\mathbf{w}})=\mathbf{P}_{N_4}^T\tilde{\mathbf{N}}_4(\tilde{\mathbf{u}},\tilde{\mathbf{w}}).\end{array}\tag{5}$$

The explicit form of $\tilde{\mathbf{N}}_1^m(\tilde{\mathbf{u}},\tilde{\mathbf{v}})$ is given by

$$\begin{aligned}&=\chi[(\underbrace{\mathbf{P}_{N_1}^T\mathbf{A}}\,\tilde{\mathbf{u}}).*(\underbrace{\mathbf{P}_{N_1}^T\mathbf{G}\mathbf{B}}\,\tilde{\mathbf{v}})+(\underbrace{\mathbf{P}_{N_1}^T\mathbf{G}_x\mathbf{A}}\,\tilde{\mathbf{u}}).*(\underbrace{\mathbf{P}_{N_1}^T\mathbf{G}_x\mathbf{B}}\,\tilde{\mathbf{v}})\\ &\quad+(\underbrace{\mathbf{P}_{N_1}^T\mathbf{G}_y\mathbf{A}}\,\tilde{\mathbf{u}}).*(\underbrace{\mathbf{P}_{N_1}^T\mathbf{G}_y\mathbf{B}}\,\tilde{\mathbf{v}})]\end{aligned}\tag{6}$$

and similarly for $\tilde{\mathbf{N}}_2^m$, $\tilde{\mathbf{N}}_3^m$, $\tilde{\mathbf{N}}_4^m$. We remark that the k-by-m matrices

$$\mathbf{E}_1 = \mathbf{A}^T\mathbf{S}^{N_1}(\mathbf{S}^{N_1}_{\mathrm{vec}(\varrho)})^{-1}, \qquad \mathbf{E}_2 = \mathbf{A}^T\mathbf{S}^{N_2}(\mathbf{S}^{N_2}_{\mathrm{vec}(\varrho)})^{-1},$$

$$\mathbf{E}_3 = \mathbf{B}^T\mathbf{S}^{N_3}(\mathbf{S}^{N_3}_{\mathrm{vec}(\varrho)})^{-1}, \qquad \mathbf{E}_4 = \mathbf{D}^T\mathbf{S}^{N_4}(\mathbf{S}^{N_4}_{\mathrm{vec}(\varrho)})^{-1},$$

can be precomputed and reused at each time step. Also, each of the m-by-k coefficient matrices in (6) grouped by the curly brackets are precomputed so that the computational complexity of each nonlinear function is independent of the dimension n of the original full-order system. Using the coefficient matrices in (3) the form of the POD-DEIM reduced system is

$$\begin{aligned}
\dot{\tilde{\mathbf{u}}}(t) &= -\mathbf{E}_1\tilde{\mathbf{N}}_1^m(\tilde{\mathbf{u}}(t),\tilde{\mathbf{v}}(t)) + d_u\mathbf{G}_u\tilde{\mathbf{u}}(t) + \mathbf{A}^T\mathbf{F}_1(\mathbf{A}\tilde{\mathbf{u}}(t)) + \mathbf{E}_2\tilde{\mathbf{N}}_2^m(\tilde{\mathbf{u}}(t),\tilde{\mathbf{w}}(t)),\\
\dot{\tilde{\mathbf{v}}}(t) &= \mathbf{E}_3\tilde{\mathbf{N}}_3^m(\tilde{\mathbf{v}}(t),\tilde{\mathbf{h}}(t)),\\
\dot{\tilde{\mathbf{h}}}(t) &= d_h\mathbf{G}_h\tilde{\mathbf{h}}(t) + \mathbf{C}^T\mathbf{F}_2(\tilde{\mathbf{u}}(t),\tilde{\mathbf{h}}(t)),\\
\dot{\tilde{\mathbf{w}}}(t) &= d_w\mathbf{G}_w\tilde{\mathbf{w}}(t) + \mathbf{D}^T\mathbf{F}_3(\mathbf{B}\tilde{\mathbf{v}}(t),\mathbf{D}\tilde{\mathbf{w}}(t)) + \mathbf{E}_4\tilde{\mathbf{N}}_4^m(\tilde{\mathbf{u}}(t),\tilde{\mathbf{w}}(t)).
\end{aligned}$$

We show DEIM improves the efficiency of the POD approximation and achieves a complexity reduction of the nonlinear terms. Numerical results are presented.

References

[1] Anderson, A.R.A., *A hybrid mathematical model of solid tumor invasion: the importance of cell adhesion*. Math. Med. Biol. IMA J. 22, 163–186 (2005).

[2] Barrault, M., Maday, Y., Nguyen, N.C., Patera, A.T.: *An "empirical interpolation" method: application to efficient reduced-basis discretization of partial differential equations*. C.R. Math. Acad. Sci. Paris 339, 667–672 (2004).

[3] Chaturantabut, S., Sorensen, D.C.: Discrete Empirical Interpolation for Nonlinear Model Reduction. TR09–05, CAAM, Rice University (2009).

Methods For Flood Hazard Mapping On The Test Area Of Svilengrad

Nina Dobrinkova

1 Objectives

SMART WATER project idea has its origin from the territorial needs of the Veneto Region - Province of Padua, in particular after the tragic flood event that has affected the area in November 2010. Main problems registered in that occasion have been the lack of an integrated communication system between regional and local Civil Protection authorities and the lack of coordination between relevant territorial actors. Such events has occured on the territories of Romania, Greece and Bulgaria during this period too. That is why the Province of Padua have contacted competent entities in Europe, in order to develop a concrete, easy to use and low cost solution for the territorial needs and built up consortia with Romanian, Bulgarian and Greek representatives who are having test cases with flood events similar to the one of Veneto Region. This objective has been shared by the entities that decided to take part in the project called SMART WATER, due to similar problems experienced in their test case areas.

2 Actions and means involved

The SMART WATER project has as main activities the following actions:

1. Analysis of the existing tools developed at European level for real time forecasting of flood events and of the linked hydraulic risk and selection of the best performing one.

2. Relevant territorial data collection, data standardization and shared data bases creation will be performed on the Italian, Romanian, Bulgarian and Greek test areas.

3. Development of a dedicated web based application, access-free at each territorial level. The application will be linked to the shared data bases and the flood hazard model will be implemented in its modules.

4. Training sessions dedicated to end-users from regional to local levels will take place at each test case area.

5. Networking with relevant territorial actors, drafting and signing of Memorandum of Understanding to assure continuous and updated data availability for the tool will give stakeholders and representative authorities sustainable results and future expansion of the SMART WATER tool.

6. Pilot testing within project area in order to calibrate and validate the flood hazard model will be conducted within the test area of Svilengrad, Bulgaria.

3 Flood Hazard Methods short description for Svilengrad test area

For Svilengrad test area will be used the free US flood hazard mapping model HEC-RAS. To set up correctly our data for the simulation with HEC-RAS model we needed to define which areas along the river will be included. The model requires the input of geometric data to represent river networks, channel cross-section data, and hydraulic structure data such as bridges, culverts, and weirs. The river networks define the connectivity of the river system, which is a collection of reaches, all oriented downstream. A reach is defined in HEC-RAS as starting or ending at junctions - locations where two or more streams join together or split apart. A river may be composed of one or more reaches with accordance to the river specifications. Channel cross-section data are used in HEC-RAS to characterize the flow carrying capacity of the river and adjacent floodplain. Cross-section data includes station-elevation data, main channel bank stations, downstream reach lengths, roughness coefficients, and contraction and expansion coefficients. Station-elevation data represent the ground surface at designated locations in a river reach. Cross-sections are taken perpendicular at the direction of flow both in the main channel and in the overbank areas. Bank stations separate the portion of the cross-section that is the main channel of the river from the adjacent floodplain areas termed the left and right overbank areas. Reach lengths are used to define the distance between cross-sections and are used for energy loss calculations in HEC-RAS. Reach lengths are considered for the left overbank, main channel, and right overbank areas and indicate the path of flow between cross sections. Roughness coefficients are an indication of the relative channel roughness. Channel roughness is considered for calculating frictional energy loss between cross sections. Typically, channel roughness is indicated by Manning's n-values. Contraction and expansion coefficients are flow dependent and characteristic of abrupt changes in flow direction [1, 2]. An example of a river cross-section is given on Figure 1.

4 WEB-GIS platform in SMART WATER project

The project Smart Water has technical specifications which are oriented to the civil protection engineers, who could apply field response for the population in risk by having webGIS tool that could support their decision making in cases of large flood events. The test areas are river sections defined for each project partner and the Bulgarian region is on the territory of municipality Svilengrad. The end user needs for the test cases cover the following types of information for the river monitoring:

- Distance from water level to river bank side
- Flooding areas

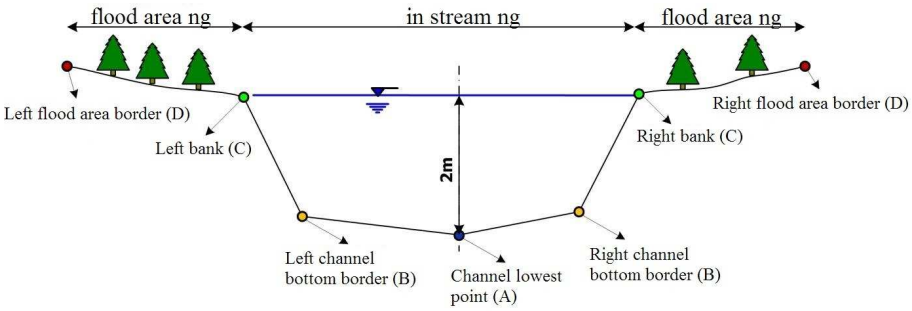

Figure 1: Example of cross-section in the test area.

- Speed and direction of the water
- Water blades
- A series of maps of predefined and variable flood scenarios, with greater frequency for the selected test case area provided in an information layer (i.e. raster images) corresponding to the information required by the civil protection units, where the reliability of forecasts is the main focus.
- A set of data in the form of graphs, tables, or files for download will be also available for the identified critical levels.
- For each simulation and for each point, the maximum water height independently from the moment, when it is reached, will display immediate worst scenario situation possible from the given initial conditions.

The standard WMS interface will be applied for displaying the hydrological model outputs on the webGIS platform. The maps in raster format like JPEG or PNG will give opportunity for punctual queries for the users. The identification of the strategic locations and data supply will have geomorphologic and hydrodynamic sets, where will be included DEM (Digital Elevation Model) for the catchment basin, ortophoto images for better justification of land use, meteorological data for precipitations and additional climatic conditions.On Figure 2 is given the structure of the information flow that the webGIS platform will have.

5 Conclusions

Increased information and awareness of citizenship thanks to widely used, innovative and low cost communication methods like (Internet/Intranet Networks, GSM/WAP/ GPRS mobile) give SMART WATER project vast options for fast and easy implementation on local, regional and national levels.

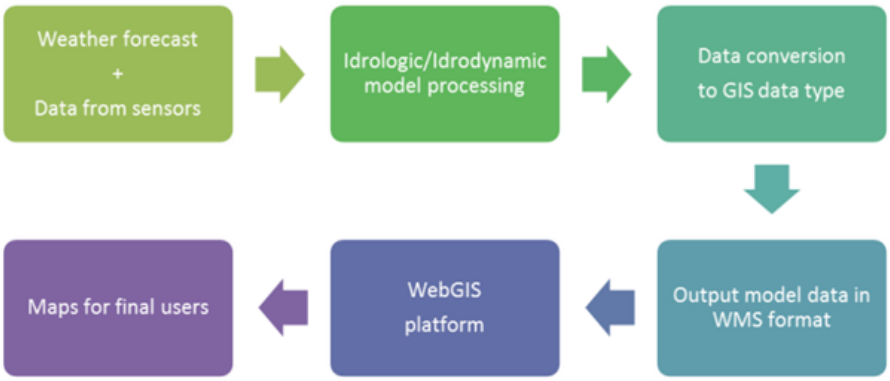

Figure 2: Information flow as it will be implemented in the webGIS tool that will be the result of Smart Water project.

6 Acknowledgements

This paper is supported by project Simple Management of Risk Through a Web Accessible Tool for EU Regions - ECHO/SUB/2012/638449. Acronym: SMART WATER. Web site: *http* : *//www.smartwaterproject.eu/*.

References

[1] EXIMAP, 2007, Handbook on Good Practices for Flood Mapping in Europe. *http* : *//ec.europa.eu/environment/water/flood_risk/flood_atlas/pdf/handbook_goodpractice.pdf*

[2] U.S. Army Corps of Engineers, 1998. HEC-RAS: River Analysis System User's Manual. Hydrologic Engineering Center, Davis, CA.

Wind Model in a Wild Fire Spread

Stefka Fidanova and Pencho Marinov

1 Introduction

The wild fires are a big problem for a countries with dry climate. Every year a big regions of forest are burn. The problem is very serious in South Europe, USA and Australia. This part of the world becomes dryer, because of the climate change and the number of wild fires and damages increase. A wild fire spread model can have several applications. The prevision of the fire front can help firemen to optimize their work. Possible scenarios can be played and train the firemen. The model can show the dangerous places for appearance of wild fire. Existing models are not satisfactory because they are very complicate and slow to be used in real situation [4, 5]. Most of them are used only for training.
In our work we apply game method for modeling with hexagonal cells to model wild fire spread. We include wind influence and the change of the form and spread of the fire front.

2 Game Method

The Game Method for Modeling (GMM) is applied of modeling different processes as biological processes, forest dynamic, natural processes etc. The idea of the GMM comes from Conway's Game of Life [3]. First the GMM is proposed by Atanassov [1]. It is a kind of cellular automate. In its first variant the GMM uses two-dimensional finite grid of squares. Every cell (square) has his own initial state, which forms the initial configuration of the hall area (grid). There is a set of rules which describes the change of the state of the cell according their previous state and according the state of the closer cells. The process is iterative, divided on time steps. The final state of a cell is a result of modifications which occurred during the certain number of application of the rules. The final configuration is the set of the final states of hall cells. The single application of the rules over a given configuration is called elementary step. The process stops after some predefined conditions, for example obtaining predefined configuration or execution of fixed number of steps.
In our previous work we use square cells for wild fire modeling [2]. In this work we apply GMM with hexagonal cells. The wild fire spread is circle when there is not a wind. The hexagon is close to the circle. Other reason is that in hexagonal mesh there is only one kind of neighbors and all neighbor cells have side contacts. In a square variant there are two kind of neighbor cells, with side contacts and with corner contacts.

3 Wind Modeling

In our wild fire model, considered area is represented by hexagonal cells. The problem is very difficult, therefore we complicate the model step by step. In this work we include modeling of the wind wile the area is flat. The parameters of our wild fire model are: burning time of the cell, time to start to burn, force of the wind, direction of the wind. The model is prepared for fixed humidity and air temperature. We suppose existing of pre-processing and recalculation of the parameters, before the start of the modeling. The burning time (burning duration) shows how many time steps are needed, the material inside the cell to be totally burned. The time to start to burn is related with ignition speed if one neighbor cell burns. If the material in the cell is unburned, than the burning duration and the speed for ignition are equal to 0. The rules of our fire model are: The modeling starts from the initial state of the area where one ore more cells are burning; Every time step the burning duration of burning cells decrease with 1 till it becomes 0 (totally burned); If a cell is burning, the speed of ignition of closer cells are changed, depending of the force and direction of the wind; When the speed of ignition becomes 0 the cell start to burn; The process continues until no other change of the parameters is possible or the number of the applied time steps is equal to the predefined time steps.

Advantage of our model is that it can start from any stage of the area, which is a realistic case, because the forest fires are discern after some acceleration. We suppose that the initial model parameters are fixed. We use average wind. The wind is represented by vector. Every cell can have its own wind vector. If some cell is burning the spread of the heat depends of the projection of the wind vector on the directions of other cells and inversely of the square of the distance of a cell to the burning cell. If the force of the wind is 0, there is not a wind, the burning cell has influence only on direct neighbors. In this case the ignition time of neighbor cells decrease with 1 every time step till it becomes 0. In the case with wind the ignition time of the affected cells decrease with number from the interval $[0, 1]$. We can have several scenarios. When the force of the wind is big and the ignition time is small, than the fire front spread on the wind direction and there are not or there is very small fire spread in the opposite direction. When force of the wind is small and the ignition time is big, than the fire front spread on the direction opposite to the wind direction, but with much less speed.

On Figure 1 is shown wind effect on the wild fire spread when the burning material is the same in all cells. The force of the wind shown on Figure 1b and Figure 1d is two times higher than this on the Figure 1a and Figure 1c. On the all figures is shown the fire front after 17 time steps. The fire is started from the black cell. We observe that on the Figure 1b and Figure 1d the distance between the fire start and the front to the wind direction is longer than on Figure 1a and Figure 1c. Other observation is that the distance from the fire start and the front on the direction opposed to the wind direction is shorter.

We tested wind with various directions and forces. We verify if the form of the fire front is the same with same wind force and different directions, when the all cells have

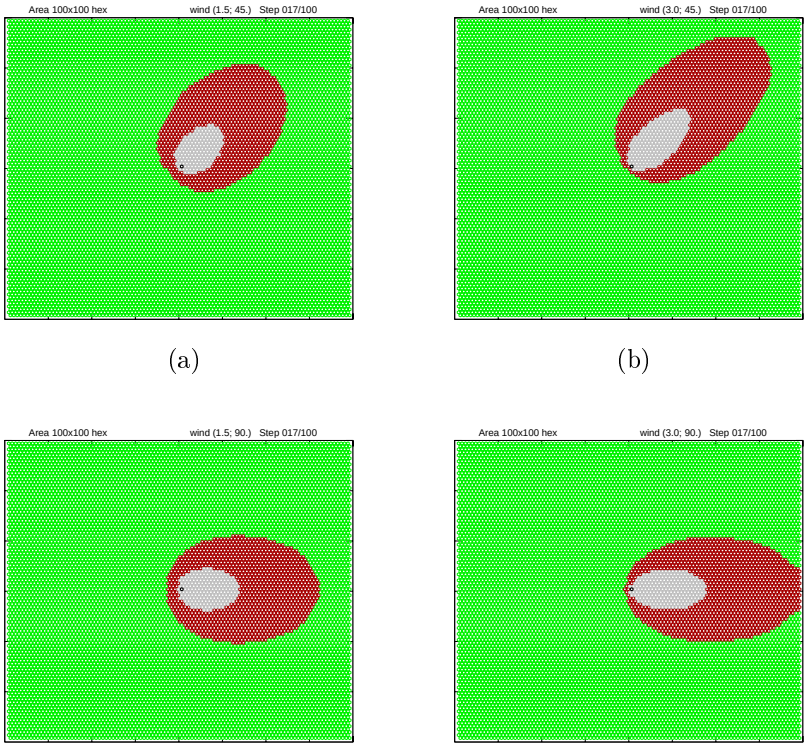

Figure 1: Wind effect with: **(a)** light wind with direction 45 degrees; **(b)** hight wind with direction 45 degrees; **(c)** light wind with direction 90 degrees; **(d)** hight wind with direction 90 degrees

same burning time and ignition time. On Figure 1c the wind force is the same as on Figure 1a only the direction is different. The same is on Figure 1b and Figure 1d. We observe that the achieved by our model front of the fire is almost similar when the force of the wind is the same.

4 Conclusion

On this paper we apply GMM on wild fire modeling. In our model we take in to account the presence of the wind and it influence on closer cells. We run various tests and verify that the fire spread looks realistic.

Acknowledgment

This work has been partially supported by the European Commission project ACOMIN and by the Bulgarian National Scientific Fund under the grant I01/0006- "Simulation of wild-land fire behavior".

References

[1] Atanassov K., On a combinatorial game-method for modeling. Advances in Modeling and Analysis, AMSE Press, Vol 19(2), 1994, pp. 41-47.

[2] Dobrinkova N., Fidanova S. and Atanasov K., Game-Method Model for Filed Fires, Large Scale Scientific Computing, Lecture Notes in Computer Science No 5910, ISSN 0302-9743, Springer, Germany, 2010, pp. 173-179.

[3] Gardner M., Mathematical Games - The fantastic combination of John Conway's new solitaire game life", Scientific American 223, ISBN 0-89454-001-7, 1970, pp. 120-123.

[4] Ferragut L., Asensio M.I., Simon J., Forest Fire Simulation: Mathematical Models and Numerical Methods, Monografias de la Real Academia de Ciencias de Zaragoza, Vol 34, 2010, 51-71.

[5] Rothermel R. C.: A Mathematical Model for Predicting Fire Spread in Wild land Fuels, General Technical Report INT-115, USDA Forest Service, International For- est and Range Experiment Station, 1972.

Computer Simulations of the Atmospheric Composition Climate of Bulgaria - Some Basic Results

Georgi Gadzhev, Kostadin Ganev, Maria Prodanova, Dimiter Syrakov, Nikolai Miloshev

1 Introduction

Recently extensive studies for long enough simulation periods and good resolution of the atmospheric composition status in Bulgaria have been carried out using up-to-date modeling tools and detailed and reliable input data [1, 2, 3, 4].
The simulations aimed at constructing of ensemble, comprehensive enough as to provide statistically reliable assessment of the atmospheric composition climate of Bulgaria - typical and extreme features of the special/temporal behavior, annual means and seasonal variations, etc.
The present paper, in which a brief review of the studies, will focus on some important characteristics of the atmospheric composition climate of Bulgaria

2 Modeling tools and input data

All the simulations are based on the US EPA Model-3 system [5]The large scale (background) meteorological data used by the study is the NCEP Global Analysis Data with 1x1 degree resolution. The MM5 and CMAQ nesting capabilities are used to downscale the problem to a 3 km horizontal resolution for the innermost domain (Bulgaria).
The TNO high resolution emission inventory [6] is exploited. A detailed description of the emission modeling is given in [4]

3 Some illustrations

As already explained, the 8-year simulated fields ensemble is large enough to allow statistical treatment. In particular the probability density functions for each of the atmospheric compounds can be calculated, with the respective seasonal and diurnal variations, for each of the points of the simulation grid or averaged over the territory of the country. Knowing the probability function we know everything about the climate of the different compound concentrations (see Figure 1).
Another important characteristic of the atmospheric composition climate of the country is the contribution of the emission of different categories to the overall atmospheric composition pattern (see Figure 2).

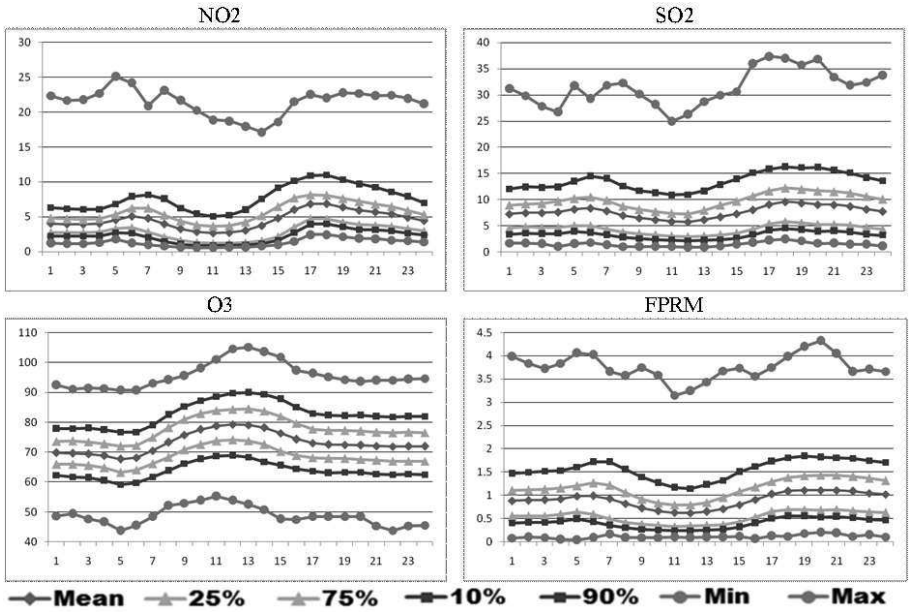

Figure 1: Annually mean diurnal variations of the averaged for the country NO2, SO2, O3 and fine PM surface concentrations [ug/m3]: curves of mean, maximal and minimal values as well as curves show the imaginary concentrations for which the probability of the simulated ones to be smaller is respectively 0.25, 0.75, 0.1 and 0.9.

4 Some basic facts about the atmospheric composition climate of Bulgaria

Some of the major findings about the atmospheric composition climate of Bulgaria are as follows:

- the behavior of the surface concentrations, averaged over the ensemble annually, or for the four seasons and over the territory of the country is reasonable and demonstrates effects which for most of the compounds can be explained from a point of view of the generally accepted schemes of dynamic influences (in particular the role of turbulent transport and its dependence on atmospheric stability) and/or chemical transformations;

- the SNAP 1 contribution to the surface SO2 concentrations is smaller than one should expect, having in mind that the 'Maritza' power plants are among the biggest sulfur sources in Europe. Probably, a significant amount of SO2 from these sources becomes a subject of larger scale transport and so is moved outside the country;

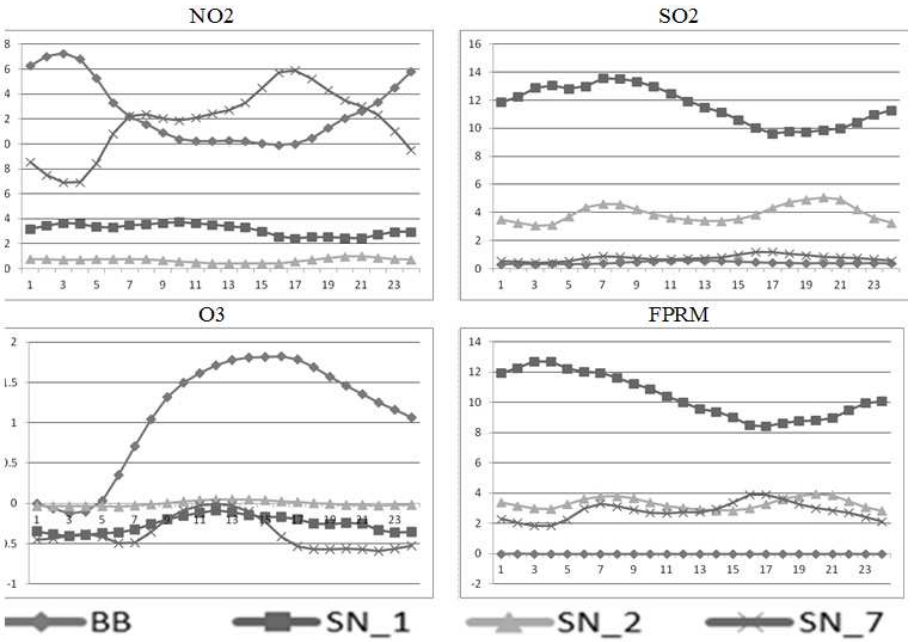

Figure 2: Annually mean diurnal variations of the averaged for the country contribution [%] of different emission categories on NO2, SO2, O3 and fine PM surface concentrations.

- the contribution of biogenic emissions to surface ozone in the country is relatively small. This indicates that local O3 production rate is limited by the availability of NOx concentration, a regime which is called NOx-limited. Obviously from a point of view of atmospheric composition climate the Balkan Peninsula and Bulgaria are predominantly 'rural' environment which explains the ozone photochemistry specifics in the region.;
- the contribution of the emission from categories 1 and 7, which are the major sources of the other ozone precursor - nitrogen oxides, is also small. This, once again is an indirect indicator, that the surface ozone in Bulgaria is to a small extend due to domestic sources, but is mostly imported;
- the results produced by the CMAQ - Integrated Process Rate Analysi s- demonstrate the very complex behavior and interaction of the different processes. The analysis of the behavior of different processes does not give simple answer of the question how the air pollution in a given point or region is formed.

Aknowledgements

The present work is supported by the Bulgarian National Science Fund (grant DCVP-02/1/29.12.2009) and the EC-FP7 grant 261323 (project EGI-InSPIRE).

References

[1] Gadzhev G., Yordanov G., Ganev K., Prodanova M., Syrakov D., Miloshev N., (2011), Atmospheric Composition Studies for the Balkan Region. LSSC 2010, LNCS, vol. 6046, pp.150-157,Springer

[2] Gadzhev G., Syrakov D., Ganev K., Brandiyska A., Miloshev N., Jordanov G., Prodanova M., (2011), Atmospheric Composition of the Balkan Region and Bulgaria - Some Numerical experiments. American Institute of Physics Conf. Proc. 1404, 200, pp. 200-209, DOI: 10.1063/1.3659921

[3] Gadzhev G., Ganev K., Syrakov D., Miloshev N., and Prodanova M., (2012), Contribution of biogenic emissions to the atmospheric composition of the Balkan Region and Bulgaria, Int. J. Environment and Pollution, Vol. 50, Nos. 1/2/3/4, pp.130-139, DOI: 10.1504/IJEP.2012.051187.

[4] Gadzhev G., Ganev K., Miloshev N., Syrakov D., Prodanova M., (2013), Numerical Study of the Atmospheric Composition in Bulgaria, Computers and Mathematics with Applications, 65, pp. 402-422.

[5] D. Byun, J. Ching, Science Algorithms of the EPA Models-3 Community Multiscale Air Quality (CMAQ) Modeling System. EPA Report 600/R-99/030, Washington DC. http://www.epa.gov/asmdnerl/models3/doc/science/science.html.

[6] Visschedijk A. J. H., Zandveld P.Y.J., H.A.C. Denier van der Gon, (2007),A High Resolution Gridded European Emission Database for the EU Integrate Project GEMS, TNO-report 2007-A-R0233/B

Air Quality Index Evaluations for Bulgaria

Ivelina Georgieva

1 Introduction

In communication with the general public providing information on the actual air quality is not meaningful to present concentration values unless the concentrations are related to the effect levels. Frequently this is done by converting the concentration into a dimensionless scale which is also associated with an intuitive color code (from green to red) and a linguistic description (e.g. from very good to very poor). Commonly the reference levels used in the conversion are based on health-protection related limit, target or guideline values set by the EU, at national or local level or by the WHO.
For describing the ambient pollutant mix, an overall air quality index (AQI) is constructed. In calculating such an overall AQI, firstly for each individual pollutant a sub-index is calculated. The overall index is set to the highest value of each of the pollutant considered.
The AQI has become part of the information routinely provided to the public. The AQI makes it possible to describe the air quality in a simple, understandable way.

2 Computer simulated atmospheric composition

Recently extensive studies for long enough simulation periods and good resolution of the atmospheric composition status in Bulgaria have been carried out using up-to-date modeling tools and detailed and reliable input data [1, 2, 3, 4, 5, 6, 7, 8, 9].
The simulations aimed at constructing of ensemble, comprehensive enough as to provide statistically reliable assessment of the atmospheric composition climate of Bulgaria - typical and extreme features of the special/temporal behavior, annual means and seasonal variations, etc.

3 Some AQI examples

Utilization of the ensemble for studying the AQI climate in Bulgaria is the goal of the present work.
The AQI, calculated in the frame of Bulgarian Chemical Weather Forecast System [10, 11], ver.3, which follows the UK Air Quality Index [12] is used in the present work as well. Due to the limited volume of the present abstract only few examples, illustrating the AQI climate in Bulgaria will be demonstrated.
Figure 1, for example, demonstrates the seasonal and diurnal variation of the recurrence of different AQI categories, averaged for the territory of Bulgaria. As it can be seen AQI2 and 3 are with highest recurrence, while all other AQI are much less

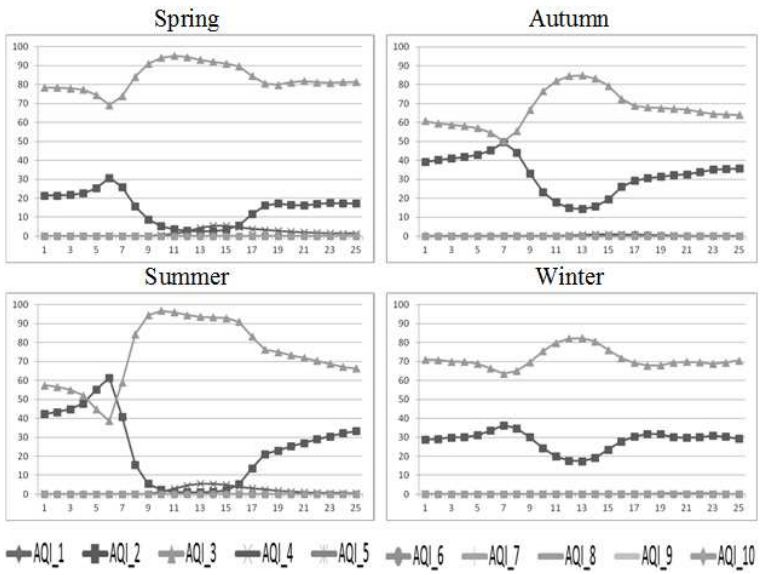

Figure 1: Diurnal and seasonal variations of the averaged over Bulgaria recurrence [%] of the different AQI.

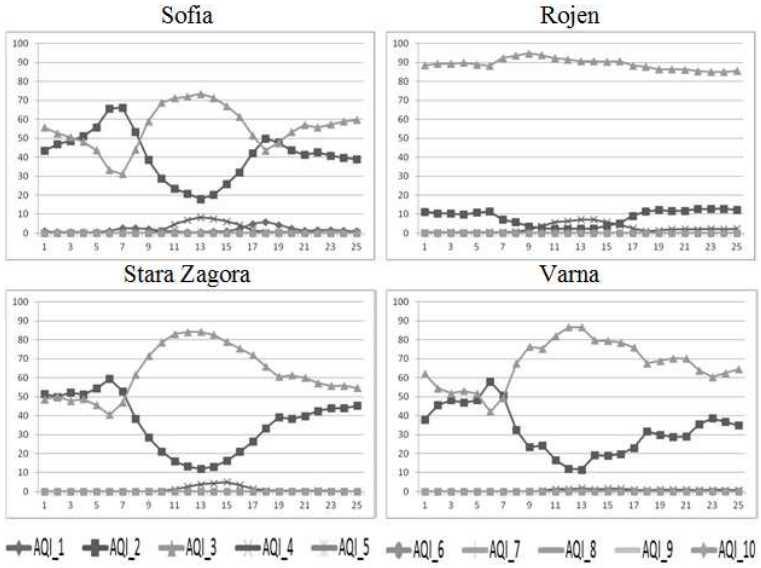

Figure 2: Diurnal variations of the annually averaged recurrence [%] of the different AQI for different points

probable. Exceptions can be seen at noon for spring and summer, when probability of AQI4 becomes higher than the one for AQI2.
The AQI probabilities have not only seasonal and diurnal, but also spatial variability. Figure 2 demonstrates the annual AQI recurrence for different points. As can be seen AQI2 and 3 have highest impact, while all others AQI are with negligible impact. AQI4 probability has local maximum at midday for Sofia, Rojen and Stara Zagora.
The general conclusion that can be made is that the air quality status of Bulgaria is rather good (evaluated with a spatial resolution of 3km) - the recurrence of high AQI values is close to zero. It should be also noted that the dominant pollutant - the one that determines the AQI value is mostly the surface ozone.

Aknowledgements

The present work is supported by the Bulgarian National Science Fund (grant DCVP-02/1/29.12.2009) and the EC-FP7 grant 261323 (project EGI-InSPIRE).

References

[1] Gadzhev G., Yordanov G., Ganev K., Prodanova M., Syrakov D., Miloshev N., (2011), Atmospheric Composition Studies for the Balkan Region. LSSC 2010, LNCS, vol. 6046, pp.150-157, Springer

[2] Gadzhev G., Syrakov D., Ganev K., Brandiyska A., Miloshev N., Jordanov G., Prodanova M., (2011), Atmospheric Composition of the Balkan Region and Bulgaria - Some Numerical experiments. American Institute of Physics Conf. Proc. 1404, 200, pp. 200-209, DOI: 10.1063/1.3659921

[3] Gadzhev G., Ganev K., Syrakov D., Miloshev N., and Prodanova M., (2012), Contribution of biogenic emissions to the atmospheric composition of the Balkan Region and Bulgaria, Int. J. Environment and Pollution, Vol. 50, Nos. 1/2/3/4, pp.130-139, DOI: 10.1504/IJEP.2012.051187.

[4] Gadzhev G., Ganev K., Miloshev N., Syrakov D., Prodanova M., (2013), Numerical Study of the Atmospheric Composition in Bulgaria, Computers and Mathematics with Applications, 65, pp. 402-422.

[5] Gadzhev G., K. Ganev, M. Prodanova, D. Syrakov, E. Atanasov, N. Miloshev, (2013), Multi-scale atmospheric composition modelling for Bulgaria, NATO Science for Peace and Security Series C: Environmental Security 137 , pp. 381-385 (CD)

[6] Ganev K., D. Syrakov, A. Todorova, G. Gadzhev, G. Jordanov, N. Miloshev, M. Prodanova, (2009), Joint analysis of dilution and transformation processes of air pollution from the road and ship transport. 7th International Conference on Air Quality Science and Application Istanbul, 24-27 March 2009. (on a CD)

[7] Ganev K., Syrakov D., Prodanova M., Miloshev N., Jordanov G., Gadjev G., and Todorova A., 2009, Atmospheric composition modeling for the Balkan region, ISBN: 978-975-403-510-0, pp. 77-85

[8] Todorova A., D. Syrakov, G. Gadjhev, G. Georgiev, K. Ganev, M. Prodanova, N. Miloshev, V. Spiridonov, A. Bogatchev, K. Slavov, (2010), Grid computing for atmospheric composition studies in Bulgaria. Earth Sci. Inform. ISSN 1865-0473 Vol.3, No.4, pp. 259-282.

[9] Todorova A., Gadzhev G., Jordanov G., Syrakov D., Ganev K., Miloshev N., Prodanova M., (2009), Application of the US EPA models 3 sysytem for numerical simulations of high PM10 levels episodes.

[10] Syrakov D., Etropolska I., Prodanova M., Ganev K., Miloshev N., Slavov K., (2012), Operational Pollution Forecast for the Region of Bulgaria, American Institute of Physics, Conf. Proc. 1487, pp. 88 - 94; DOI: 10.1063/1.4758945.

[11] Syrakov D., M. Prodanova, I. Etropolska, K. Ganev, N. Miloshev, K. Slavov, G. Jordanov, 2011 Automated system for chemical weather forecast in Bulgaria, Bulgarian Journal of Meteorology and Hydrology, v. 16, No. 1, pp.30-40. de Leeuw F.,W. Mol, (2005),Air Quality and Air Quality Indices: a world apart.ETC/ACC Technical Paper 2005/5

[12] de Leeuw F., W. Mol, (2005), Air Quality and Air Quality Indices: a world apart. ETC/ACC Technical Paper 2005/5
http://acm.eionet.europa.eu/docs/ETCACC_TechnPaper_2005_5_AQ_Indices.pdf.

Statistical Estimation of Brown Bears Population in Rhodope Mountains

Todor Gurov, Emanouil Atanassov, Aneta Karaivanova, Ruslan Serbezov, and Nikolai Spassov

The brown bear (Ursus arctos) is the most widespread bear in the world. It can be found across Europe, Asia and North America in habitats ranging from forests to dry deserts and tundra. One of the best bear habitats in Europe are located in Bulgaria. They are situated in the mountains of Rhodopa, Stara planina, Rila, Pirin, Vitosha. Until 1992 the bear had been a game target. By Order 1023 dated 31.12.1992 of the Ministry of Environment and Water (MoEW)the species has been declared protected, in compliance with the Nature protection act. This status has been kept also after the Biodiversity act was passed in 2002. The Habitat directive requires strict protection of the species and declaration of special protected areas for conservation of its habitats [5]. The main habitats of the bear in Bulgaria are included in the ecological network NATURA 2000 [6]. For the purposes of protection of the habitats and the management of the network NATURA 2000 a mapping and determination of their environmental status was carried out in the frame of project under the EU operational programmes environment. The acquired information are used for elaboration of plans for management of the protected areas and the populations of the species as well as for regulation of the investment projects therein. That is why it is important to estimate habitat use and population dynamics of brown bears in the country. In this work we study the population of brown bears in Rhodopa Mountains, using data received from the monitoring that was carried out in Autumn 2011. Recommendations regarding the obtained estimators and the necessary sample sizes are presented, as well as some ways to improve data collection during future monitoring.

1 Evaluation of the population size of the brown bear

In this study, we use the transect method and statistical approches [1, 3, 4] to estimate population size of the brown bear. The transect method is based of collection of traces of brown bear on predefined set of routes (transects) and analysis to determine the unique traces. It is a popular and cheap method for monitoring the bear population. The numerical analysis of brown bear population is made using statistical methods, by using the data collected on size of front/rear paw of bears obtained during the National Monitoring (26-27 October 2011) in the Western Rhodopes, the territory of Pazardzhik region and parts of the Plovdiv region. These data, together with data for nutritional importance of forest types, enable us to evaluate the numerical population throughout Western area of Rhodope mountains where there are large areas with a permanent presence of the species.

The number of transects used during the National Monitoring was 48 covering 14 forest administrative units, see Table 1. For determining the unique traces of brown

FORESTRY AREA: (administrative unit or forest farm)	Asenovgrad			Chekeritsa					Batak		Belovo		
Transects	3			5					2		3		
Number of traces	0	0	0	0	4	1	1	1	0	1	0	0	2
FORESTRY AREA:	Peshtera			Selishte					Alabak		Beglika		
Transects	3			3					2		3		
Traces	1	0	0	2	0	0			2	0	2	3	1
FORESTRY AREA:	Borovo			Rakitovo					Rodopi		Shiroka polyana		
Transects	3			2					2		3		
Traces	1	2	2	3		0			2	1	1	1	1
FORETRY AREA:	Chepino/Chehlyovo										Yundolau		
Number of transects	11										3		
Number of bear's traces	1	0	1	0	1	2	4	0	1	2	0	0	0
Total transects :	48					Traces:					47		

Table 3: Distribution of the bear's traces on the forestry areas and on the transects.

Deviation	Min deviation	Mean value	Max deviation	Round to a whole number	Level of significance x_β	Confidence interval β
1.0742885	45.89	49.04	52.19	**45-53**	3.00	99.7%
1.0742885	47.21	49.04	50.79	**47-51**	1.67	95%

Table 4: Number of unique traces by using different confidence interval.

bears the main quantitative indicator was the width of the front paw of the bear, while the width of the rear paw of the bear was used as a secondary indicator.
The Table 4 shows results for mean value and standard diviation of the non-groupped data, presented in Table 3
The GPS data was used to perform classification based on a statistical method (Mahalanobis distance - D2) [2].
For this purpose, 412 GPS locations of brown bears are used (traces marked trees, burrows, observations, genetic samples collected from sites in the hair bear habitat, excrement, etc.).
Based on this data, we performed statistical extrapolation, taking into account the suitability of different types of woodland, namely 4 groups of woodland were considered:

Fit areas bear habitats	„other land cover"	coniferous forest	mixed forests	deciduous forest	Total
14 Forestry areas with transects	271.72	835.99	399.51	343.73	1850.95
Other forestry areas (Pazardjik and Plovdiv) without transects	351.619	896.9119	452.226	448.6128	2149.369
all fit areas bear habitats in Smolyan and Kardjalii	671.28	988.36	609.9237	447.5292	2717.094

Table 5: 4 fit areas bear habitats in square kilometres (km2), grouped by regions of the Rhodope mountain.

Fit areas bear habitats	Other land cover	Coniferous forest	Mixed forests	Deciduous forest	Total
14 Forestry areas with transects ; Other forestry areas (Pazardjik and Plovdiv) without transects	4.75	20.08	19.35	12.43	56.61
Round to a whole number	5	21	20	13	57/59
All fit areas bear habitats in Smolyan and Kardjalii	9.07	22.13	26.09	12.40	69.69
Round to a whole number	10	23	27	13	70/73
Total size population	**15**	**44**	**47**	**26**	**127/132**

Table 6: Results for population size of the brown bear in Rhodope mounting.

- other land cover (like blackberries, shrubs, forest herbs - mean value of D2 - 11.4;
- coniferous forest - mean value of D2 - 6.8;
- mixed forests - mean value of D2 - 3.6;
- deciduous forest - mean value of D2 - 5.56.

The distribution of forest area per woodland type is shown in Table 5. The final results, which offer an estimate of the brown population in the whole Rhodopi mountain, are shown in Table 6.
Based on the estimated statistical error of about 8%, the population size should be between 137 and 143.

2 Conclusion

Data from national monitoring the size of bear paws can be used to determine height, age and sex of bears. It is a task, the results of which will be presented in a later publication. When collecting data during national monitoring, several sources of subjective errors were observed, namely: (i) availability of feeders on some of the routes leading to correlation of the results and increase the error in the calculations. (ii) uneven number of routes in the forestry areas (administrative unit or forest farm). In some forest farms there were large number of routes, while others need to be supplemented with new routes. It is recommended that the average number of routes per farm depend on the size of the areas that are fit for habitat. (iii) accuracy of trace determination - wrong determination of front/rear paws.
To improve the mathematical model to assess the brown bear population need for a National Monitoring each fall , usually in the middle or end of October. Provision is also generating simulation data using high performance computing systems with the main objective to improve the model. The introduction of the principle of repeatability for the transects will allow to compare the data with those from previous monitoring and observe the tendencies. It is important to collect information about the type of forest where each trace was found. The accumulation of data from several

national monitorings will allow to assess the development trend of the population - if we have a sustained increase or decrease.

3 Future work

Based on the developed methodology, an estimate for population size in the whole country can be obtained when more data is available. In addition to that an estimate the trend of growth for the brown bear population in the country shall be obtained, when data from consecutive and consistent monitorings can be used. Our ambition is to create a program product for solving the above problems.

Acknowledgment

This work was supported by the National Science Fund of Bulgaria under Grant DCVP 02/1 CoE SuperCA++ and by PUDOOS under the Contract No 9190.

References

[1] Kalos, M.A., Whitlock, P.A., Monte Carlo Methods, Wiley Interscience, New York, 1986.

[2] Zlatanova, D., Modeling habitat suitability of bear (Ursus arctos L.), wolf (Canis lupus L.) and lynx (Lynx lynx L.) in Bulgaria, PhD Thesis , Sofia University - Faculty of Biology, 2010, pp. 287. (in Bulgarian).

[3] Yoccoz, N.G., Nichols J.D., and Boulinior Th., Monitoring of biological diversity in space and time, J. TRENDS in Ecology&Evolution, Vo. 16 (8), August 2001, 446-453.

[4] Beier, P., Cunningham, St.C., Power of track surveys to detect changes in cougar populations, Wildlife Society Bulletin 1996, 24 (3); 540-546.

[5] Red Data Book of The Republic Bulgaria, Vol. 2 - Animals, http://e-ecodb.bas.bg/rdb/en/, Sofia, 2011.

[6] Natura2000, http://natura2000.moew.government.bg/

Structure Analysis of HLA Complexes in the Presence of Co-Receptors

Nevena Ilieva, Damyan Grancharov, Peicho Petkov, Michael Kenn, Reiner Ribarics, and Wolfgang Schreiner

The major histocompatibility complex (MHC) molecule and the T cell antigen receptor (TCR) are the primary components of the immunological synapse which realises the cell-cell interactions of the adaptive immune response. MHC molecules (in humans also called human leukocyte antigen – HLA) are highly polymorphic proteins which bind protein fragments (epitops) and present them on the cell surface. TCR is responsible for the antigen recognition and succeeding signal transmission into the cell interior. The binding of the antigen within the MHC is not covalent, also its interaction with the TCR is of relatively low affinity, so there are many factors which can influence the stability of the immunological synapse.

Molecular dynamics (MD) is a powerful method for modelling and investigation of the structure and behaviour of biomolecules, which provides an insight into dynamics of the processes they undergo and is a valuable completion to the experimental studies. In a previous work, we have critically investigated the reliability of the RMSD-based MD analysis [1] and have emphasized the importance of identifying semi-rigid domains in the biomolecules [2] on the example of LC13 TCR/ABCD3/HLA-B*44:05, which has been crystallized by MacDonald et al [3]. In the present paper, we extend the investigated system by including also the CD8 co-receptor, which is believed to intervene in the dynamics of the whole process [4]. However, the specific mechanisms behind this influence are still not clarified, not least because of limited experimental data (some recent work is contained in [5, 6]).

As there is no structure available for this extended complex, we engineered it from the PDB entries 3KPS (LC13 TCR in complex with HLA B*4405 bound to EEYLQAFTY – a self peptide from the ABCD3 protein, [3]) and 1AKJ (a complex between human CD8$\alpha\alpha$, HLA-A*0201 and a HIV reverse transcriptase epitope). The alignment was based on a contact map between CD8 and MHC molecules, including the close-contact C-α atoms of MHC, with a cutoff of 1.5nm.

The two complexes (with and without CD8 co-receptors) were subjected to 200ns GROMACS 4.0.7 simulations at 310K, with the GROMOS96 53a6 force field, time step of 5fs (after removing the hydrogen motions), v-rescale temperature coupling with a time constant of 0.1ps and Berendsen pressure coupling with a time constant of 0.5ps. Both Van-der-Waals and Coulomb interactions were computed with 1.4nm cutoff, and for the long-range electrostatics PME method with standard parameters was applied.

Based on an extensive analysis, encompasssing RMSD distributions for functionally critical parts of the investigated complexes, such as the binding groove of the MHC molecule, its α3 domain and the TCR, interface surface area between α3 domain of

MHC and the CD8, hydrogen-bond dynamics and relative distances between MHC and TCR, conclusions may be drawn about the stabilizing role of the CD8 co-receptor on the whole complex. The influence of the CD8 presence on the semi-rigid domain formation is to be kept in mind as well. The present analysis may also be envisaged as a proof-of-concept for the engineering protocol, to be used in forthcoming sudies of the allorecognition patterns in complexes with point mutations of the MHC molecule.

Aknowledgements

The MD trajectories used in the present work were generated on the IBM-BlueGene/P computer facility at Bulgarian National Centre for Supercomputing Applications (NCSA). The work was supported in part by BSF and OeAD under Grants DCVP 02/1/2009, DNTS-A 01-2/2013 and WTA-BG 06/2013.

References

[1] W. Schreiner, R. Karch, B. Knapp, and N. Ilieva, *Relaxation Estimation of RMSD in Molecular Dynamics Immunosimulations.* Comp. and Math. Meth. in Med., Vol. 2012; doi: 10.1155/2012/173521.

[2] M. Kenn, R. Ribarics, N. Ilieva, W. Schreiner, *Finding Semi-Rigid Domains in Biomolecules by Clustering Pair-Distance Variations.*BioMed Res. Int. (Comp. and Bioinf. Techn. for Immunology) *(to appear)*

[3] W.A. Macdonald et al., *T Cell Allorecognition via Molecular Mimicry.* Immunity **31**: 897–908 (2009).

[4] Y. Li, Y. Yin, and R.A. Mariuzza, *Structural and biophysical insight into the role of CD4 and CD8 in T cell activation.* Review article. Frontiers in Immmunology, Vol. 4 (July 2013); doi: 103389/fimmu.2013.00206

[5] Y. Shi, J. Qi, A. Iwamoto, G. Gao, *Plasticity of human CD8αα binding to peptide–HLA-A*2402.* Mol. Immunology **48** (2011) 2198–2202.

[6] J. Borger, R. Zamoyska, D. Gakamsky, *Proximity of TCR and its CD8 coreceptor controls sensitivity of T cells.* Immun. Lett. **157** (2014) 16–22.

Structured Low-Rank Approximation by Factorization

Mariya Ishteva, Konstantin Usevich, Ivan Markovsky

We consider the problem of approximating an affinely structured matrix, for example a Hankel matrix, by a low-rank matrix with the same structure. This problem occurs in system identification, signal processing and computer algebra, among others. We consider a factorization approach and enforce the structure on the approximation by introducing a penalty term in the objective function. The proposed local optimization algorithm is able to solve the weighted structured low-rank approximation problem, as well as to deal with the cases of missing or fixed elements.

1 Introduction

Low-rank approximations are widely used in data mining, machine learning and signal processing as a tool for dimensionality reduction and factor analysis. In system identification, signal processing and computer algebra, the matrices are often structured, e.g., (block) Hankel, (block) Toeplitz, Sylvester, or banded matrices with fixed bandwidth. The goal of structured low-rank approximation is to preserve the given structure while obtaining a low-rank approximation. Although each of the "constraints" can easily be handled separately, imposing both low-rank and fixed structure on the approximation is nontrivial.
To deal with the rank constraint, we consider a matrix factorization approach, i.e., given a structured matrix $D \in \mathbb{R}^{m\times n}$ and a number r such that $r \ll m, n$, find two factors $P \in \mathbb{R}^{m\times r}$ and $L \in \mathbb{R}^{r\times n}$, such that

$$D \approx PL \quad \text{and} \quad PL \text{ is a structured matrix.}$$

The structure will be enforced by introducing a penalty term in the objective function.

2 Problem formulation

Affine structures can be defined as

$$\mathcal{S}(p) = S_0 + \sum_{k=1}^{n_p} S_k p_k,$$

where $S_0, S_1, \ldots, S_{n_p} \in \mathbb{R}^{m\times n}$, $p \in \mathbb{R}^{n_p}$ and $n_p \in \mathbb{N}$ is the (minimal) number of parameters. Let $\mathrm{vec}(X)$ denote the vectorized matrix X and let

$$\mathbf{S} = \begin{bmatrix} \mathrm{vec}(S_1) & \cdots & \mathrm{vec}(S_{n_p}) \end{bmatrix} \in \mathbb{R}^{mn\times n_p}.$$

Since n_p is minimal, $\mathbf{S}$ has full column rank. For simplicity, we assume that the elements of $\mathbf{S}$ are only 0 and 1, and there is at most one nonzero in each row (non-overlap across S_k), i.e., every element of the structured matrix corresponds to only one element of p.

2.1 Orthogonal projection on image($\mathcal{S}$)

It can be shown that the orthogonal projection of a matrix X on image($\mathcal{S}$) is given by

$$\mathcal{P}_{\mathcal{S}}(X) := \mathcal{S}(\mathbf{S}^{\dagger} \operatorname{vec}(X)), \quad \textit{where} \quad \mathbf{S}^{\dagger} := (\mathbf{S}^{\top}\mathbf{S})^{-1}\mathbf{S}^{\top}. \tag{1}$$

The effect of applying the pseudo-inverse $\mathbf{S}^{\dagger}$ on a vectorized matrix X is producing a p_X structure vector by averaging elements corresponding to the same S_k. Note that applying $\mathbf{S}^{\dagger}$ on a (vectorized) structured matrix extracts its structure vector, since $\mathbf{S}^{\dagger}\mathbf{S}\,p = p$. Finally,

$$\operatorname{vec}(\mathcal{P}_{\mathcal{S}}(X)) = \operatorname{vec}(S_0) + \Pi_{\mathbf{S}} \operatorname{vec}(X), \tag{2}$$

where $\Pi_{\mathbf{S}} = \mathbf{S}\,\mathbf{S}^{\dagger} = \mathbf{S}(\mathbf{S}^{\top}\mathbf{S})^{-1}\mathbf{S}^{\top}$ is the orthogonal projector on the image of $\mathbf{S}$.

2.2 Optimization problem

We solve a series of related simpler subproblems, the solution of each subsequent problem being forced closer to the feasible region of the main problem. One of the requirements (low-rank or structure) will always be imposed, while the other one will be satisfied only upon convergence. We have the following two choices (see Figure 1):

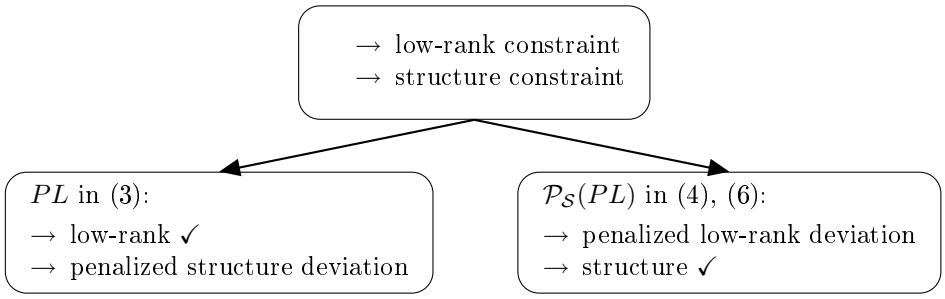

Figure 1: Optimization problems

- Penalize the structure deviation

$$\min_{P,\,L} \|D - PL\|_W^2 + \lambda \|PL - \mathcal{P}_{\mathcal{S}}(PL)\|_F^2, \tag{3}$$

where λ is a penalty parameter, $\|\cdot\|_F$ stands for the Frobenius norm, $\mathcal{P}_{\mathcal{S}}(PL)$ is defined in (1), and $\|\cdot\|_W$ is a semi-norm on the space of matrices $\mathbb{R}^{m\times n}$, induced by a positive semidefinite matrix $W \in \mathbb{R}^{mn\times mn}$ as $\|D\|_W^2 := (\operatorname{vec}(D))^{\top} W \operatorname{vec}(D)$.

- Penalize the low-rank deviation

$$\min_{P,\,L} \|D - \mathcal{P}_{\mathcal{S}}(PL)\|_W^2 + \lambda \|PL - \mathcal{P}_{\mathcal{S}}(PL)\|_F^2. \tag{4}$$

Note that for $\lambda = \infty$, the term $\|PL - P_{\mathcal{S}}(PL)\|$ has to be 0 and problems (3) and 4) are equivalent. The interpretations of (3) and (4) are however different. In (4) the main part is the structure and the low rank is 'secondary'. In (3) it is the other way around, although in both cases both constraints are satisfied at the solution.
In the literature [2], the weighted structured low-rank approximation problem is often formulated as

$$\min_{\hat{p}} \|p - \hat{p}\|_{\overline{W}}, \quad \text{such that} \quad \operatorname{rank}(\mathcal{S}(\hat{p})) \leq r, \tag{5}$$

where $\overline{W} \in \mathbb{R}^{n_p \times n_p}$ is a symmetric positive definite matrix of weights. (If $\overline{W}$ is the identity matrix, $\|\cdot\|_{\overline{W}} = \|\cdot\|_2$.)
Note that (4) can be formulated using $\overline{W}$ in the following way

$$\boxed{\min_{P,\,L} \|p - \mathbf{S}^\dagger \operatorname{vec}(PL)\|_{\overline{W}}^2 + \lambda \|PL - \mathcal{P}_{\mathcal{S}}(PL)\|_F^2.} \tag{6}$$

3 The proposed algorithm

3.1 Main idea

We solve the minimization problem (6) by alternatingly improving the approximations of P and of L,

$$\begin{aligned} &\min_{L} \|p - \mathbf{S}^\dagger \operatorname{vec}(PL)\|_{\overline{W}}^2 + \lambda \|PL - \mathcal{P}_{\mathcal{S}}(PL)\|_F^2, \\ &\min_{P} \|p - \mathbf{S}^\dagger \operatorname{vec}(PL)\|_{\overline{W}}^2 + \lambda \|PL - \mathcal{P}_{\mathcal{S}}(PL)\|_F^2, \end{aligned} \tag{7}$$

until convergence.
Let I_n be the $n \times n$ identity matrix, '$\otimes$' denote the Kronecker product and $\overline{W} = \overline{M}^\top \overline{M}$. Then (7) can be reformulated as

$$\begin{aligned} &\min_{L} \left\| \begin{bmatrix} \overline{M}\,\mathbf{S}^\dagger \\ \sqrt{\lambda}\Pi_{\mathbf{S}_\perp} \end{bmatrix} (I_n \otimes P) \operatorname{vec}(L) - \begin{bmatrix} \overline{M}p \\ \sqrt{\lambda}\operatorname{vec}(S_0) \end{bmatrix} \right\|_2^2, \\ &\min_{P} \left\| \begin{bmatrix} \overline{M}\,\mathbf{S}^\dagger \\ \sqrt{\lambda}\Pi_{\mathbf{S}_\perp} \end{bmatrix} (L^\top \otimes I_m) \operatorname{vec}(P) - \begin{bmatrix} \overline{M}p \\ \sqrt{\lambda}\operatorname{vec}(S_0) \end{bmatrix} \right\|_2^2, \end{aligned}$$

$\Pi_{\mathbf{S}_\perp} = (I_{mn} - \Pi_{\mathbf{S}})$ being the orthogonal projector on the left kernel of $\mathbf{S}$.
These are least squares problems and can easily be solved by standard techniques. The matrix P can be initialized by a matrix representing the left dominant subspace of A. We declare that PL is a structured matrix if

$$\|PL - P_{\mathcal{S}}(PL)\|_F^2 < 10^{-12}.$$

3.2 Parameter λ

In theory, if we fix $\lambda = \infty$, then we have the exact structured low-rank approximation problem. In practice, we start from a small value and increase it with each iteration until it reaches a "large enough" value. This way we allow the algorithm to move to a "good region" quickly and then impose more strictly all constraints. For convergence properties, we rely on the theory of quadratic penalty method from [3, §17.1].

4 Conclusions

The proposed algorithm solves the weighted structured low-rank approximation problem and can deal with the cases of missing elements in the data matrix or fixed elements in the structure. This is interesting not only from optimization point of view, but also has great impact on the applicability of the proposed approach. Practically relevant simulation examples from system identification, computer algebra (finding a common divisor of polynomials with noisy coefficients), and symmetric tensor decomposition are presented in [1], demonstrating its consistently good performance.

Acknowledgments

The research leading to these results has received funding from the European Research Council under the European Union's Seventh Framework Programme (FP7/2007-2013) / ERC Grant agreement number 258581 "Structured low-rank approximation: Theory, algorithms, and applications", the Research Foundation Flanders (FWO-Vlaanderen), the Flemish Government (Methusalem Fund, METH1), and the Belgian Federal Government (Interuniversity Attraction Poles programme VII, Dynamical Systems, Control, and Optimization). MI is an FWO Pegasus Marie Curie Fellow.

References

[1] M. Ishteva, K. Usevich, I. Markovsky. Regularized structured low-rank approximation with applications. Available from `http://arxiv.org/abs/1308.1827`.

[2] I. Markovsky. *Low Rank Approximation: Algorithms, Implementation, Applications*. Springer, 2012.

[3] J. Nocedal, S. J. Wright. *Numerical Optimization*. Springer Series in Operations Research. Springer, 2nd edition, 2006.

LScalable implementation of the parallel multigrid method on massively parallel computer

Kab Seok Kang

Fast elliptic solvers are a key ingredient of massively parallel Particle-in-Cell (PIC) and Vlasov simulation codes for fusion plasmas. This applies for both, gyrokinetic and fully kinetic models. The currently available most efficient solver for large elliptic problems is the multigrid method, especially the geometric multigrid method which requires detailed information of the geometry for its discretization.

The multigrid method is a well-known, fast and efficient algorithm to solve many classes of problems [1, 5]. In general, the ratio of the communication costs to computation costs increases on the coarser level, i.e., the communication costs are high on the coarser levels in comparison to the computation costs. Since, the multiplicative multigrid algorithm is applied on each level, the bottleneck of the parallel multigrid lies on the coarser levels, including the exact solver at the coarsest level. The additive multigrid method could combine all the data communication for the different levels in one single step. Unfortunately, this version can be used only for the preconditioner and usually needs almost twice as many iterations instead. The multiplicative version can be used both as a solver and as a preconditioner, so we consider the multiplicative version only.

The feasible coarsest level of operation of the parallel multigrid method depends on the number of cores since there must be at least one degree of freedom (DoF) per core (the coarsest level limitation). Thus, the total number of DoF of the coarsest level problem increases with increasing number of cores. To improve the performance of the parallel multigrid method, we consider reducing the number of executing cores to one (the simplest case) after gathering data from all cores on a certain level (gathering the data) [3]. This algorithm avoids the coarsest level limitation. Numerical experiments on large numbers of cores show a very good performance improvement. However, this implementation may still be further improved, if we manage to reduce the number of MPI tasks to yield better scaling properties.

Modern computer architectures have highly hierarchical system design, i.e., multi-socket multi-core shared-memory computer nodes which are connected via high-speed interconnects. This trend will continue into the foreseeable future, broadening the available range of hardware designs even when looking at high-end systems. Consequently, it seems natural to employ a hybrid programming model which uses OpenMP for parallelization inside the node and MPI for message passing between nodes.

Expected benefits with OpenMP/MPI hybridzation are a good usage of shared memory system resources (memory, cache, latency, and bandwidth), and a reduced memory footprint [2]. OpenMP coarsens the granularity at the MPI level (larger message sizes) and allows increased and/or dynamic load balancing. This is preferential for some problems which have naturally two-level parallelism or only use a restricted number of MPI tasks. Consequently, such a programming model can have better scalability than both pure MPI and pure OpenMP. The most important benefit of applying the

hybrid OpenMP/MPI programming model to the parallel multigrid method is that it can reduce the number of MPI tasks and thus decrease the communication cost of the coarser level. This simple fact leads to better scalability on the same number of cores.

In this paper, we consider a structured triangulation of a hexagonal domain for an elliptic partial differential equation as a test problem [4]. The matrix-vector multiplication is the key component of iterative methods such as CGM, GMRES, and the multigrid method. Many researchers have developed parallel solvers for partial differential equations on unstructured triangular meshes. In [4], we considered a new approach to handle a structured grid of a regular hexagonal domain with regular triangle elements. In this context we showed that the matrix-vector multiplication of this approach has an almost perfect scaling property [4]. We modify the parallel multigrid algorithm, which was implemented using MPI, by adding OpenMP parallelization at the node level.

To get performance results we run the program on the HELIOS machine. The HELIOS machine is located in the International Fusion Energy Research Centre (IFERC) at Aomori, Japan. IFERC was built in the framework for the EU(F4E)-Japan broader approach collaboration. The machine is made by 4410 Bullx B510 Blades nodes of two 8-core Intel Sandy-Bridge EP 2.7 GHz processors with 64 GB memory and connected by Infiniband QDR. So it has a total of 70 560 cores total and 1.23 Petaflops Linpack performance.

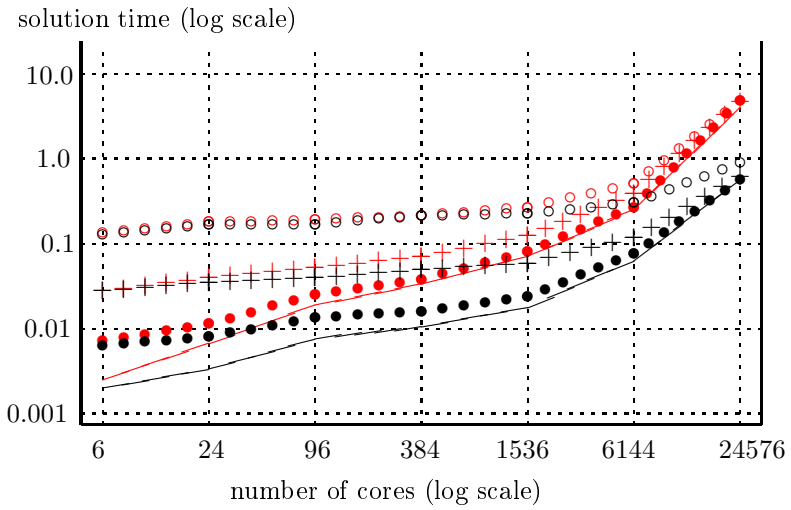

Figure 1: **(Semi-weak scaling)** The solution time in seconds of the multigrid method with a Gauss-Seidel smoother as a preconditioner for the PCGM with (in black) and without (in red) gathering the data as a function of the number of cores for domains with 2K DoF (solid line), 8K DoF (•), 32K DoF(+), and 132K DoF(∘) per core.

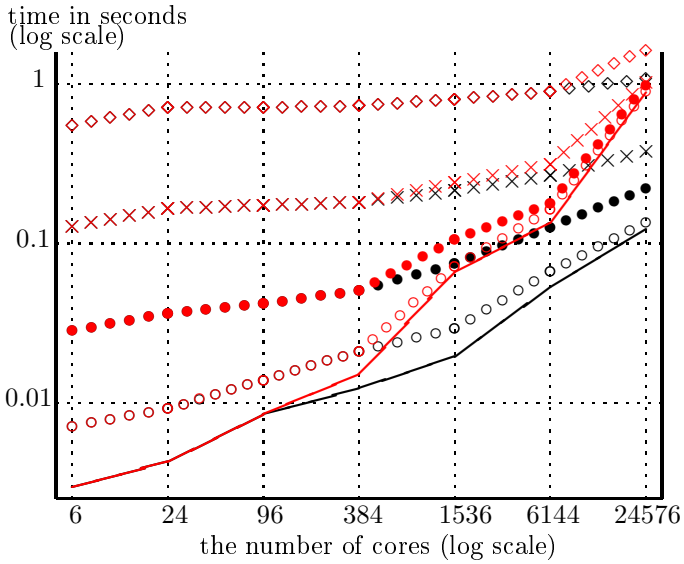

Figure 2: **(Semi-weak scaling OpenMP/MPI)** The solution time in seconds of the multigrid method with a Gauss-Seidel smoother as a preconditioner for the PCGM as a function of the number of cores for a fixed number of DoF per core. (The best results of the hybrid model in black, pure MPI in red. 2K (solid), 8K (○), 32K (•), 130K (×) and 500K (◇) per core).

The parallel multigrid method with gathering the data avoids the coarsest level limitation and numerical experiments on large numbers of cores show a very good performance improvement as can be seen in Fig. 1. There, we depict the semi-weak scaling results which measure the solution time of a problem with almost the same number of DoF per core. For the multigrid method a pure weak scaling seems to be hard to achieve as the number of operations per core has to be fixed. However, increasing the problem size according to the number of cores automatically leads to introducing additional multigrid levels to keep the size of the coarsest level problem constant. Therefore, the number of operations per core slightly increases in our semi-weak scaling due to additional multigrid levels. The numerical results in Fig. 1 show that this implementation still needs improvements for large number of MPI tasks and small numbers of DoF per core.
Next, we depict in Fig. 2 the semi-weak scaling results for the selected test cases: 2k, 32k, 32k, 130k, and 500k DoF per core. There we compare the pure MPI case occupying all 16 cores on each node (in red) with the best performing hybrid cases of 1, 4, or 16 OpenMP threads per MPI task, i.e., 16, 4, or 1 MPI task per node (in black). For the pure MPI case the performance significantly degrades when the number of cores becomes large for cases with a small number of DoF per core. This situation

improves with the hybrid model, i.e., problems with small number of DoF can be solved with a larger number of threads on a larger number of cores. The threads work on the shared memory of a node which makes this method more efficient by avoiding part of the internode communication of the MPI method.

References

[1] W. Hackbush, *Multigrid Methods and Applications*, Springer-Verlag, Berlin, Germany, 1985.

[2] G. Hager, G. Jost, and R. Rabenseifner, Communication Characteristics and Hybrid MPI/OpenMP Parallel, Programming on Clusters of Multi-core SMP Nodes *Cray User Group 2009 Proceedings*.

[3] K. S. Kang, Parallelization of the Multigrid Method on High Performance Computers, IPP-Report 5/123, 2010.

[4] K. S. Kang, A parallel multigrid solver on a structured trianglation of a hexagonal domain, *DD21 proceedings*.

[5] P. Wesseling, *An Introduction to Multigrid Methods*, Wiley, Chichester, 2003.

Finite element based finite difference method for multidimensional convection-diffusion-reaction equations

Adem Kaya, Dr. Ali Şendur

Abstract

An efficient finite difference method is proposed for multidimensional convection-diffusion-reaction equations which is obtained from finite element method, particularly designed to treat the (most interesting) case of small diffusion, but is able to adapt naturally from the diffusion-dominated regime to the convection-dominated and/or to the reaction-dominated regime.

1 Introduction

The multidimensional convection-diffusion-reaction equation (CDR) is an active research area. It is well known that standard methods such as Galerkin finite element method and central differencing produce undesired oscillations that pollute whole domain when convection or reaction dominates and sharp layers occur in the solution of CDR equation. To cure this situation many methods have been proposed so far, especially in finite element approach. Streamline-Upwind Petrov Galerkin (SUPG) is one of the first approach to cure this situation. Another approach is Residual-Free-Bubble (RFB) method which is based on enriching the finite element space. It is first studied to find a suitable value of stabilizing parameter for SUPG method. The main problem with this method is that it requires the solution of a local PDE which is as difficult as solving the original problem.

Most of finite element methods depend on mesh dependent parameters. Altough, there exist stabilization parameters that give nodally exact solutions in $1D$, finding optimal mesh dependent parameters is intractable in $2D$ and $3D$. Furthermore, in multi-dimensions it is more difficult to design numerical methods which are robust (that is, monotone) in all regimes.

Link-cutting bubble strategy (LCB) [1] is a stabilized finite element method which is nodally exact in 1D. It aims to stabilize the Galerkin method by using a suitable refinement near the layer region. LCB strategy uses the piecewise linear bubble functions to find the suitable sub-grid nodes. It works as the plain Galerkin method on augmented meshes. It is extended to time-dependent convection-diffusion-reaction problem in $1D$ in [2]. Implementation of the LCB method in multi-dimension is not easy.

I will propose a new strategy which is robust in all regimes and depends on LCB method for multidimensional CDR equation. It can be easily implemented even for $4D$ and $5D$ CDR equations. Discretization of domain contains two steps: first, we will do an initial discretization then, we will place subgrid nodes into the initial

discretization using some arguments in [1]. After solving equation on augmented grid we exclude subgrid nodes to simulate the numerical solution.

2 Link-cutting Bubble strategy

Link-Cutting Bubble strategy introduced in [1] was designed for one-dimensional convection-diffusion-reaction equation (1);

$$\begin{cases} \mathcal{L}u = -\epsilon u'' + \beta u' + \sigma u = f(x) \text{ on } I, \\ u(0) = u(1) = 0. \end{cases} \tag{1}$$

It aims to approximate the basis bubble functions with piecewise linear functions including subgrid nodes into elements. If we consider a typical element $K = (x_1, x_2)$ and assume $\beta > 0$ and $\sigma > 0$, then the subgrid nones are obtained by placing two extra nodes, say z_1 and z_2, such that $x_1 < z_1 < z_2 < x_2$ where locations of z_1 and z_2 depend on problem parameters. After derivation of sub-grid nodes Link-cutting bubble strategy works as plain Galerkin method with piecewise linear basis functions on augmented mesh.
It is well known that in one space dimension standard Galerkin finite element method with piecewise linear basis functions corresponds to following finite difference method for CDR equation on uniform mesh:

$$-\epsilon\frac{u_{j+1} - 2u_j + u_{j-1}}{h^2} + \beta\frac{u_{j+1} - u_{j-1}}{2h} + \sigma\frac{u_{j+1} + 4u_j + u_{j-1}}{6} = \frac{f_{j-1} + 4f_j + f_{j+1}}{6} \tag{2}$$

where h is the length of each element. On non-uniform meshes it corresponds to following difference method:

$$-\epsilon\frac{u_{j+1}}{h_2} + \epsilon\frac{u_j}{h_2} + \epsilon\frac{u_j}{h_1} - \epsilon\frac{u_{j-1}}{h_1} + \beta\frac{u_{j+1} - u_{j-1}}{2} + \sigma\frac{h_2u_{j+1} + 2h_2u_j + 2h_1u_j + h_1u_{j-1}}{6}$$

$$= \frac{h_2f_{j+1} + 2h_2f_j + 2h_1f_j + h_1f_{j-1}}{6} \tag{3}$$

where $h_2 = x_{i+1} - x_i$, $h_1 = x_i - x_{i-1}$.

3 The numerical approach

In two space dimensions we will consider the following constant coefficient linear elliptic convection-diffusion-reaction problem in a polygonal domain Ω:

$$\begin{cases} -\epsilon\left(\frac{\partial^2 u}{\partial x^2} + \frac{\partial^2 u}{\partial y^2}\right) + b.\left(\frac{\partial u}{\partial x}, \frac{\partial u}{\partial y}\right) + \sigma u = f(x, y) \text{ on } \Omega \\ u(x, y) = g \text{ on } \partial\Omega \end{cases} \tag{4}$$

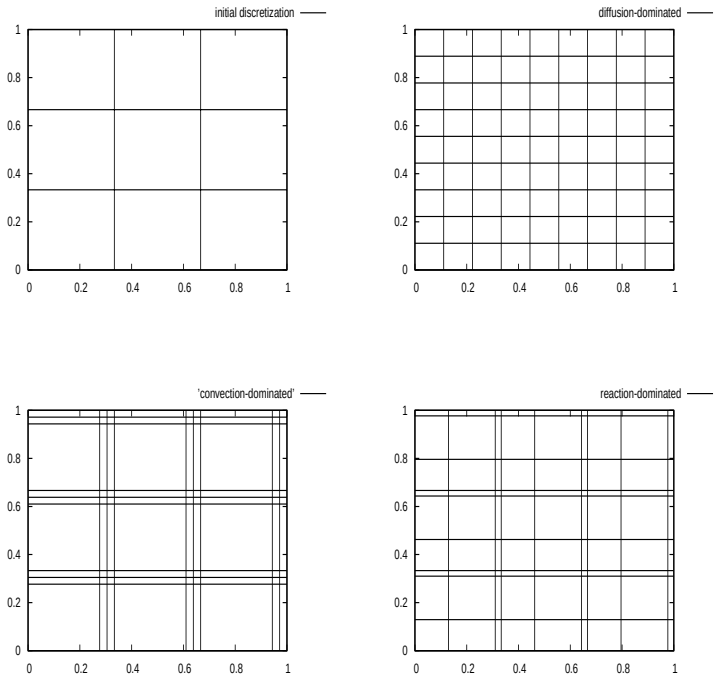

Figure 1: Initial discretization and modified discretizations in three different regimes for $N = M = 4$.

where $\epsilon > 0$, $b = (b_1, b_2)$ and $\sigma \geq 0$. We can write equation (4) as follows:

$$\begin{cases} -\epsilon\left(\frac{\partial^2 u}{\partial x^2}\right) + b_1\left(\frac{\partial u}{\partial x}\right) + \sigma\frac{|b_1|}{|b_1|+|b_2|}u - \epsilon\left(\frac{\partial^2 u}{\partial y^2}\right) + b_2\left(\frac{\partial u}{\partial y}\right) + \sigma\frac{|b_2|}{|b_1|+|b_2|}u \\ = \frac{|b_1|}{|b_1|+|b_2|}f(x,y) + \frac{|b_2|}{|b_1|+|b_2|}f(x,y) \text{ on } \Omega \\ u(x,y) = g \text{ on } \partial\Omega. \end{cases} \tag{5}$$

where b_1 and b_2 are not equal zero, simultaneously. We can consider equation (4) as a sum of the following equations;

$$-\epsilon\left(\frac{\partial^2 u}{\partial x^2}\right) + \beta_1\left(\frac{\partial u}{\partial x}\right) + \sigma\frac{|b_1|}{|b_1|+|b_2|}u = \frac{|b_1|}{|b_1|+|b_2|}f(x,y) \tag{6}$$

and

$$-\epsilon\left(\frac{\partial^2 u}{\partial y^2}\right) + \beta_2\left(\frac{\partial u}{\partial y}\right) + \sigma\frac{|b_2|}{|b_1|+|b_2|}u = \frac{|b_2|}{|b_1|+|b_2|}f(x,y). \tag{7}$$

Applying finite difference method in (3) to the equations (6-7) and summing up we get the finite difference formulation for equation (4).

3.1 Discretization of the domain

We start the discretization of the domain with an initial discretization which can be structured or unstructured. For simplicity, let N denotes the number of uniformly spaced grid points in x-direction , M in y-direction and K in z-direction on initial discretization. Second discretization (modified discretization) is derived by placing subgrid nodes which are obtained with applying Link-cutting bubble strategy in x, y and z-direction, separately. x-coordinates of modified discretization is obtained by applying the procedure in Link-cutting bubble strategy to the equation (6) and y-coordinates to the equation (7) in $2D$. The modified discretization consists of $(3N-2)\times(3M-2)$ points in $2D$ and $(3N-2)\times(3M-2)\times(3K-2)$ points in $3D$. Figure 1 shows an example of initial discretization and modified discretizations obtained from the initial discretization in different regimes in $2D$.

References

[1] Brezzi, F., Hauke, G., Marini, L.D. & Sangalli, G.(2003) Link-cutting bubbles for the stabilization of convection-diffusion-reaction problems. *Math. Models Methods Appl. Sci.,* **13**, 445-461.

[2] Asensio, M.I., Ayuso, B. & Sangalli, G. (2007) Coupling stabilized finite element methods with finite difference time integration for advection-diffusion-reaction problems. *Comput. Methods Appl. Mech. Engrg.,* **196**, 3475-3491.

A Fast Parallel Algorithm for Direct Simulation of Particulate Flows Using Conforming Grids

Johnwill Keating and Peter D. Minev

This study presents a development of the direction splitting algorithm for problems in complex geometries proposed in [1] to the case of flows containing rigid particles. The main novelty of this method is that the grid can be very easily fit to the boundaries of the particle and therefore the spatial discretization is very accurate. This is made possible by the direction splitting algorithm of [1]. It factorizes the parabolic part of the operator direction wise and this allows to discretize in space each of the one-dimensional operators by adapting the grid to fit the boundary only in the given direction. Here we use a MAC discretization stencil but the same idea can be applied to other discretizations. Then the equations of motion of each particle are discretized explicitly and the so-computed particle velocity is imposed as a Dirichlet boundary condition for the momentum equations on the adapted grid. The pressure is extended within the particles in a fictitious domain fashion.

The incompressible Navier-Stokes equations for the fluid occupying a domain Ω_f are given by:

$$\frac{D\mathbf{u}}{Dt} = -\nabla p + \frac{1}{\mathrm{Re}}\nabla^2\mathbf{u}, \quad \nabla\mathbf{u} = 0, \text{ in } \Omega_f. \tag{1}$$

The equations of motion of the i^{th} rigid particle with a density $\rho_{p,i}$, occupying the domain $\Omega_{p,i}$, $i = 1, \ldots, N$, are given by

$$\mathbf{U}_i = \frac{d\mathbf{X}_i}{dt}, \tag{2}$$

$$\eta_i \frac{d\mathbf{U}_i}{dt} = (\eta_i - 1)\frac{1}{\mathrm{Fr}}\mathbf{e}_g + \frac{1}{V_i}\mathbf{F}_i, \tag{3}$$

$$\eta_i \mathbf{I}_i \frac{d\omega_i}{dt} = \mathbf{T}_i. \tag{4}$$

Here, $\mathbf{X}_i$ is the center of mass of the i^{th} particle, $\mathbf{U}_i$ is its velocity, $\eta_i = \rho_{p,i}/\rho_f$ is its relative density, V_i is its volume, $\mathbf{I}_i$ is its inertia tensor, $\mathbf{F}_i = \int\limits_{\partial\Omega_{p,i}} \boldsymbol{\sigma}\cdot\mathbf{n}\, dS$ is the hydrodynamic force acting on the particle, $\mathbf{n}$ is the unit normal pointing out of the particle, $\boldsymbol{\sigma} = -p\boldsymbol{\delta} + 1/\mathrm{Re}(\nabla\mathbf{u} + (\nabla\mathbf{u})^T)$ is the stress tensor of the fluid, and $\mathbf{T}_i = \int\limits_{\partial\Omega_{p,i}} (\mathbf{x} - \mathbf{X}_i) \times (\boldsymbol{\sigma}\cdot\mathbf{n})\, dS$ is the hydrodynamic torque acting on the particle. For spherical particles, $\mathbf{I}_i = \mathrm{diag}(2/5 V_i r_i^2)$, where r_i is the radius of the i^{th} particle.

2000 Mathematics Subject Classification. 65N12, 65N15 , 35Q30.

Key words and phrases. Direction Splitting, Particulate Flows, Direct Numerical Simulation, Navier-Stokes Equations

The discretization of this mixed system of ODEs and PDEs proceeds by first discretizing the particle equations by a second order explicit scheme:

$$\mathbf{F}_i^n = \int\limits_{\partial\Omega_{p,i}^n} \boldsymbol{\sigma}^n \cdot \mathbf{n}\, dA, \tag{5}$$

$$\mathbf{T}_i^n = \int\limits_{\partial\Omega_{p,i}^n} (\mathbf{x} - \mathbf{X}_i^n) \times (\boldsymbol{\sigma}^n \cdot \mathbf{n})\, dA, \tag{6}$$

$$\eta_i V_i \left(\frac{\mathbf{U}_i^{n+1} - \mathbf{U}_i^n}{\Delta t} \right) = (\eta_i - 1)\frac{V_i}{\mathrm{Fr}}\mathbf{e}_g + \frac{3}{2}\mathbf{F}_i^n - \frac{1}{2}\mathbf{F}_i^{n-1}, \tag{7}$$

$$\eta_i \mathbf{I}_i \left(\frac{\boldsymbol{\omega}_i^{n+1} - \boldsymbol{\omega}_i^n}{\Delta t} \right) = \frac{3}{2}\mathbf{T}_i^n - \frac{1}{2}\mathbf{T}_i^{n-1} \tag{8}$$

$$\frac{\mathbf{X}_i^{n+1} - \mathbf{X}_i^n}{\Delta t} = \frac{1}{2}(\mathbf{U}_i^{n+1} + \mathbf{U}_i^n), \tag{9}$$

where the stress tensor at time level n in (5) and (6) is approximated by

$$\boldsymbol{\sigma}^n = -\frac{1}{2}\left(p^{n-\frac{1}{2}} + p^{*,n+\frac{1}{2}} \right) \boldsymbol{\delta} + \frac{1}{\mathrm{Re}}(\nabla \mathbf{u}^n + (\nabla \mathbf{u}^n)^T). \tag{10}$$

Equation (7) may also include an additional force to prevent overlapping of particles or to model their collisions (see for example [2]). Various approaches for treatment of collisions can be used and easily incorporated in the present scheme. The so-computed velocity of the particles is then used as boundary conditions for the Navier-Stokes equations on the particle boundaries. However, imposing these boundary conditions in the traditional manner would require to grid the fluid domain and apply classical discretizations like finite elements or finite volumes. Such an ALE procedure would therefore require to re-grid the fluid domain very often that is absolutely unfeasible if the flow involves more than several particles. The goal of this study is to perform simulations involving millions or even billions of particles and therefore we used an approach based on the modified Douglas scheme that is essentially a direction splitting scheme. If Ω is an extension of the fluid domain Ω_f that includes all domains occupied by particles then the scheme proceeds as follows:

1 Pressure predictor

The pressure is predicted in the entire extended domain Ω by:

$$p^{*,n+\frac{1}{2}} = p^{n-\frac{1}{2}} + \phi^{n-\frac{1}{2}}. \tag{11}$$

2 Velocity update

The velocity is computed in the velocity domain Ω_f^{n+1} via:

$$\begin{aligned}
&\frac{\boldsymbol{\xi}^{n+1}-\mathbf{u}^n}{\Delta t}+\frac{3}{2}(\mathbf{u}^n\cdot\nabla)\mathbf{u}^n-\frac{1}{2}(\mathbf{u}^{n-1}\cdot\nabla)\mathbf{u}^{n-1}=\\
&-\nabla p^{*,n+\frac{1}{2}}+\frac{1}{\mathrm{Re}}\left(\partial_{xx}\boldsymbol{\eta}^n+\partial_{yy}\boldsymbol{\zeta}^n+\partial_{zz}\mathbf{u}^n\right),\\
&\frac{\boldsymbol{\eta}^{n+1}-\boldsymbol{\xi}^{n+1}}{\Delta t}=\frac{1}{2\mathrm{Re}}\partial_{xx}\left(\boldsymbol{\eta}^{n+1}-\boldsymbol{\eta}^n\right),\\
&\frac{\boldsymbol{\zeta}^{n+1}-\boldsymbol{\eta}^{n+1}}{\Delta t}=\frac{1}{2\mathrm{Re}}\partial_{yy}\left(\boldsymbol{\zeta}^{n+1}-\boldsymbol{\zeta}^n\right),\\
&\frac{\mathbf{u}^{n+1}-\boldsymbol{\zeta}^{n+1}}{\Delta t}=\frac{1}{2\mathrm{Re}}\partial_{zz}\left(\mathbf{u}^{n+1}-\mathbf{u}^n\right).
\end{aligned}\tag{12}$$

The rigid body velocity $\mathbf{u}^{n+1}=\mathbf{U}^{n+1}+\omega^{n+1}\times(\mathbf{x}-\mathbf{X}^{n+1})$ (computed from (7) and (8)) is prescribed at all points of the grid that lie inside $\Omega_{p,i}^{n+1}$ and on $\partial\Omega_{p,i}^{n+1}$. While discretizing (12) in space, the grid is fitted to the boundary of the fluid domain $\partial\Omega_f^{n+1}$. As mentioned above, if this fitting needs to be performed in multi dimensions and many particles, the problem is not treatable by contemporary mesh generators. However, since (12) requires only the solution of one dimensional problems in each direction, it would be necessary to adult the grid only on each individual grid line in a given direction. In fact, the current procedure does not require to adjust positions of grid nodes on a given line but only to adjust the finite difference stencil around points of intersection of this line with particle boundaries. More details on this procedure can be founds in [1] and [5].

3 Pressure correction

The pressure time-increment ϕ is approximated by solving

$$(I-\partial_{xx})(I-\partial_{yy})(I-\partial_{zz})\phi^{n+\frac{1}{2}}=-\frac{\eta_{\min}}{\Delta t}\nabla\mathbf{u}^{n+1}\tag{13}$$

over the entire domain $\Omega=[0,X]\times[0,Y]\times[0,Z]$. The scaling factor $\eta_{\min}=\min\left\{1,\min\limits_{1\le i\le N}\{\eta_i\}\right\}$ is included following an idea proposed in [3] for modification of the classical projection schemes for flows with discontinuous density. This scheme avoids the need to solve a pressure Poisson equation with a discontinuous coefficient resulting from the density discontinuity. Indeed, particulate flows can be interpreted as flows of a variable density fluid over a simply-shaped domain. The stability and optimality of such formulations is analyzed in [4]. Equation (13) is supplemented by homogeneous Neumann boundary conditions on $\partial\Omega$, and can be solved as the

following series of one-dimensional problems:

$$\begin{aligned} &\theta - \partial_{xx}\theta = -\tfrac{\eta_{\min}}{\Delta t}\nabla \mathbf{u}^{n+1}, && \partial_x\theta|_{x=0,X} = 0, \\ &\psi - \partial_{yy}\psi = \theta, && \partial_y\psi|_{y=0,Y} = 0, \\ &\phi^{n+\frac{1}{2}} - \partial_{zz}\phi^{n+\frac{1}{2}} = \psi, && \partial_z\phi^{n+\frac{1}{2}}|_{z=0,Z} = 0 \end{aligned} \tag{14}$$

4 Pressure update

The pressure is corrected in the entire extended domain Ω by:

$$p^{n+\frac{1}{2}} = p^{n-\frac{1}{2}} + \phi^{n+\frac{1}{2}} - \frac{\chi}{2\mathrm{Re}}\nabla(\mathbf{u}^{n+1} + \mathbf{u}^n) \text{ in } \Omega. \tag{15}$$

where $0 \leq \chi \leq 1$ is a parameter of the scheme.
Finally, the presentation will demonstrate the accuracy and stability of the method on various benchmark problems involving rigid particles (see [5]). In addition, some results of direct simulations of fluidized beds involving thousands and millions of particles will be presented. Further details of these simulations can be found in [6].

References

[1] Ph. Angot, J. Keating, and P. Minev. A direction splitting algorithm for incompressible flow in complex geometries. *Comput. Methods Appl. Mech. Engrg*, 117:111–120, 2012.

[2] R. Glowinski, T. Pan, T. Hesla, D. Joseph, and J. Periaux. A fictitious domain approach to the direct numerical simulation of incompressible viscous flow past moving rigid bodies: Application to particulate flow. *J. Comput. Phys.*, 169:363, 2001.

[3] J.-L. Guermond and Abner Salgado. A splitting method for incompressible flows with variable density based on a pressure Poisson equation. *Journal of Computational Physics*, 228(8):2834 – 2846, 2009.

[4] J.-L. Guermond and Abner Salgado. Error analysis of a fractional time-stepping technique for incompressible flows with variable density. *SIAM J. Numer. Anal.*, 49(3):917 – 944, 2011.

[5] J. Keating and P. Minev. A fast algorithm for direct simulation of particulate flows using conforming grids. *J. Comp. Phys.*, 255:486–501, 2013.

[6] John William Keating. *Direction-splitting schemes for particulate flows.* PhD thesis, University of Alberta, Edmonton, 2013. http://hdl.handle.net/10402/era.33972.

Robust preconditioning of Darcy problem for highly heterogeneous media

J. Kraus, R. Lazarov, M. Lymbery, S. Margenov, L. Zikatanov

1 Darcy problem

Consider the following second order elliptic boundary value problem written in mixed form for the unknown scalar functions $p(x)$ and the vector function $\mathbf{u}$:

$$\mathbf{u} + K(x)\nabla p = 0 \qquad \text{in } \Omega, \tag{1a}$$

$$\operatorname{div} \mathbf{u} = f \qquad \text{in } \Omega, \tag{1b}$$

$$p = 0 \qquad \text{on } \Gamma_D\ , \tag{1c}$$

$$\mathbf{u}\cdot\mathbf{n} = 0 \qquad \text{on } \Gamma_N. \tag{1d}$$

Here $K(x)$ is uniformly bounded positive function in Ω, $f \in L^2(\Omega)$, and $\Omega \subset \mathbb{R}^d$ ($d = 2, 3$) is a bounded polyhedral domain with its boundary $\partial\Omega$ split into two non-overlapping parts Γ_D and Γ_N. For the pure Neumann problem assume that f satisfies the compatibility condition $\int_\Omega f dx = 0$. In this case the solution is determined uniquely by taking $\int_\Omega p\, dx = 0$. To simplify the presentation, assume that Γ_D is a non-empty set with strictly positive measure, so the above problem has a unique solution. This equation is a model used for example in heat and mass transfer, flows in porous media, diffusion of passive chemicals, electromagnetics, and other applied areas. The methods presented in this note are targeting applications of equations (1a)–(1d) to flows in highly heterogeneous porous media. The goal is to design a preconditioner for the mixed finite element approximation of the above problem that will lead to efficient iterative methods which converge independently of the contrast in $K(x)$. The construction is based on the method developed in [4, 5].
A fundamental role in the analysis plays the weighted inner product

$$\Lambda_\alpha(\mathbf{u},\mathbf{v}) = (\alpha\ \mathbf{u},\mathbf{v}) + (\operatorname{div}\mathbf{u}, \operatorname{div}\mathbf{v}), \quad \alpha(x) = K^{-1}(x), \tag{2}$$

in the space

$$\boldsymbol{H}(\operatorname{div}) := \boldsymbol{H}(\operatorname{div};\Omega) = \{\mathbf{v} \in L^2(\Omega)^d : \ \operatorname{div}\mathbf{v} \in L^2(\Omega)\}. \tag{3}$$

Multigrid methods for $\boldsymbol{H}(\operatorname{div})$-systems have been designed earlier, see, e.g., the work by Arnold, Falk, and Winther [2] who considered the weighted bilinear form $\Lambda_d(\mathbf{u},\mathbf{v}) = \alpha(\mathbf{u},\mathbf{v}) + \beta(\operatorname{div}\mathbf{u}, \operatorname{div}\mathbf{v})$ with constants $\alpha > 0$ and $\beta > 0$. A key moment in their study was robustness with respect to α and β. The important difference between our form Λ_α and Λ_d, however, is that in Λ_α the parameter α is a highly heterogeneous function with very large ratio between the smallest and the largest values.

1991 Mathematics Subject Classification. 65F10, 65N20, 65N30.
Key words and phrases. weighted $\boldsymbol{H}(div)$-norm, mixed finite elements, least-squares, high contrast media, robust preconditioners

This makes the design of a robust multigrid method and also the proof of a proper *inf-sup* condition much more difficult. To present the dual mixed weak form define the function spaces

$$\begin{aligned} \boldsymbol{V} &\equiv \boldsymbol{H}_N(\mathrm{div};\Omega) = \{\mathbf{v} \in L^2(\Omega)^d : \ \mathrm{div}\,\mathbf{v} \in L^2(\Omega), \ \text{ and } \ \mathbf{v} = 0 \ \text{ on } \ \Gamma_N\} \\ W &\equiv \{q \in L^2(\Omega) \ \text{ and } \ \int_\Omega q \, dx = 0 \quad \text{if} \quad \Gamma_N = \partial\Omega\}. \end{aligned}$$

Then the weak form of the problem (1a)–(1d) is: Find $\mathbf{u} \in \boldsymbol{V}$ and $p \in W$ such that

$$\mathcal{A}^{DM}(\mathbf{u}, p; \mathbf{v}, q) = -(f, q) + (f, \mathrm{div}\,\mathbf{v}) \quad \forall (\mathbf{v}, q) \in \boldsymbol{V} \times W, \tag{4}$$

where the bilinear form $\mathcal{A}^{DM}(\mathbf{u}, p; \mathbf{v}, q) : (\boldsymbol{V}, W) \times (\boldsymbol{V}, W) \to \mathbf{R}$ is defined as

$$\mathcal{A}^{DM}(\mathbf{u}, p; \mathbf{v}, q) := (\alpha \mathbf{u}, \mathbf{v}) + (\mathrm{div}\,\mathbf{u}, \mathrm{div}\,\mathbf{v}) - (p, \mathrm{div}\,\mathbf{v}) - (\mathrm{div}\,\mathbf{u}, q). \tag{5}$$

Obviously the form $\mathcal{A}^{DM}(\mathbf{u}, p; \mathbf{v}, q)$ is symmetric but indefinite. Note that this is a slightly modified mixed method, which yields the same solution but offers some advantages in designing efficient solution methods, see e.g. [2, 8]. Consider a stable mixed method, e.g., Raviart-Thomas method, to approximate the solution of (4): Find $(\mathbf{u}_h, p_h) \in \boldsymbol{V}_h \times W_h$ such that

$$(\alpha\, \mathbf{u}_h, \mathbf{v}_h) + (\nabla \cdot \mathbf{v}_h, p_h) = 0 \quad \forall \mathbf{v}_h \in \boldsymbol{V}_h, \tag{6a}$$

$$(\nabla \cdot \mathbf{u}_h, q_h) = (f, q_h) \quad \forall q_h \in W_h. \tag{6b}$$

The saddle point problem (6) is equivalent to the following indefinite system of linear algebraic equations

$$\begin{bmatrix} M_h & B_h \\ B_h^T & 0 \end{bmatrix} \begin{bmatrix} \mathbf{u} \\ \mathbf{p} \end{bmatrix} = \begin{bmatrix} \mathbf{0} \\ \mathbf{f} \end{bmatrix}. \tag{7}$$

In short one can write (7) in the form

$$\mathcal{A}_h \mathbf{m} x_h = \mathbf{m} f_h \tag{8}$$

where $\mathcal{A}_h : X_h \to X_h^\star$ is a self-adjoint and indefinite operator and $X_h = \boldsymbol{V}_h \times W_h$. As it has been shown in [3] the operator norms

$$\|\mathcal{A}_h\|_{\mathcal{L}(X_h, X_h^\star)} \ \text{ and } \ \|\mathcal{A}_h^{-1}\|_{\mathcal{L}(X_h^\star, X_h)} \ \text{ are uniformly bounded} \tag{9}$$

for stable mixed finite element disretizations of problem (6).

2 Two-level preconditioner

Following [1], the goal is to construct a positive definite self-adjoint operator $\mathcal{B}_h : X_h \to X_h^\star$ such that all eigenvalues of $\mathcal{B}_h^{-1}\mathcal{A}_h$ are bounded uniformly independent of h and independent of the variations of the coefficient α, i.e., independent of the contrast. From (9) it follows that

$$\|\mathcal{B}_h\|_{\mathcal{L}(X_h, X_h^\star)} \ \text{ and } \ \|\mathcal{B}_h^{-1}\|_{\mathcal{L}(X_h^\star, X_h)} \ \text{ being uniformly bounded in } \ h \ \text{ and } \ \alpha \tag{10}$$

is a sufficient condition for $\mathcal{B}_h$ to be a uniform and robust preconditioner for the minimum residual (MinRes) iteration.
Let the block diagonal preconditioner $\mathcal{B}_h$ be defined as

$$\mathcal{B}_h := \begin{bmatrix} A_h & 0 \\ 0 & I_h \end{bmatrix} \tag{11}$$

where I_h is the identity on W_h, and $A_h : \boldsymbol{V}_h \to \boldsymbol{V}_h^*$ is given by $(A_h \mathbf{u}_h, \mathbf{v}_h) = \Lambda_\alpha(\mathbf{u}_h, \mathbf{v}_h)$, see (2).
Then condition (10) reduces to $\|A_h\|_{\mathcal{L}(\boldsymbol{V}_h, \boldsymbol{V}_h^\star)}$ and $\|A_h^{-1}\|_{\mathcal{L}(\boldsymbol{V}_h^\star, \boldsymbol{V}_h)}$ being uniformly bounded in h and α, see [1].
Hence the crucial step is to construct a robust and uniformly convergent iterative method for solving systems with $A = A_h$. The method of fictitious space preconditioning, first proposed in [7], and later refined in [9], provides the framework. Let B denote the auxiliary space two-grid preconditioner, which is implicitly defined by

$$B^{-1} := \overline{M}^{-1} + (I - M^{-T}A)C^{-1}(I - AM^{-1}) \tag{12}$$

where C is a fictitious (auxiliary) space preconditioner approximating A. Here the operator M denotes an A-convergent smoother, and $\overline{M} = M(M + M^T - A)^{-1}M^T$ the symmetrized smoother. Further, let $V = \mathbb{R}^N$ and $\widetilde{V} = \mathbb{R}^{\widetilde{N}}$ where $\widetilde{N} > N$. Then a surjective mapping $\Pi : \widetilde{V} \to V$ can be defined such that the preconditioner (12) can be written in the form

$$B^{-1} = \overline{M}^{-1} + \tau^{-1}\Pi\widetilde{A}^{-1}\Pi^T \tag{13}$$

where $\widetilde{A}$ is a certain domain decomposition auxiliary matrix and the value of the scaling parameter τ can be chosen such that the two-grid method with iteration matrix $I - B^{-1}A$ is convergent.
The proposed auxiliary space two-grid method differs from the classical two-grid methods in replacing coarse-grid correction by a subspace correction with iteration matrix $I - C^{-1}A$.
The following theorem provides a bound for the relative condition number $\kappa(B^{-1}A)$.

Theorem 1. *([5]) Let B be defined according to (13) and assume that M satisfies the smoothing property*

$$\underline{c}\langle \mathbf{v}, \mathbf{v}\rangle \le \rho_A \langle \overline{M}^{-1}\mathbf{v}, \mathbf{v}\rangle \le \bar{c}\langle \mathbf{v}, \mathbf{v}\rangle \quad \textit{and} \quad \|AM^{-T}\mathbf{v}\|^2 \le \frac{\eta}{\rho_A}\|\mathbf{v}\|_A^2$$

where $\rho_A = \lambda_{\max}(A)$ denotes the spectral radius of A and the constant η is non-negative. Further, let $\Pi : \widetilde{V} \to V$ be energy-stable, i.e., $\|\Pi\tilde{\mathbf{v}}\|_A^2 \le c_\Pi \|\tilde{\mathbf{v}}\|_{\widetilde{A}}^2$ for all $\tilde{\mathbf{v}} \in \widetilde{V}$. Then the extremal eigenvalues of $B^{-1}A$ satisfy $\lambda_{\max}(B^{-1}A) \le \bar{c} + \frac{c_\Pi}{\tau}$ and $\lambda_{\min}(B^{-1}A) \ge \frac{1}{\tau + \eta/\underline{c}}$, and thus $\kappa(B^{-1}A) \le (\bar{c} + c_\Pi/\tau)(\tau + \eta/\underline{c})$.

3 Auxiliary space multigrid method

Let $k = 0, 1, \ldots, \ell-1$ be the index of mesh refinement where $k = 0$ corresponds to the finest mesh, i.e., $A^{(0)} := A_h = A$ denotes the fine-grid matrix. Consider the sequence of domain decomposition auxiliary matrices $\widetilde{A}^{(k)}$, in two-by-two block factorized form

$$(\widetilde{A}^{(k)})^{-1} = (\widetilde{L}^{(k)})^T \widetilde{D}^{(k)} \widetilde{L}^{(k)}, \tag{14}$$

where

$$\widetilde{L}^{(k)} = \begin{bmatrix} I & \\ -\widetilde{A}_{21}^{(k)} (\widetilde{A}_{11}^{(k)})^{-1} & I \end{bmatrix}, \quad \widetilde{D}^{(k)} = \begin{bmatrix} (\widetilde{A}_{11}^{(k)})^{-1} & \\ & Q^{(k)^{-1}} \end{bmatrix}. \tag{15}$$

The construction is such that the Schur complement $Q^{(k)} = \widetilde{A}_{22}^{(k)} - \widetilde{A}_{21}^{(k)} (\widetilde{A}_{11}^{(k)})^{-1} \widetilde{A}_{12}^{(k)}$ of $\widetilde{A}^{(k)}$ is sparse and defines an (additive) approximation of the dense Schur complement $S^{(k)} = A_{22}^{(k)} - A_{21}^{(k)} A_{11}^{(k)^{-1}} A_{12}^{(k)}$. Then $Q^{(k)}$ serves as the next coarser-level matrix, i.e.,

$$A^{(k+1)} := Q^{(k)}, \tag{16}$$

and the two-level block factorization can be applied recursively. The algebraic multilevel iteration (AMLI)-cycle auxiliary space multigrid (ASMG) preconditioner $B^{(k)}$ of $A^{(k)}$ is defined on all levels $k < \ell$ via the following relation

$$B^{(k)^{-1}} := \overline{M}^{(k)^{-1}} + (I - M^{(k)^{-T}} A^{(k)}) \Pi^{(k)} (\widetilde{L}^{(k)})^T \overline{D}^{(k)} \widetilde{L}^{(k)} \Pi^{(k)^T} (I - A^{(k)} M^{(k)^{-1}}) \tag{17}$$

where

$$\overline{D}^{(k)} := \begin{bmatrix} (\widetilde{A}_{11}^{(k)})^{-1} & \\ & B_\nu^{(k+1)^{-1}} \end{bmatrix} \tag{18}$$

and $B_\nu^{(k+1)}$ is the coarse-level preconditioner of $A^{(k+1)}$, i.e., $B_\nu^{(k+1)^{-1}} \approx A^{(k+1)^{-1}}$, and

$$B_\nu^{(\ell)} := A^{(\ell)}. \tag{19}$$

In the linear AMLI-cycle method $B_\nu^{(k+1)^{-1}}$ is a polynomial approximation of $A^{(k+1)^{-1}}$ whereas the nonlinear AMLI-cycle ASMG method uses a nonlinear mapping $B_\nu^{(k+1)^{-1}} = B_\nu^{(k+1)^{-1}}[\cdot]$ whose action on a vector $\mathbf{d}$ is realized by ν iterations of a preconditioned Krylov subspace method. For further details on the construction and analysis of ASMG preconditioners for weighted $\boldsymbol{H}(\mathrm{div})$-norm see [6].

Acknowledgments

This work was partially supported by the Bulgarian NSF Grant DCVP 02/1, FP7 Grant AComIn, and the Austrian NSF Grant P22989. R. Lazarov was supported in parts by US NSF Grant DMS-1016525, by Award No. KUS-C1-016-04, made by KAUST. L. Zikatanov was supported in part by US NSF Grants DMS-1217142 and DMS-101652.

References

[1] D. Arnold, R. Falk, and R. Winther, *Preconditioning in H(div) and applications*, Mathematics of Computation, **66** (1997), 957–984.

[2] D. Arnold, R. Falk, and R. Winther, *Multigrid in H(div) and H(curl)*, Numerische Mathematik, **85**:2 (2000), 197–217.

[3] F. Brezzi and M. Fortin, *Mixed and Hybrid Finite Element Methods*, Springer, New York, 1991.

[4] J. Kraus, *Additive Schur complement approximation and application to multilevel preconditioning*, SIAM Journal on Scientific Computing, **34**:6, (2012), A2872–A2895.

[5] J. Kraus, M. Lymbery, and S. Margenov, *Auxiliary space multigrid method based on additive Schur complememt approximation*, Numerical Linear Algebra with Applications, (submitted Oct. 2013).

[6] J. Kraus, R. Lazarov, M. Lymbery, S. Margenov, and L. Zikatanov, *Preconditioning of weighted $\boldsymbol{H}(div)$-norm and applications to numerical simulation of highly heterogeneous media*, (in preparation).

[7] S. Nepomnyaschikh, *Mesh theorems on traces, normalizations of function traces and their inversion*, Soviet J. Numer. Anal. Math. Modelling, **6**:3 (1991), 223–242.

[8] P. Vassilevski and R. Lazarov, *Preconditioning mixed finite element saddle-point elliptic problems*, Numerical Linear Algebra with Applications, **3**:1 (1996), 1–20.

[9] J. Xu, *The auxiliary space method and optimal multigrid preconditioning techniques for unstructured grids*, Computing, **56** (1996), 215–235.

A Computational Approach for the Seismic Damage Response of Adjacent Tall RC Structures Environmentally Degradated and Strengthened by Ties

Angelos Liolios, George Hatzigeorgiou, Konstantinos Liolios, Stefan Radev, Krassimir Georgiev, Ivan Georgiev

Dedicated to Professor Svetozar Margenov's 60th anniversary.

In Civil Engineering, pounding is one of the non-usual extremal actions (seismic, environmental etc.), which can cause significant strength degradation and damages on existing structures [1]. Pounding concerns the seismic interaction between adjacent structures, e.g. neighboring buildings in city centers constructed in contact. On the common contact interface, during an earthquake excitation, appear at each time-moment either compressive stresses or relative removal displacements (separating gaps) only. These requirements result to inequality conditions in the mathematical problem formulation. To overcome strength degradation effects, various repairing and strengthening procedures can be used for the seismic upgrading of existing buildings [1]. Among them, cable-like members (ties) can be used as a first strengthening and repairing procedure. These cable-members can undertake tension, but buckle and become slack and structurally ineffective when subjected to a sufficient compressive force. So, in the mathematical problem formulation, the constitutive relations for cable-members are also inequality conditions. Due to above considerations, the full problem of the earthquake response of pounding adjacent structures strengthened by cable-elements bracings has as governing conditions both, equalities as well as inequalities. Thus the problem becomes a high nonlinear one. For the strict mathematical treatment of the problem, the concept of variational and/or hemivariational inequalities can be used and has been successfully applied [2]. As concerns the numerical treatment, non-convex optimization algorithms are generally required [3]. The present study deals with two numerical approaches for the earthquake analysis of existing adjacent reinforced concrete (RC) building frames, which can come in unilateral contact and have to be strengthened by cable elements. The unilateral behaviours of both, the cable-elements and the interfaces contact-constraints, are taken strictly into account and result to inequality constitutive conditions. The finite element method is used for space discretization in combination with a time discretization scheme. First, the structural system of the two adjacent RC frames (A) and (B) is discretized in space by using finite elements. The usual frame elements are used for the reinforced concrete frames. As concerns the interfaces of unilateral contact, where pounding is expected to take place, unilateral constrained elements are used. On the other hand, for the cable strengthening system, pin-jointed bar elements are used. The behaviour of both, the cable elements and unilateral contact elements, includes loosening, elastoplastic or/and elastoplastic-softening-fracturing and unloading - reloading effects. All

these characteristics concerning both constitutive laws, on the one hand of the cable elements and on the other hand of the unilateral contact elements, can be expressed mathematically by non-convex relations of the the general form:

$$s_i(d_i) \in \hat{\partial} S_i(d_i) \tag{1}$$

Here s_i and d_i are generalized stress and deformation quantities, respectively, $\hat{\partial}$ is the generalized gradient and S_i is the superpotential function, see Panagiotopoulos [2]. In specializing details, for the cables, s_i is the tensile force (in [kN]) and d_i the deformation (elongation) (in [m]), of the i-th cable element. Similarly, concerning the unilateral contact simulation, s_i is the compressive force p_i (in [kN]) and $d_i$the deformation (shortening) (in [m]), of the i-th unilateral constraint element. By definition -see [2] - the relation (1) is equivalent to the following hemivariational inequality, expressing the Virtual Work Principle:

$$S_i^{\uparrow}\left(d_i, e_i - d_i\right) s_i\left(d_i\right) \cdot \left(e_i - d_i\right) \tag{2}$$

where $S_i^{\uparrow}$ denotes the subderivative of S_i and e_i, d_i are kinematically admissible (virtual) deformations.
Next, incremental dynamic equilibrium for the two frames (A) and (B) of the structural system, considered as uncoupled and unstrengthened, i.e. without pounding and without cables, is expressed by the usual matrix relations of Structural Dynamics:

$$\begin{aligned} \mathbf{M_A}\ddot{\mathbf{u}}_\mathbf{A} + \mathbf{C_A}(\dot{\mathbf{u}}_\mathbf{A}) + \mathbf{K_A}(\mathbf{u_A}) &= \mathbf{f_A} \\ \mathbf{M_B}\ddot{\mathbf{u}}_\mathbf{B} + \mathbf{C_B}(\dot{\mathbf{u}}_\mathbf{B}) + \mathbf{K_B}(\mathbf{u_B}) &= \mathbf{f_B} \end{aligned} \tag{3}$$

Here $\mathbf{u}$ and $\mathbf{f}$ are the displacement and the loading forces time dependent vectors, respectively. The damping and stiffness terms, $\mathbf{C}(\dot{\mathbf{u}})$ and $\mathbf{K}(\mathbf{u})$, respectively, concern the general non-linear case. Dots over symbols denote derivatives with respect to time. For the case of ground seismic excitation $\mathbf{x_g}$, the loading history term $\mathbf{f}$ becomes

$$\mathbf{f} = -\mathbf{M}\mathbf{r}\ddot{\mathbf{x}}_\mathbf{g} \tag{4}$$

where $\mathbf{r}$ is the vector of stereostatic displacements. When both, cable-elements and pounding are taken into account, equations (3) for the assembled system of the two frames (A) and (B), considered as coupled and strengthened, become

$$\begin{aligned} \mathbf{M_A}\ddot{\mathbf{u}}_\mathbf{A} + \mathbf{C_A}(\dot{\mathbf{u}}_\mathbf{A}) + \mathbf{K_A}(\mathbf{u_A}) &= \mathbf{f_A} + \mathbf{T_A}\mathbf{s_A} + \mathbf{B}\mathbf{p} \\ \mathbf{M_B}\ddot{\mathbf{u}}_\mathbf{B} + \mathbf{C_B}(\dot{\mathbf{u}}_\mathbf{B}) + \mathbf{K_B}(\mathbf{u_B}) &= \mathbf{f_B} + \mathbf{T_B}\mathbf{s_B} + \mathbf{B}\mathbf{p} \\ \mathbf{p} &= \mathbf{p_N} + \mathbf{P_T}. \end{aligned} \tag{5}$$

Here $\mathbf{s_A}$ and $\mathbf{s_B}$ are the cable elements stress vectors for frames (A) and (B), respectively; $\mathbf{p}$ is the contact elements stress vector and $\mathbf{T_A}$, $\mathbf{T_B}$, $\mathbf{B}$ are transformation matrices. The pounding stress vector $\mathbf{p}$ is decomposed to the vectors $\mathbf{p_N}$, of the normal, and $\mathbf{p_T}$ of the tangential interaction forces between frames (A) and (B). The

system of the above relations (1)-(5), combined with the initial conditions, provide the problem formulation, where, for given $\mathbf{f}$ and/or $\ddot{\mathbf{x}}_\mathbf{g}$, the vectors $\mathbf{u_A}$, $\mathbf{u_B}$, $\mathbf{p}$ and $\mathbf{s_A}$, $\mathbf{sB}$ have to be computed.
The relevant computational approach is described in [3, 4]. A piecewise linearization of the above constitutive relations as in elastoplasticity (see Figure 1) is used. By applying a time-integration scheme, in each time-step Δt a relevant non-convex linear complementarity problem of the following matrix form is eventually solved :

$$\mathbf{v} \geq \mathbf{0}, \quad \mathbf{Av} + \mathbf{a} \leq \mathbf{0}, \quad \mathbf{v^T} \cdot (\mathbf{Av} + \mathbf{a}) = \mathbf{0}. \tag{6}$$

Here $\mathbf{v}$ is the vector of unknown unilateral quantities at the time âĂŞmoment t, $\mathbf{v^T}$ is the transpose of $\mathbf{v}$, $\mathbf{a}$ is a known vector dependent on excitation and results from previous time moments $(t - \Delta t)$, and $\mathbf{A}$ is a transformation matrix. An alternative approach for treating numerically the problem is the incremental one. Now, relations (5), taking into account also second-order geometric effects (P-Delta effects), are written in incremental form:

$$\begin{array}{c} \mathbf{M_A \Delta \ddot{u}_A + C_A \Delta \dot{u}_A + (K_A + G_A) \Delta U_A = -M_A \Delta \ddot{u}_g + T_A \Delta s_A + B \Delta p} \\ \mathbf{M_B \Delta \ddot{u}_B + C_B \Delta \dot{u}_B + (K_B + G_B) \Delta U_B = -M_B \Delta \ddot{u}_g + T_B \Delta s_B + B \Delta p} \end{array}. \tag{7}$$

Here $\mathbf{G_A}$ and $\mathbf{G_B}$ are the geometric stiffness matrices, by which P-Delta effects are taken into account. On such incremental approaches is based the structural analysis software Ruaumoko [5]. Ruaumoko software uses the finite element method and permits an extensive parametric study on the inelastic response of structures. Concerning the time-discretization, implicit or explicit approaches can be used. Here the Newmark implicit scheme is chosen and Ruaumoko is used to provide results which are related to the following critical parameters: local or global structural damage, maximum displacements, interstorey drift ratios, development of plastic hinges. The decision about a possible strengthening for an existing structural system of interacting structures, damaged by a seismic event, can be taken after a relevant evaluation of suitable damage indices. After Park/Ang [7], the global damage is obtained as a weighted average of the local damage at the section ends of each structural element or at each cable element. First the local damage index DIL is computed by the following relation:

$$DI_L = \frac{\mu_m}{\mu_u} + \frac{\beta}{F_y d_u} E_T \tag{8}$$

where: μ_m is the maximum ductility attained during the load history, μ_u the ultimate ductility capacity of the section or element, β a strength degrading parameter, F_y the yield force of the section or element, E_T the dissipated hysteretic energy, and d_u the ultimate deformation. Next, the dissipated energy $\mathbf{E_T}$ is chosen as the weighting function and the global damage index $\mathbf{DI_G}$ is computed by using the following relation:

$$DI_G = \frac{\sum_{i=1}^{n} DI_{Li} E_i}{\sum_{i=1}^{n} E_i} \tag{9}$$

where: DI_{Li} is the local damage index after Park/Ang at location i, E_i is the energy dissipated at location i and n is the number of locations at which the local damage

is computed. The applicability of the proposed methods is verified in numerical examples, where a system of two tall reinforced concrete frames (A) and (B) under pounding is considered for cable-strengthening. The constitutive law of cable-elements is shown in Figure 1. Other details, concerning the seismic response of cable-braced RC systems subjected to multiple earthquakes, are described in [6].

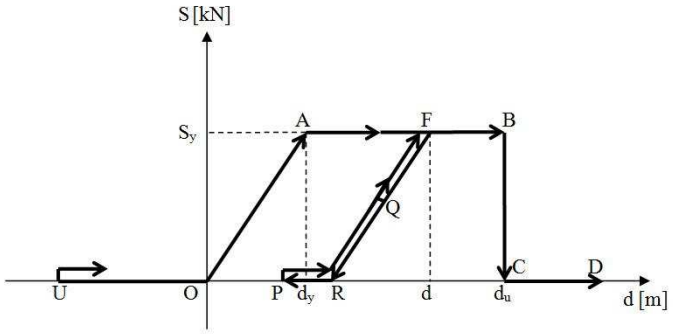

Figure 1: The constitutive law of cable-elements.

References

[1] Bertero V. V., Whittaker A. S., Seismic upgrading of existing buildings, *5as Jornadas Chilenas de SismologÃηa e IngenierÃηa AntisÃηsmica*, 1 (1989), 27-46.

[2] Panagiotopoulos P.D., Hemivariational Inequalities. Applications in Mechanics and Engineering, Springer-Verlag, Berlin, New York, (1993).

[3] Liolios A., A linear complementarity approach for the non-convex seismic frictional interaction between adjacent structures under instabilizing effects, Journal of Global Optimization, 17 (2000), 259-266.

[4] Liolios Ang., Chalioris K., Liolios Ast., Radev St., and Liolios Kon., A Computational Approach for the Earthquake Response of Cable-braced Reinforced Concrete Structures under Environmental Actions, LNCS, 7116 (2012), 590-597.

[5] Carr A.J., RUAUMOKO - Inelastic Dynamic Analysis Program, Department of Civil Engineering, University of Canterbury, Christchurch, New Zealand, 2008.

[6] Liolios Ang., Liolios Ast., Hatzigeorgiou G., A Numerical Approach for Estimating the Effects of Multiple Earthquakes to Seismic Response of Structures Strengthened by Cable-Elements, Journal of Theoretical and Applied Mechanics, 43(3) (2013), 21-32.

[7] Park Y.J., A.H.S. Ang, Mechanistic seismic damage model for reinforced concrete, Journal of Structural Division ASCE, 111(4), (1985), 722-739.

Robust Balanced Semi-Coarsening Multilevel Preconditioning for Bicubic FEM Discretizations

Maria Lymbery

Let

$$A_h \mathfrak{u}_h = F_h \tag{1}$$

be the linear system of algebraic equations derived from the application of finite element method for the discretization of the elliptic boundary value problem

$$-\nabla \cdot (a(x)\nabla u(x)) = f(x) \quad in\ \Omega, \tag{2a}$$

$$u = 0 \quad on\ \Gamma_D, \tag{2b}$$

$$(a(x)\nabla u(x)) \cdot \mathbf{n} = 0 \quad on\ \Gamma_N. \tag{2c}$$

where conforming bicubic elements have been utilized.
The notations used in (1) and (2) are as follows:

- A_h is the global stiffness matrix;
- F_h is the given right hand side;
- h is the mesh parameter of the underlying partition $\mathcal{T}_h$ of Ω;
- $\Omega \subset R^2$ is a polygonal complex domain with a boundary $\Gamma = \Gamma_D \cup \Gamma_N$;
- $f(x)$ is a given function in $L_2(\Omega)$;
- $a(x) = (a_{ii}(x))$, $i = 1, 2$ is a diagonal positive definite coefficient matrix that is uniformly bounded in Ω;
- $\mathbf{n}$ is the outward unit vector normal to Γ.

An initial mesh $\mathcal{T}_0$ has been set in Ω in such a way that the coefficients $a_{ii}, i = 1, 2$ are constants over each element of $\mathcal{T}_0$. A recursive balanced semi-coarsening refinement procedure has been applied to it resulting in the sequence of nested meshes $\mathcal{T}_0 \subset \mathcal{T}_1 \subset ... \subset \mathcal{T}_\ell = \mathcal{T}_h$ where ℓ is an even number. The solution of (1) is sought over the finest mesh $\mathcal{T}_\ell = \mathcal{T}_h$ which best approximates (2a)-(2c).
The Algebraic Multilevel Iteration (AMLI) preconditioner $B = B^{(\ell)}$ has the following recursive definition, e.g [2, 3, 7],

$$B^{(0)} = A^{(0)},$$

$$B^{(k)} = {J^{(k)}}^{-T} \begin{bmatrix} A_{11}^{(k)} & 0 \\ \tilde{A}_{21}^{(k)} & P^{(k-1)} \end{bmatrix} \begin{bmatrix} I & {A_{11}^{(k)}}^{-1} \tilde{A}_{12}^{(k)} \\ 0 & I \end{bmatrix} {J^{(k)}}^{-1},\ k = 1, \ldots, \ell \tag{3}$$

where

$$P^{(k-1)^{-1}} = [I - p_{\beta_{k-1}}(B^{(k-1)^{-1}}, A^{(k-1)})] A^{(k-1)^{-1}}.$$

Here β_{k-1} denotes the degree of the stabilization Chebyshev polynomial $p_{\beta_{k-1}}$. When it is cyclicly varied the resulting AMLI algorithm is called *hybrid V-cycle*, cf. [6].

Theorem 1. *The AMLI method is of optimal order under the following conditions, see [3, 6]:*

- *the properly scaled approximation* $C_{11}^{(k+1)}$ *satisfies the estimate*

$$\kappa(C_{11}^{(k+1)^{-1}} A_{11}^{(k+1)}) = O(1);$$

- *solving systems with* $C_{11}^{(k+1)}$ *requires* $O(N_{k+1} - N_k)$ *arithmetic operations;*
-

$$\beta_k = 1 \quad \textit{if } (k \bmod k_0) \neq 0, \qquad \frac{1}{\sqrt{1-\gamma^{(k_0)^2}}} < \beta_k < \rho_{k_0} \quad \textit{if } (k \bmod k_0) = 0.$$

Here ρ_{k_0} *is the mesh refinement ratio of* k_0 *consecutive mesh refinement steps,* N_k *is the number of degrees of freedom belonging to* $\mathcal{T}_k$ *and* $\gamma^{(k_0)}$ *is the constant in the strengthened Cauchy-Bunyakowski-Schwarz(CBS) inequality that is related to the nested finite element spaces* $V_{(j+1)k_0}$ *and* V_{jk_0}.

Lemma 1. *Consider the balanced semi-coarsening AMLI algorithm with parameter* $\rho = 2$. *The CBS constant* $\gamma^{(2)}$ *corresponding to bicubic conforming finite elements is uniformly bounded with respect to the anisotropy ratio and it holds that*

$$(\gamma^{(2)})^2 \quad \leq \quad \frac{203 + 5\sqrt{46}}{288} \quad \approx \quad 0.823, \qquad\qquad \varrho = 2. \tag{4}$$

Solving (1) with an AMLI algorithm results in a sequence of smaller subproblems with the pivot block matrices $A_{11}^{(k+1)}$. In the general setting of anisotropic problems $\kappa(A_{11}^{(k+1)})$ is not uniformly bounded with respect to the related number of degrees of freedom and special robust preconditioning techniques have to be developed for the pivot blocks systems, e.g. [4].
When using balanced semi-coarsening mesh refinement, however, the degrees of freedom can be ordered in such way that the blocks $A_{11}^{(k+1)}$ to be block diagonal with uniformly bounded semi-bandwidth, [5]. Therefore, any direct solver for banded matrices has computational complexity of optimal order, i.e.

$$\mathcal{N}(A_{11}^{(k+1)^{-1}} \mathrm{v}) = O(N^{(k+1)} - N^{(k)}).$$

.
The last result combined with the uniform estimates (4) and the optimality conditions from Theorem 1 leads to the main result.

Theorem 2. *The balanced semi-coarsening AMLI preconditioner* (3) *with even* k *and* $\rho = 3$, $3 \leq \beta \leq 8$ *has an optimal order of computational complexity and the estimate is uniform with respect to mesh and coefficient anisotropy.*

References

[1] Axelsson, O., Vassilevski, P.: Algebraic multilevel preconditioning methods I, Numer. Math. 56 (1989), 157-177.

[2] Kraus, J.: Additive Schur complement approximation and application to multilevel preconditioning, SIAM J. Sci. Comput., 34 (2012), A2872-A2895.

[3] Kraus, J., Margenov, S.: Robust Algebraic Multilevel Methods and Algorithms. De Gruyter, Germany (2009).

[4] Kraus, J., Margenov, S., Synka, J.: On the Multilevel Preconditioning of Crouzeix-Raviart Elliptic Problems, *Num. Lin. Alg. Appl.*, 15 (2008), 395-416.

[5] Margenov, S: Semicoarsening AMLI Algorithms for Elasticity Problems, Num. Lin. Alg. Appl., 5 (1998), 347-362.

[6] Vassilevski, P.: Hybrid V-cycle algebraic multilevel preconditioners, Math. Comp. 58 (1992), 489-512.

[7] Vassilevski, P.: Multilevel Block Factorization Preconditioners: Matrix-based Analysis and Algorithms for Solving Finite Element Equations,Springer, New York (2008).

Large amplitude vibrations of heated Timoshenko beams with delamination

Emil Manoach and Jerzy Warminski

Abstract

In this work, the large amplitude vibration of a heated Timoshenko composite beam having delamination is studied. The model of delamination takes into account contact interaction between sublaminates including normal forces, shear forces and additional damping due to the sublaminate interaction. Numerical calculations are performed in order to estimate the influence of the delamination, the geometrically nonlinear terms and elevated temperature on the response of the beam.

1 Introduction

Delamination is a major problem in multilayer composite structures. Due to this reason the development of adequate models describing the phenomena arising in the delaminated part of the structure is a very important topic in real engineering applications. Models which describe the dynamic behaviour of the delaminated structures could be very useful in the development of the vibration based methods for delamination detection. In most of the models for the dynamic behavior of the beam with delamination the shear forces during the sublaminate interaction and the additional damping arising due to sliding between sublaminates are neglected. A model of the dynamic response of a composite Timoshenko beam which takes into account the above mentioned phenomena was recently developed in [1]. Most of the models describing the dynamic behavior of beam with delamination use the Bernoulli-Euler or the Timoshenko beam theories considering the small deflections only. As a rule, the environmental conditions and especially the temperature influence are not taken into account in these models. In the present work the model of a Timoshenko beam with delamination developed in [1] and [2] is extended considering the large deflections of the beams at elevated temperature environment.

2 Theoretical consideration and numerical modelling

The composite laminated beam was conditionally considered to consist of four sections (Fig. 1). Section 1 and section 4 are without defects. The cross section between these two parts contains a delamination. Sections 2 and 3 denote the parts of the beamï£¡s cross section divided by the delamination.
By h_i $(i = 2,\ 3)$ the thicknesses of the delaminated parts of the cross-section are denoted and z_d is the z-coordinate of the delamination. The governing equations for

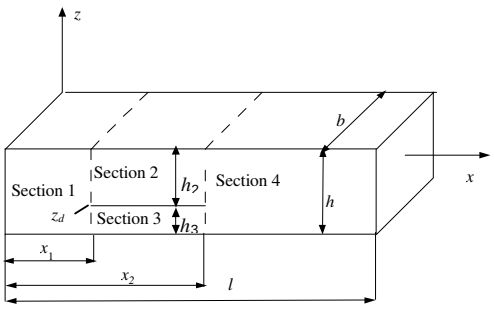

Figure 1: Geometry of the beam. x_1 and x_2 denote the beginning and the end of delaminated area.

the large amplitude thermoelastic vibration of the beam could be written as follow:

$$\begin{aligned} E_i bh_i \frac{\partial^2 u_i}{\partial x^2} &= -E_i bh_i \frac{\partial w_i}{\partial x}\frac{\partial^2 w_i}{\partial x^2} + E_i b\alpha_{iT}\frac{\partial \gamma_T}{\partial x}, \\ \chi_T = \int_{-h/2}^{h/2} T\,(x,z,t)\,z dz, \quad \gamma_T &= \int_{-h/2}^{h/2} T(x,z,t) dz \end{aligned} \tag{1}$$

$$\begin{aligned} \rho_i I_i \frac{\partial^2 \psi_i}{\partial t^2} =& E_i I_i \frac{\partial^2 \psi_i}{\partial x^2} - c_{2i}\frac{\partial \psi_i}{\partial t} - kG_i F_i\left(\frac{\partial w_i}{\partial x} - \psi_i\right) + \alpha_{iT} bE_i \frac{\partial \chi_T}{\partial x} \\ &+ (-1)^i K^S \gamma \left[\frac{\partial}{\partial x}(h_2 w_2 - h_3 w_3) - (h_2\psi_2 - h_3\psi_3)\right] \\ &- (-1)^i \dot{K}^S \gamma \left(h_2\dot{\psi}_2 - h_3\dot{\psi}_3\right) \end{aligned} \tag{2}$$

$$\begin{aligned} \rho_i bh_i \frac{\partial^2 w_i}{\partial t^2} =& kG_i bh_i\left(\frac{\partial^2 w_i}{\partial x^2} - \frac{\partial \psi_i}{\partial x}\right) - c_{1i}\frac{\partial w_i}{\partial t} \\ &+ E_i bh_i\left[\frac{\partial u_i}{\partial x} + \frac{1}{2}\left(\frac{\partial w_i}{\partial x}\right)^2 - \alpha_{iT}\gamma_T\right]\frac{\partial^2 w_i}{\partial x^2} \\ &+ (-1)^i K^N \gamma(w_2 - w_3) + (-1)^i \dot{K}^N \gamma(\dot{w}_2 - \dot{w}_3) - q(x,t) \end{aligned} \tag{3}$$

Here u_i and w_i denote the longitudinal and transverse displacement of i-th beam section, ψ_i is the angle of rotation of the normal of the cross-section to the beam mid-axes, E_i and G_i are the Youngï£¡s and shear modulus, α_{iT} is the coefficient of thermal expansion, I_i is the geometrical inertia moment of the i^{th} cross-section, T is the temperature.
K^N, K^S, $\dot{K}^N$ and $\dot{K}^S$ are constants depending on the material parameters of the sublaminates. They are different from zero only when the sublaminates are in contact. The parameter γ has been introduced to take into account the fact, that for section 1

and 4 the terms containing K^N, K^S, $\dot{K}^N$ and $\dot{K}^S$ disappear i.e. $\gamma = 1$ for $i = 2$ and 3 and $\gamma = 0$ for $i = 1$ and 4. The equations (1) are solved for the case of clamped - clamped boundary conditions and corresponding continuity conditions which equalize the displacements, angular rotations, bending moments and shear forces in sections 1 with these in section 2 and 3 and in section 4 with the ones in sections 2 and 3 (see [1]).

3 Solution of the problem

A numerical approach and algorithm are proposed to solve the above formulated problem. It is based on the assumptions that the longitudinal inertia effect can be neglected, that the beam gets the elevated temperature instantly, and that the temperature is uniformly distributed along the beam length and thickness. In order to consider the longitudinal displacements in delaminated beam the model is considered to consist of two parallel beams - I and II. Beam I consists of section 1,2 and 4 and beam II consists of sections 1, 3 and 4. The Eq. (2) and Eq. (3) are discretized by the finite difference method and the obtained system ordinary differential equations in time is solved by an implicit method using the backward differentiation formulas and an iteration procedure.

4 Numerical results and conclusions

Numerical results of the large amplitude vibration of intact and damaged beams were provided and comparisons with the case of result obtained by the small deflection beam theory (SDBT) were performed. The influence of the elevated temperature on the response of the damaged beam was also studied. Selected results are presented in Fig. 2 and 3. The elevated temperature can lead to complex nonlinear behavior of delaminated beam as buckling and non-periodic motion (see Fig. 3).

Acknowledgments

The first author wishes to acknowledge the support received from the Bulgarian NSF Grant DCVP-02/1. The financial support of Structural Funds in the Operational Programme Innovative Economy (IE OP) financed from the European Regional Development Fund - Project 'Modern material technologies in aerospace industry', Nr POIG.01.01.02-00-015/08-00 is gratefully acknowledged by the second author

References

[1] E. Manoach, J. Warminski, A. Mitura, S. Samborski, Dynamics of a composite Timoshenko beam with delamination, Mechanics Research Communications, 47-53, 46, 2012.

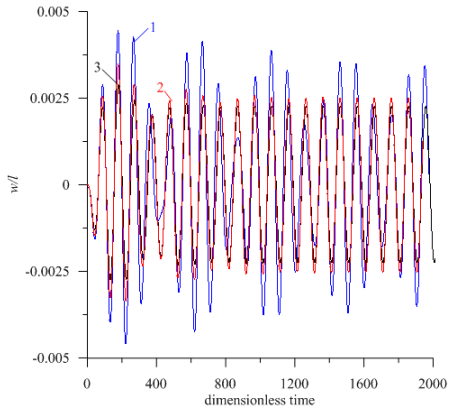

Figure 2: Time history diagram of the response of the beam subjected to a harmonic loading with $p = 2.4kN$ and $\omega_e = 1360rad.s^{-1}$. 1 (blue line) - SDBT with delamination; 2 (Red line) - Large deflections beam theory (LDBT) with delamination; 3 (black line) - LDBT without delamination.

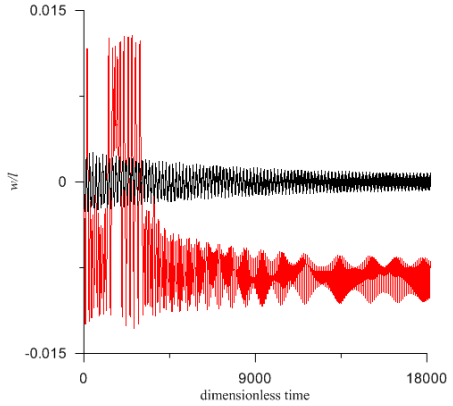

Figure 3: Time history diagrams for beam described by LDBT subjected to harmonic loading at elevated temperature. $1-\Delta T = 30K$; $2-\Delta T = 50K$. $p(x,t) = p_0 sin(\omega_e t)$. $p_0 = 3kN$, $\omega_e = 1360rad.s^{-1}$

[2] E. Manoach, J. Warminski, A. Mitura, S. Samborski, Dynamics of a laminated composite beam with delamination and inclusions, Eur. Phys. J. Special Topics, 1649 - 1664, 222, 2013.

Data-Driven Signal Processing: A Low-Rank Approximations Approach

Ivan Markovsky

State-of-the-art signal processing and control methods are model based and require a model identification step prior to solving the actual data processing problem. Starting with a review of classical system identification, this talk presents a model-free data processing approach, in which model parameters need not be explicitly estimated. The underlying computational tool in the new setting is low-rank approximation of a structured matrix constructed from the data. Preserving the structure in the approximation leads to statistically optimal estimators and fast computational methods.

1 Structured low-rank approximation

Structured low-rank approximation is the problem of approximating a given matrix D by another matrix $\widehat{D}$, which is as close as possible to D, has the same structure as D, and reduced rank. An example where a rank deficient structured matrix arises is when a sequence $p = (p_1, \ldots, p_{n_p})$ satisfies a difference equation with lag $\ell < \lceil n_p/2 \rceil$

$$R_0 p_t + R_1 p_{t+1} + \cdots + R_\ell p_{t+\ell} = 0, \qquad \text{for } t = 1, \ldots, n_p - \ell. \tag{DE}$$

The system (DE) is linear in the vector of parameters $R := \begin{bmatrix} R_0 & R_1 & \cdots & R_\ell \end{bmatrix}$, so that it can be written as $R\mathcal{H}_{\ell+1,n_p-\ell}(p) = 0$, where $\mathcal{H}_{\ell+1,n_p-\ell}(p)$ is a *Hankel matrix* constructed from p. Therefore, for $R \neq 0$, the fact that p satisfies a difference equation (DE) is equivalent to rank deficiency of $\mathcal{H}_{\ell+1,n_p-\ell}(p)$. With noisy data p, the matrix $\mathcal{H}_{\ell+1,n_p-\ell}(p)$ is generically full rank and the model identification problem becomes a Hankel strutured low-rank approximation problem.
Formally the strutured low-rank approximation problem is defined as follows [4, 5]. Given: structure specification $\mathcal{S}$, vector of structure parameters $p \in \mathbb{R}^{n_p}$, and desired rank r, find a structure parameter vector $\widehat{p}$, such that the corresponding matrix $\mathcal{S}(\widehat{p})$ has rank at most r, and is as close as possible to p in the sense of a semi-norm $\|\cdot\|$

$$\begin{aligned} &\text{minimize} \quad \text{over } \widehat{p} \in \mathbb{R}^{n_p} \quad \|p - \widehat{p}\| \\ &\text{subject to} \quad \operatorname{rank}\bigl(\mathcal{S}(\widehat{p})\bigr) \leq r. \end{aligned} \tag{SLRA}$$

2 Solution methods

In general, the structured low-rank approximation problem (SLRA) is NP-hard.
There are three fundamentally different solution approaches: heuristics based on convex relaxations [1] and subspace methods [7], local optimization methods, and global optimization methods [6]. The approach used in the subspace type methods is to relax the structure constraint and solve the resulting unstructured low-rank approximation

problem via the singular value decomposition. The subspace methods are found to be very effective in model reduction, system identification, and signal processing.
The methods based on local optimization split into two main categories: *alternating projections* [3] and *variable projections* [2] type algorithms. Both alternating projections and variable projections exploit the bilinear structure of the low-rank approximation problems. In the statistical literature, the alternating projections algorithm is given the interpretation of *expectation maximization*.

Acknowledgments

The research leading to these results has received funding from the European Research Council under the European Union's Seventh Framework Programme (FP7/2007-2013) / ERC Grant agreement number 258581 "Structured low-rank approximation: Theory, algorithms, and applications".

References

[1] M. Fazel. *Matrix rank minimization with applications*. PhD thesis, Elec. Eng. Dept., Stanford University, 2002.

[2] G. Golub and V. Pereyra. Separable nonlinear least squares: the variable projection method and its applications. *Inverse Problems*, 19:1–26, 2003.

[3] M. Ishteva, K. Usevich, and I. Markovsky. Regularized structured low-rank approximation. Technical report, Vrije Univ. Brussel, 2013.

[4] I. Markovsky. Structured low-rank approximation and its applications. *Automatica*, 44(4):891–909, 2008.

[5] I. Markovsky. *Low Rank Approximation: Algorithms, Implementation, Applications*. Springer, 2012.

[6] K. Usevich and I. Markovsky. Optimization on a Grassmann manifold with application to system identification. *Automatica*, 2014.

[7] P. Van Overschee and B. De Moor. *Subspace identification for linear systems: Theory, implementation, applications*. Kluwer, Boston, 1996.

Fuzzy Logic Nonlinear Control of an Inverted Pendulum on a Chart

Aydın Özbey, Erol Uzal, Aşkın Mutlu, Hüseyin Yıldız

Abstract

Stabilization at the top vertical position of an inverted pendulum on a cart by applying a force to the cart is considered. This is an underactuated mechanical system for which the main nonlinear control scheme, feedback linearization, fails. A single control law producing the force on the cart using cart velocity, and position and velocity of the pendulum is developed and shown to stabilize the pendulum at the top position while bringing the cart to its origin. In order to avoid the singularity problems faced in feedback linearization process, fuzzy logic has used.

1 Introduction

Inverted pendulums are widely studied mechanical systems since their dynamics is simple enough to allow detailed studies, and also complicated enough to serve as test problems for various control strategies. In this study, we propose a single control law (meaning that it does not consist of pieces valid at different pendulum angles) and verify by numerical experiments.

2 Governing Equations and fuzzy logic nonlinear Control Strategy

A schematic of the system is shown in Fig. 1 The masses of the cart and the pendulum are M and m, respectively. The aim is to hold the pendulum angle at zero while driving the cart to its origin x = 0. When the non-dimensional variables chosen as follows

$$x^* = \frac{x}{l} \quad t^* = \sqrt{\frac{g}{l}}t \quad u^* = \frac{u}{mg}$$

The governing equations are

$$(1+k)\ddot{x} + \ddot{\theta}\cos\theta - \dot{\theta}^2\sin\theta = u$$
$$\ddot{x}\cos\theta + \ddot{\theta} - \sin\theta = 0$$

where

$$k = \frac{M}{m}$$

Solving for second derivatives in results in

$$\ddot{\theta} = f_1(\theta, \dot{\theta}) + f_2(\theta)u$$
$$\ddot{x} = f_3(\theta, \dot{\theta}) + f_4(\theta)u$$

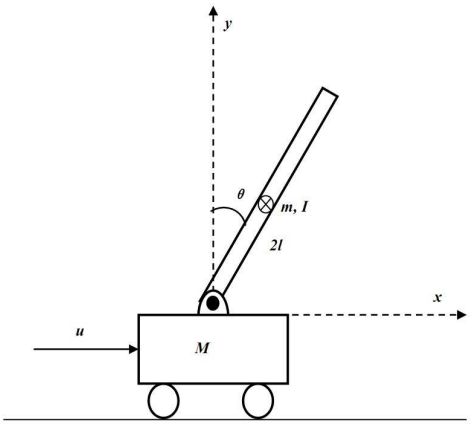

Figure 1: Inverted Pendulum on a Chart

The control law proposed is

$$u = \frac{1}{f_2^*}(-K_1\theta - K_2\dot{\theta} - f_1) + K_3 x + K_4\dot{x}$$

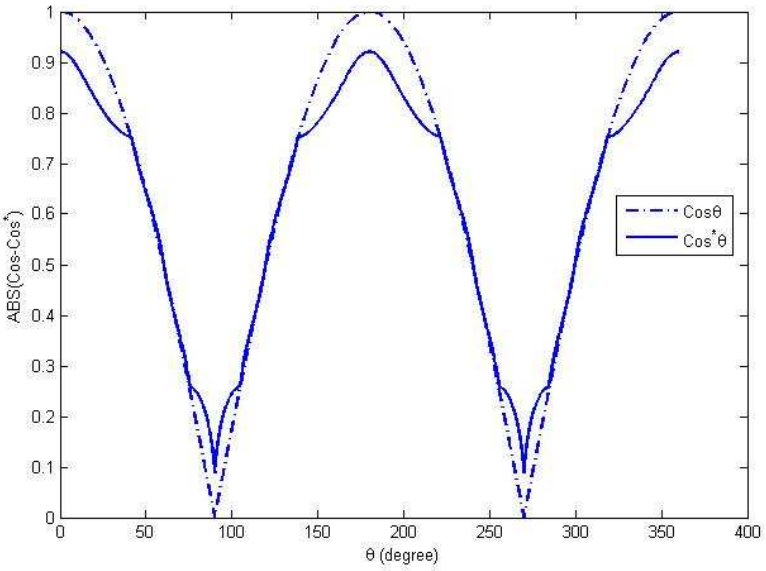

Figure 2: comparison of the real cosine and the values produced by fuzzy logic

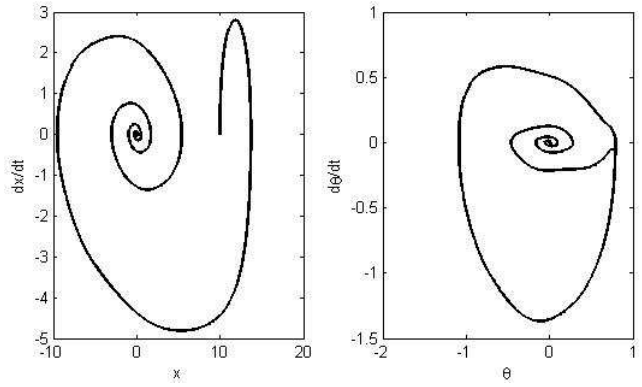

Figure 3: Phase Plane Analyse

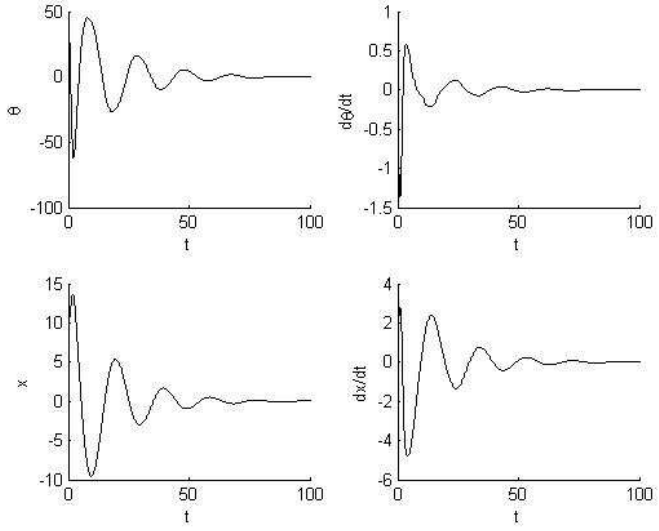

Figure 4: Simulation Results

where

$$f_1(\theta, \dot{\theta}) = \frac{3\dot{\theta}^2 \sin\theta\cos\theta - 3(1+k)\sin\theta}{3\cos^2\theta - 4(1+k)}$$

$$f_2(\theta) = \frac{3\cos\theta}{3\cos^2\theta - 4(1+k)}$$

$$f_3(\theta,\dot{\theta}) = \frac{3\sin\theta\cos\theta - 4\dot{\theta}^2\sin\theta}{3\cos^2\theta - 4(1+k)}$$

$$f_4(\theta) = \frac{-4}{3\cos^2\theta - 4(1+k)}$$

$$f_2^*(\theta) = \frac{3\cos^*\theta}{3(\cos^*\theta)^2 - 4(1+k)}$$

The K coefficients in the control law are calculated by using the actual cosine values. But the $\cos^*\theta$ values used in the control law are calculated by fuzzy logic and then substituted for $\cos\theta$. The cosine values calculated by fuzzy logic have close values to the real cosine values, but never become zero. By doing that, the singularity problem due to the cosine becoming zero is avoided. A comparison of the real cosine and the values produced by fuzzy logic is shown in Fig. 2.

3 Results and Discussion

As seen from the phase plane graphs of the variables Fig. 3, the system is stable. Simulation results show Fig. 4 that the proposed control law can stabilize the system in a reasonable time.

Control of a Robot Arm Using Magnetic Forces

Aydın Özbey, Erol Uzal, Hüseyin Yıldız, Aşkın Mutlu

Abstract

In this study, a single d.o.f. robot arm made of permanent magnet (Figure 1) is intended to follow the known reference angle θ (t). The magnetic properties of the arm are modeled by a magnetic dipole. Mathematical model of the system has been developed and a PID controller is applied to the system that uses feedback linearization. The success of the control law has been examined against disturbance effects by means of simulation programs and the results were interpreted.

1 Introduction

One of the difficulties of controlling micro-electromechanical systems (MEMS) is the dimensional limitations. In the motor driven circular motion systems, the size of the electric motor is important. In this study, an alternative approach for driving the robot arm by using its magnetic properties instead of an electric motor is presented. In place of an electric motor, use of a magnetic field generated by passing an alternating current through the wires placed at specific distances from the robot arm is proposed. In this way, manufacture of a micro scale electric motor can be avoided and also the system is simplified.

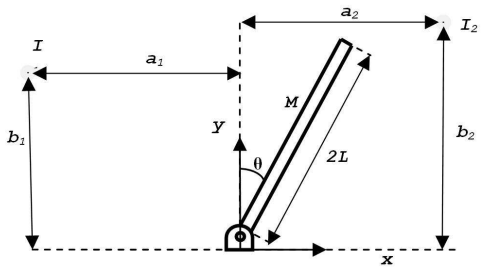

Figure 1: Single DOF robot arm

As seen in Figure 1, the robot arm with length 2L and mass M has a magnetic dipole strength of m, and can be freely rotated around the origin. The wires placed perpendicular to xy plane at the points $(-a_1, b_1)$ and (a_2, b_2) carry electric currents I_1 and I_2. It is proposed that the robot arm moves on the desired trajectory by changing the currents. To simplify the analysis, magnetic properties of the arm is modeled by a magnetic dipole, placed in the middle. Direction of the dipole is in the direction of the arm.

2 Mathematical Model of the System

Moment of inertia of the magnetic rod is

$$I = \frac{1}{2}ML^2$$

Equation of the motion of the system is

$$\ddot{\theta} = \frac{3}{4L}g\sin\theta + \frac{3}{4ML}Q$$

where Q is the resultant of the external forces (weight and the force due to the currents) on the centre of gravity.

3 Defining the Control Law

PID control in which the coefficients are calculated by applying pole placement to the feedback linearized system has been used. Then the control law can be defined as follows

$$Q = \begin{cases} |I_1| < |I_2|\,; & I_1\left(C_1\cos\theta - C_2\sin\theta\right) \\ |I_1| \geq |I_2|\,; & I_2\left(C_3\cos\theta - C_4\sin\theta\right) \end{cases} .$$

After applying feedback linearization to the system, the mathematical model of the system can be written as
when $|I_1| < |I_2|$

$$\ddot{\theta} = k_1 e(t) + k_2\frac{d}{\mathrm{d}t}e(t) + k_3\int_0^t e(\zeta)\mathrm{d}\zeta$$

when $|I_1| \geq |I_2|$

$$\ddot{\theta} = k_4 e(t) + k_5\frac{d}{\mathrm{d}t}e(t) + k_6\int_0^t e(\zeta)\mathrm{d}\zeta$$

4 Robustness of the Controller

In order to see the success of feedback linearization, robustness of the controller to external disturbances is examined. Thus, without making any change in the control law of the idealized system, a constant external torque of 10^{-7} Nm was applied and dipole moment of the magnet is assumed to be given inaccurately by 5%.

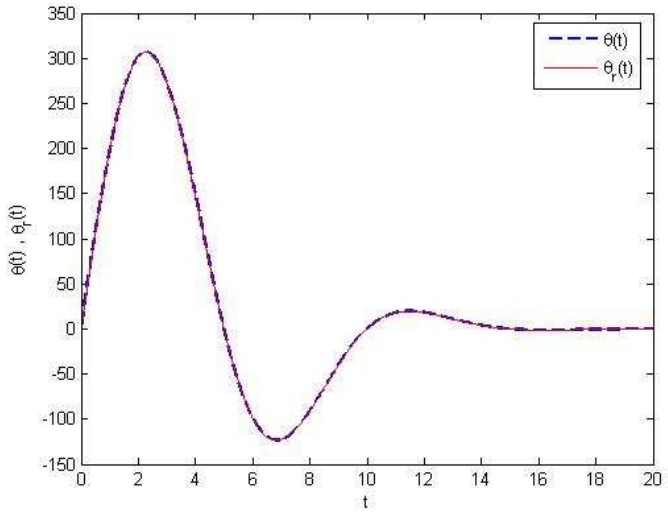

Figure 2: Angular position-time graph

5 Simulations and Results

The simulation results show that, under various disturbing effects (constant external torque and unknown dipole moment), the proposed methodology and the control law is successful.

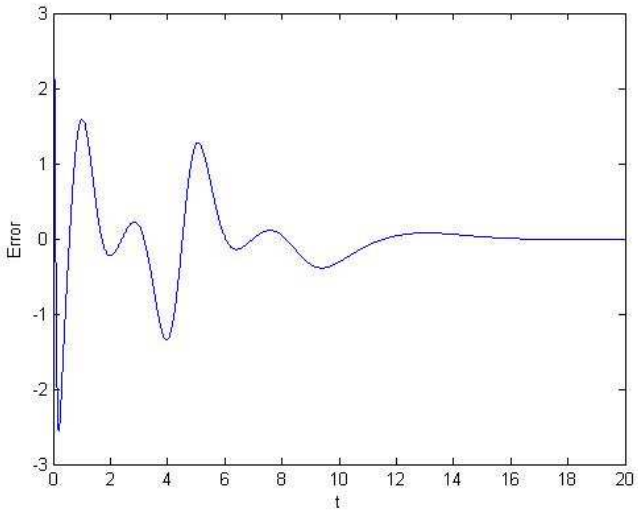

Figure 3: Error-time graph

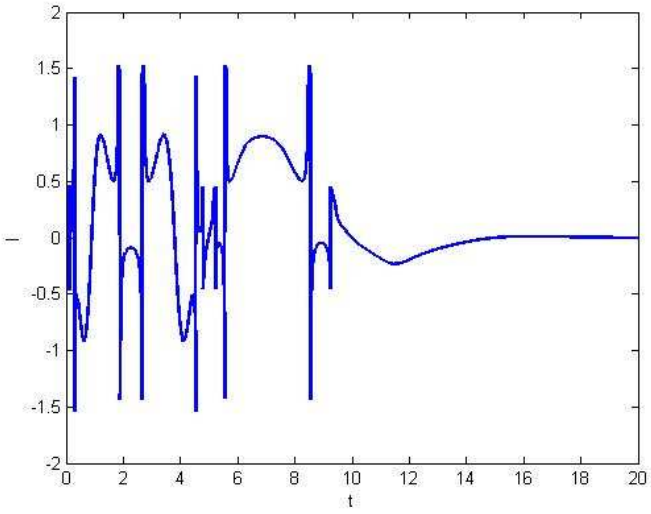

Figure 4: Total Electric Current-time graph

Libraries for treatment of electrostatic interactions for Intel Xeon Phi

Peicho Petkov, Elena Lilkova, Damyan Grancharov, Stoyan Markov, Nevena Ilieva, Leandar Litov

Computer applications for determining and analysing molecular properties are in abundance nowadays but with most of them the scope of current improvements is more and more focused on efficiency. It is a common practice not only to try to improve the algorithms, but to write architecture dependent implementations that take full advantage of the intrinsic characteristics of a particular machine or technologie. With the emerging diversity of new technologies many already existing codes need to be revised or rewritten in order to be suitable for the promising new architectures and machines.

Here, we present implementations of two libraries, optimized for Intel Xeon Phi co-processor native execution based on previously developed codes [1, 2]. One of them implements the AGBNP2 (Analytical Generalized Born plus Nonpolar model 2) implicit solvent model [3] and the other — a grid-based Poisson solver.

Molecular Dynamics (MD) simulations are mostly performed in the presence of water, since it is the most common solvent for most biological reactions and determines the structure and dynamics of proteins. There are two options to take into account the interactions of the investigated biological system with the solvent: by treating the latter either explicitly or implicitly, each approach having its strong sides. In the implicit treatment, the solvent is considered as a continuum with the dielectric and "hydrophobic" properties of water, thus avoiding the disadvantage of having a big number of local "noise" minima that arise from the small vibrations of the solvent molecules [4].

The AGBNP2 is based on a parameter-free conformational-dependent algorithm that is used to calculate hydration free energies and contributions to the forces acting on each atom in the system. It estimates the pairwise descreening scaling coefficients in the evaluation of the Born radii and adds a nonpolar part, consisting of a cavity formation term, proportional to surface area and an attractive dispersion energy term, describing Van der Waals interactions.

The second aforementioned library solves Poisson's equation on a grid, giving the electrostatic potential, created by a set of charges. The solution is obtained iteratively, with a stabilized biconjugated gradient method with a 27-stencil approximation scheme being used [5].

Both libraries are written in the C programming language with OpenMP parallelization utilizing the rather big amount of processing units with shared memory on the Intel Xeon Phi. Special efforts were devoted to vectorization of the codes, since vector instrunctions are hardwarely embedded in the Xeon Phi. In addition, data

was aligned to 64B, according to Intel MIC programming guidelines [6] and the fast memset/memcpy library from Intel was used.

Despite all optimizations efforts on computational site, the implicit solvent library didn't bring in the expected speed-up. As it turned out, it is not calculations themselves but data access that determines to the largest extent the execution time. Thus, in the case of the Poissson-solver library, an improved scalability was gained only after introducing a special variable with the only function of supplying a parallel vectorized loop with better structured data. Still both libraries remain behind the performance of the standard CPU execution.

Acknowledgements

This work was financially supported by the PRACE project funded in part by the EUs 7th Framework Programme (FP7/2007-2013) under grant agreement no. RI-261557.

References

[1] P. Petkov, S. Markov, and I. Todorov, Development of AGBNP2 Implicit Solvent Model Library for MD Simulations, PRACE Whitepaper No 111, http://www.prace-ri.eu/IMG/pdf/wp111.pdf

[2] Markov S., Petkov P., Grancharov D. and Georgiev G., High Performance Poisson Equation Solver for Hybrid CPU/GPU Systems, PRACE Whitepaper No 112, http://www.prace-ri.eu/IMG/pdf/wp112.pdf

[3] E. Gallicchio, K. Paris and R.M. Levy, The AGBNP2 Implicit Solvation Model, J. Chem. Theory Comput. 5(9), 2544âĂŞ2564 (2009).

[4] Al. Onufriev, The generalized Born model: its foundation, applications, and Limitations, Sept. 8, 2010; http://people.cs.vt.edu/ onufriev/PUBLICATIONS/gbreview.pdf

[5] Laurence Tianruo Yangyz, Richard P. Brent, Improved BiCGStab Method for Large and Sparse Unsymmetric Linear Systems on Parallel Distributed Memory Architectures (http://maths-people.anu.edu.au/ brent/pd/rpb206.pdf)

[6] Intel Xeon Phi Coprocessor High-Performance Programming, Jim Jeffers, James Reinders; Morgan Kaufmann (an Elsevier imprint), 2013

Electronic Transport in Generalized Fibonacci Lattices: A Real-Space Renormalization Approach to the Kubo-Greenwood Formula

Vicenta Sanchez, Fernando Sanchez, Chumin Wang

1 Introduction

The electronic transport in macroscopic aperiodic lattices is an interesting but not widely addressed subject, since the transport of quantum particles and large aperiodic systems both per se are not easy topics. Nowadays, the study of electronic states in artificial structures is of great importance in the condensed matter physics, because they introduce many new physical properties essential for industrial applications of atomic-scale devices. These structures can be multilayers, quantum wires, rings, or dots, etc. In particular, quasiperiodic and aperiodic systems become a subject of remarkable interest since the discovery of quasicrystals [1] and the fabrication of high-quality superlattices. Much attention has been devoted to the Fibonacci lattice, because it provides a prototype structure for studying quasiperiodic systems and possesses critically localized electronic states. The corresponding energy spectrum is neither absolutely continuous nor pure point, but singular continuous [2]. Hence, the transport properties of these critically localized states are a fascinating and still unclear theme. There is a generalization of the Fibonacci sequence and in this work we present an analysis of the electronic transport in macroscopic generalized Fibonacci systems by using the Kubo-Greenwood formalism and the real-space renormalization method [3].

2 Formalism

Let us consider the bond problem on a generalized Fibonacci chain (GFC), which can be constructed by using a unique type of atom and alternating two sorts of bonds, A and B, following the substitution rules A$\rightarrow$A^{m}B^n and B$\rightarrow$A, being m and n positive integer numbers. For example, the generation $k = 5$ of GFC with $m = 1$ and $n = 1$ has the sequence of $F_{1,1}(5) = ABAABABA$. The electrical conductivity within the linear response theory can be analyzed by means of the Kubo-Greenwood formula [4]

$$\sigma(\mu,\omega,T) = \frac{2e^2\hbar}{\pi\Omega m^2}\int_{-\infty}^{\infty} dE \frac{f(E)-f(E+\hbar\omega)}{\hbar\omega} Tr[p_x ImG^+(E+\hbar\omega)p_x ImG^+(E)] \quad (1)$$

where Ω is the system volume, $p_x = (im/\hbar)[H,x]$ is the projection of the momentum operator along the applied electrical field with frequency ω, G^+ is the one-particle retarded Green's function, and $f(E) = [\exp(\frac{E-\mu}{k_B T})+1]^{-1}$ is the Fermi-Dirac distribution with the Fermi energy μ and temperature T. In order to isolate the quasicrystalline

effects on the conductivity, we consider a simple s-band tight-binding Hamiltonian given by $H = \sum_j t_{j,j+1} |j\rangle \langle j+1| + t_{j,j-1} |j\rangle \langle j-1|$, where $t_{i,j} = t_A$ or t_B being the hopping integral between nearest-neighbor atoms i and j. For an periodic linear chain with null self-energies and hopping integral t, the dc conductivity at zero temperature is given by [3] $\sigma_P = \frac{e^2 a}{\pi \hbar}(N-1)$, where N is the number of atoms.
On the other hand, the Landauer formalism [5] expresses conductance (g) in terms of scattering properties. The impurities present in conductors leads to scattering of incident electrons resulting in a fraction of transmitted incident electrons. This transmitted fraction is called transmission coefficient $T(E)$ and it is related to g by

$$g(E) = \frac{2e^2}{h} M T(E) \tag{2}$$

where M is the number of transverse channels and $T(E)$ can be obtained as follows.

$$H |\psi\rangle = E |\psi\rangle \Rightarrow t_{i,i+1} c_{i+1} + t_{i,i-1} c_{i-1} = E c_i \tag{3}$$

$$\Rightarrow \begin{pmatrix} c_{i+1} \\ c_i \end{pmatrix} = \begin{pmatrix} \frac{E}{t_{i+1}} & -\frac{t_{i-1}}{t_{i+1}} \\ 1 & 0 \end{pmatrix} \begin{pmatrix} c_i \\ c_{i-1} \end{pmatrix} = T_i \begin{pmatrix} c_i \\ c_{i-1} \end{pmatrix} \tag{4}$$

$$\Rightarrow \begin{pmatrix} c_{N+1} \\ c_N \end{pmatrix} = T_N T_{N-1} \ldots T_1 \begin{pmatrix} c_1 \\ c_0 \end{pmatrix} = \begin{pmatrix} \tau_{11} & \tau_{12} \\ \tau_{21} & \tau_{22} \end{pmatrix} \begin{pmatrix} c_1 \\ c_0 \end{pmatrix} \tag{5}$$

$$\Rightarrow T(E) = \frac{4 - (E/t)^2}{[\tau_{21} - \tau_{12} + (\tau_{22} - \tau_{11})E/(2t)]^2 + (\tau_{22} + \tau_{11})^2 [1 - E^2/(4t^2)]} \tag{6}$$

3 Results

In Figure 1, the dc electrical conductivity at zero temperature $\sigma(\mu, 0, 0)$ obtained from Equation (1) is shown for GFC with $t_A = \tau t_B$ and (a) $m = n = 1$ and $k = 42$, (b) $m = 2$, $n = 1$ and $k = 22$ (c) $m = 1$, $n = 2$ and $k = 28$, and (d) $m = n = 2$ and $k = 20$, where $\tau = (\sqrt{5} - 1)/2$. The imaginary part of the energy is $10^{-13}|t|$. Notice that the GFC with $n = 1$ possess selfsimilar spectra, but the other two with $n = 2$ have a wide high-conductivity band around $E = 0$.
Magnifications of Figures 1 are presented in Figure 2. Observe that at $E = 0$ the conductivity $\sigma = \sigma_P$ for the cases (a), (b) and (d). In order to ensure the existence of transparent states, an analytical analysis is developed within the Landauer formalism. Evaluating Equation (6) at $E = 0$ we have

$$T(E = 0) = \frac{4}{[\tau_{21} - \tau_{12}]^2 + [\tau_{22} + \tau_{11}]^2} \tag{7}$$

For the case of $m = 1$ and $n = 1$, the resulting matrix elements are

$$\tau_{ij} = -rf(i+j)[P(r)\theta(k)\gamma^{[1+\theta(k)]\theta(i)} + f(r)\gamma^{\theta(i)}] - (j-1)\theta(k)(1 - \lceil \frac{r}{2} \rceil)\gamma^{\theta(k)(j-i)}, \tag{8}$$

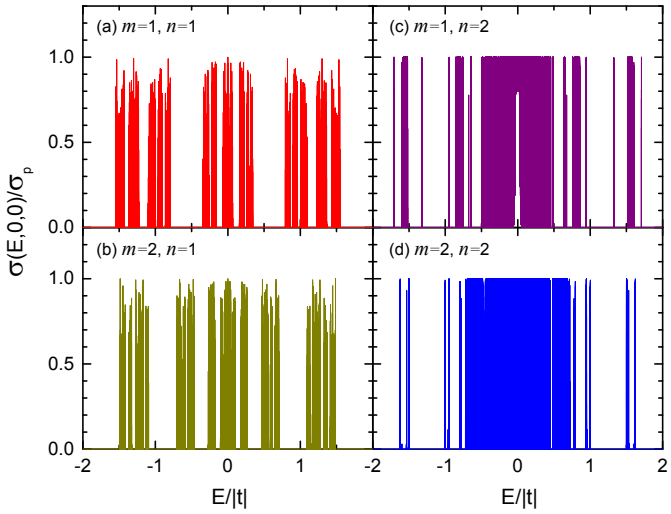

Figure 1: (Color online) DC conductivity spectra $\sigma(\mu, 0, 0)$ of GFC with $t_A = \tau t_B$ and (a) 433494438, (b) 131836324, (c) 178956972 and (d) 268377089 atoms.

where $\gamma = t_A/t_B$, $f(r) = [1 + (-1)^r]/2$, $p(r) = [(-1)^r - 1]/2$, $s = 1 - 2\lfloor q/2 \rfloor$, $q = (k-2) \bmod 4 \in [0, 3]$, $r = (k-2) \bmod 3 \in [0, 2]$ and $\theta(i) = -(-1)^i$. Hence,

$$T(0) = 4[f(r)(\gamma + \gamma^{-1})^2 + (1 - (-1)^r)(\gamma^{1+\theta(k)} + \gamma^{-(1+\theta(k))})^2/2]^{-1} \tag{9}$$

determines the existence of a transparent state for $k = 6, 12, 18, ...$ regardless the value of γ. For the case of $m = 2$ and $n = 1$,

$$\tau_{ij} = \begin{cases} \gamma^{(p(k)(-1)^i)} s, & \text{if } i = j \\ 0, & \text{if } i \neq j \end{cases} \Rightarrow T(0) = \frac{4}{[\gamma^{p(k)} + \gamma^{-p(k)}]^2}, \tag{10}$$

which leads to a transparent state at $E = 0$ for $k = 2, 4, 6, ...$ Finally, for the case of $m = 2$ and $n = 2$,

$$\tau_{ij} = \begin{cases} (-1)^i, & \text{if } i \neq j \\ 0, & \text{if } i = j \end{cases} \Rightarrow T(0) = 1, \tag{11}$$

i.e., there is always a transparent state at $E = 0$.

4 Conclusions

We have presented a detailed study of the dc conductivity spectra of macroscopic GFC with bond disorder by using a previously developed renormalization method for the

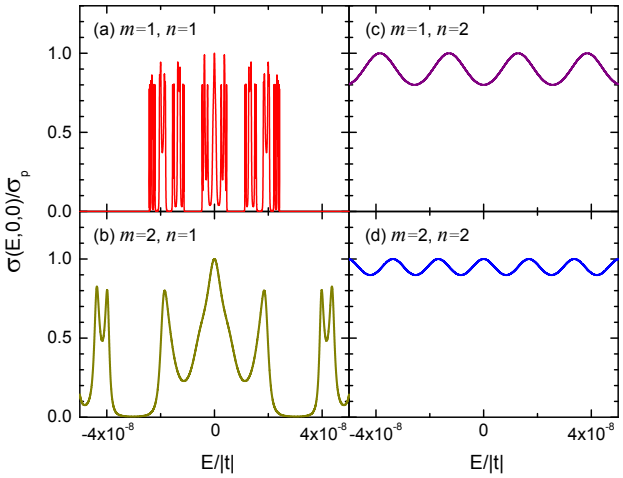

Figure 2: (Color online) Magnifications of Figure 1 around $E = 0$.

Kubo-Greenwood formula. The results show qualitatively different spectra between $n = 1$ and $n = 2$. In particular, magnifications of these spectra suggest the possible existence of transparent states at $E = 0$. Hence, we further investigate analytically such existence by means of the Landauer formalism. The results ensure that we have transparent states at $E = 0$ every 6 generations for the Fibonacci chains, every 2 generations in GFC with $m = 2$ and $n = 1$, always in GFC with $m = 2$ and $n = 2$, and never for GFC with $m = 1$ and $n = 2$. This study of transparent states could be useful for the design of new electronic heterostructural filters.

Acknowledgements

This work has been partially supported by UNAM-IN113813, UNAM-IN113714 and CONACyT-131596. Computations were performed at Miztli of DGTIC, UNAM.

References

[1] D. Shechtman, I. Blech, D. Gratias and J. W. Cahn, *Phys. Rev. Lett.* **53**, 1951 (1984).

[2] A. Suto, *J. Stat. Phys.* **56**, 525 (1989).

[3] V. Sanchez, and C. Wang, *Phys. Rev. B* **70** 144207 (2004).

[4] E.N. Economou, *Green's functions in quantum physics*, 3rd ed. (Springer, Berlin, 2006) pp 184.

[5] Y. Imry and R. Landauer, *Rev. Mod. Phys.* **71**, S306 (1999).

Acceleration of iterative algorithm for calculation of unsteady, viscous, compressible and heat-conductive gas flows on GPU

Kiril S. Shterev

1 Introduction

The Navier-Stokes-Fourier (NSF) continuum model is widely used in many areas of present day science and industry to study different microfluidic phenomena and develop and improve various microfluidic devices. Some applications of these equations are related to aerodynamics of jets, jet engines, micro-nozzles of jet printers, micro-nozzles of nano- and micro-satellites and many others.
In this paper, extrapolation technique is introduced in the SIMPLE-TS finite volume iterative algorithm for calculation of compressible Navier-Stokes-Fourier equations subject of slip and jump boundary conditions. While in the last few decades significant effort has been put in developing effective preconditioning techniques that minimize the condition number of the matrix $\mathbf{A}$ and maximize its sparsity (see [1]), very little work has been published on attempts to obtain a good initial state to initialize the iterative solver. The common practice is to use for the initial guess of iterative solver the solution from previous time step $\boldsymbol{\phi}^n$. An approximate solution for $\boldsymbol{\phi}^{n+1}$ can be obtained using various techniques. Depending on the method and smoothness of $\boldsymbol{\phi}(t)$, $\boldsymbol{\phi}^{ap}$ can be significantly closer to $\boldsymbol{\phi}^{n+1}$ than $\boldsymbol{\phi}^n$, which leading to significantly reduction of the number of iterations.
The case of linear systems with a symmetric positive definite matrix and a series of right hand sides is considered in [2], [3]. Markovinović and Jansen [6] employed Proper Orthogonal Decomposition (POD) to accelerate convergence of iterative solvers, and tested it in simulations of two-phase flow through heterogeneous porous media. They reported 67% reduction in the computing time. Tromeur-Dervout and Vassilevski [9] suggested the method of fully implicit time stepping, the algorithm INB-POD, a choice of initial guess for series of linear systems with different unsymmetric matrices and right hand sides, based on a model reduction. The idea is that solution of a reduced model provides much better initial guess than that from the previous time step. A $\sim$ (2-6)-fold acceleration of a incompressible solver on a test case 2D cavity flow and $\sim$ 1.5-fold actual speedup of a compressible solver on a test case 3D flow past a circular cylinder are reported. Grinberg and Karniadakis [4] presented POD-based extrapolation and initial guess approximation by polynomial extrapolation of values from previous time steps for each node. The test cases are incompressible turbulent flow in a stenosed carotid artery, and incompressible flow in the intracranial arterial tree. The reported acceleration, for both approaches, is (2.6-2.7)-fold. However, the polynomial extrapolation of initial guess is not related to calculated equations and is independent of neighbour nodes. This, in turn, do not requires any additional work

for model reduction and parallel implementation.
In this paper, the polynomial extrapolation of initial guess is applied to GPU implementation of algorithm SIMPLE-TS [5]. The acceleration is investigated on microfluidic problems calculated on GPU.

2 Extrapolation approach

The primary dependent variables (u, v, p and T) are extrapolated at each node in computational domain using values of previous time step of the same node (see Fig. 1).

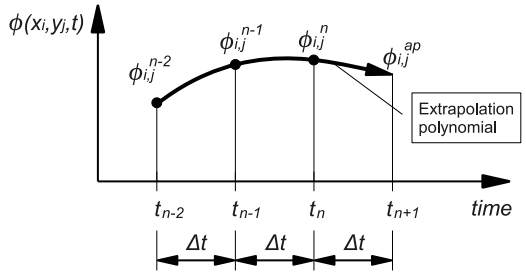

Figure 1: Extrapolation of primary dependent variable.

3 Results and Considerations

The discretization of the compressible Navier-Stokes-Fourier equations is accomplished by using a backward staggered velocity grid, in which all dependent field variables (pressure, temperature and density) are calculated at a cell centre and all flow variables (velocity components) are calculated at the surfaces of a cell. For interpolation between two neighbour points a piecewise-linear profile is used to approximate the derivations of second order [7]. A first order upwind scheme is used for interpolation of convective terms. More details about algorithm SIMPLE-TS can be found in paper [8].
In this paper are presented results consider acceleration of GPU algorithm SIMPLE-TS [5]. The results are obtained on the fine mesh (14100x300) and first order upwind scheme for approximation of convective terms and density in middle points, so that they can be used to validate the algorithm SIMPLE-TS, when the convection terms and density in middle points are approximated by the second order schemes. As a example, we consider a 2D steady-state laminar flow around a small square particle confined in a plane microchannel as shown in Fig. 2. The Knudsen number is $Kn =$

0.0103, the Mach number is $M = 0.4$. The time step is $\Delta t = 0.001$. The initial guess is extrapolated using Lagrange polynomial of first order (linear extrapolation). Acceleration of 2.4-fold is obtained, when a Karman vortex street appears, Fig. 2.

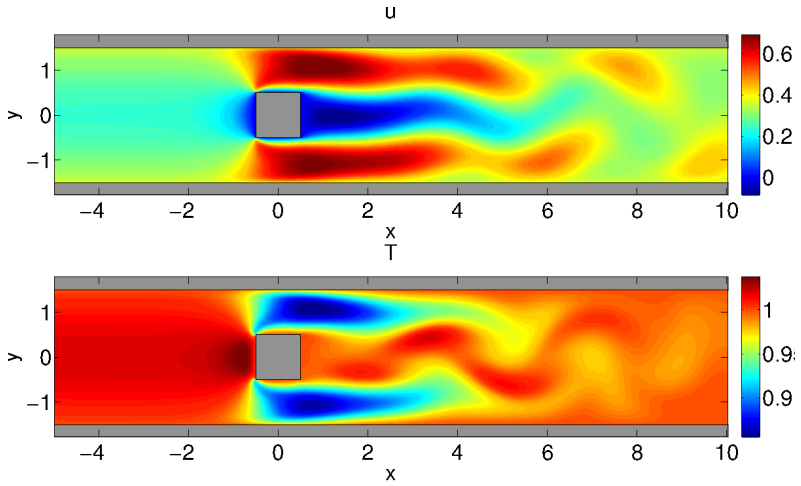

Figure 2: Fields of horizontal component of velocity (upper part) and temperature (lower part), $Kn = 0.0103$, $M = 0.4$ and corresponding $Re \approx 63$, obtained extrapolate initial guess using Lagrange polynomial of order 1.

4 Conclusion

The extrapolation of initial guess using Lagrange polynomials is simple, fast and easy for implementation in serial and parallel codes. GPU implementation of algorithm SIMPLE-TS is accelerated 2.4-fold in the case under consideration flow pas a square in a microchannel.

Acknowledgments

The authors appreciate the financial support by the NSF of Bulgaria under Grant (SuperCA++) - 2009 No DCVP 02/1. The author would like to tank Prof. DSc Stefan Stefanov for valuable remarks and considerations.

References

[1] Michele Benzi. Preconditioning Techniques for Large Linear Systems: A Survey. *Journal of Computational Physics*, 182(2):418–477, 2002.

[2] Tony F. Chan and W. L. Wan. Analysis of projection methods for solving linear systems with multiple right-hand sides. *SIAM Journal on Scientific Computing*, 18(6):1698–1721, November 1997.

[3] Jocelyne Erhel and Frederic Guyomarc'h. An augmented conjugate gradient method for solving consecutive symmetric positive definite linear systems. *SIAM J. Matrix Anal. Appl.*, 21(4):1279–1299, 2000.

[4] L. Grinberg and G. Karniadakis. Extrapolation-Based Acceleration of Iterative Solvers: Application to Simulation of 3D Flows. *Communications in Computational Physics*, 9(3):607–626, 2010.

[5] E. Atanassov K. Shterev and St. Stefanov. GPU calculations of unsteady viscous compressible and heat conductive gas flow at supersonic speed. In *Large-Scale Scientific Computing*, Large-ScaleScientific Computations. Springer-Verlag Berlin Heidelberg, June 03-07 2013.

[6] R. Markovinović and J. D. Jansen. Accelerating iterative solution methods using reduced-order models as solution predictors. *International Journal for Numerical Methods in Engineering*, 68(5):525–541, 2006.

[7] S. V. Patankar. *Numerical heat transfer and fluid flow, (Hemisphere Publishing Corporation*. Hemisphare Publishing Corporation, New York, 1980.

[8] Kiril S. Shterev and Stefan K. Stefanov. Pressure based finite volume method for calculation of compressible viscous gas flows. *Journal of Computational Physics*, 229(2):461–480, January 2010.

[9] Damien Tromeur-Dervout and Yuri Vassilevski. Acceleration of iterative solution of series of systems due to better initial guess. In Damien Tromeur-Dervout, Gunther Brenner, David R. Emerson, and Jocelyne Erhel, editors, *Parallel Computational Fluid Dynamics 2008*, volume 74 of *Lecture Notes in Computational Science and Engineering*, pages 29–40. Springer Berlin Heidelberg, 2011.

The influence of geometrical nonlinearity on the dynamics of elastic structures

Stanislav Stoykov

1 Introduction

The dynamical behavior of nonlinear mechanical systems is becoming increasingly popular among researchers, in the recent decades. The interest of the scientists is due to the fact that linearity is just a first order approximation to reality, but also due to the fact that the nonlinear terms at the equation of motion, can change the behavior of the system significantly. The nonlinearity can introduce into the system multiple solutions, jumps, sub-harmonic, super-harmonic, combination or internal resonances, symmetry-breaking and period multiplying bifurcations, chaotic or quasi periodic motions. These phenomena do not occur in linear systems. The aim of the current paper is to summarize the most popular numerical techniques used in the nonlinear dynamical analysis of elastic structures.

Fundamental properties of linear vibrating systems are the linear modes of vibration and the linear natural frequencies. They determine the dynamical behavior of the linear systems. They also have useful mathematical properties: they can be used to decouple the equations of motion; they can be used for reduction of the degrees of freedom of the system; free and forced vibrations can be expressed as linear combination of the linear normal modes. Nevertheless, linearity is a rude approximation to the reality and nonlinearity occurs frequently in real life engineering problems. Typical nonlinearities of mechanical systems include: material type of nonlinearity, which occurs when the stresses are nonlinear functions of strains; geometrical nonlinearity, which is associated with large displacements of solids and results into nonlinear strain-displacement relations; nonlinearity due to inertia forces, Coriolis or centripetal accelerations can introduce in the system nonlinearity; nonlinearity due to body forces, mainly due to magnetic and electric forces; nonlinearity due to friction, it occurs because the friction force is a nonlinear function of the displacement and the velocity like Coulomb friction or hysteretic damping.

Since nonlinear models are essential for better and more accurate modeling of the mechanical systems, there is need of tools for analyzing the resulting systems of nonlinear differential equations. For continuous systems, the equation of motion is nonlinear partial differential equation. After application of space discretization method, such as finite element method, a nonlinear system of second order ordinary differential equations is obtained. Probably the most common and comprehensive technique for analyzing systems of nonlinear ordinary differential equations is based on the concept of nonlinear normal modes (NNM) and nonlinear frequency response functions (NFRF). There are two main definitions of NNM in the literature. Rosenberg [1] defined a nonlinear normal mode of conservative system as a vibration in unison, i.e. the system performs synchronous oscillation in which all material points vibrate with

the same period and achieve simultaneously their extreme values and static equilibrium positions. Shaw and Pierre [2] defined a nonlinear normal mode as a motion which takes place on a two-dimensional invariant manifold in the phase space. Kerschen et al. [3], extended the RosenbergâĂŹs definition for NNM, to a non-necessarily synchronous but periodic motion. This definition is appropriate in the presence of internal resonances and it is used in the current work. The NFRFs are closely related to NNMs. Forced oscillations occur in the neighborhood of the free oscillations, the shape of vibration of the forced response is analogous to that of the neighboring free response, appearance of bifurcation point in free vibration, indicates that similar bifurcation can appear in forced vibration. Finally, the NNMs and the NFRFs have conceptual relation to the linear normal modes and to the linear frequency response functions. Lyapunov showed that, for n degree of freedom (DOF) conservative system, there are at least n different families of periodic solutions. These n families of periodic solutions, which define n NNMs, can be considered as the nonlinear extensions of the n linear normal modes of the linear conservative system. However, in the presence of internal resonance, the nonlinear system can possess more than n NNMs, while the linear systems cannot. The concepts of NNM and NFRF can be considered as the natural continuation of the linear normal modes and the linear frequency response functions.
In the next section, the most common methods, used for computation of the NNM and NFRF, are presented, without attempting to provide a complete list of these methods. In the third section of the paper are given typical examples of NNM and NFRF of elastic structures, considering geometrical type of nonlinearity.

2 Computation of NNM and NFRF

The elastic structures, such as beams, plates, shells or three-dimensional structures, are continuous systems and they are represented by partial differential equations. There are several methods for treating the PDEs, such as variational, weighted-residual or analytical. One of the most common methods is the finite element method (FEM), which was initially based on variational principles. After application of the FEM for space discretization of elastic structure, considering geometrical type of nonlinearity, the equation of motion is obtained in the following form:

$$\mathbf{M}\ddot{\mathbf{q}}(t) + \mathbf{C}\dot{\mathbf{q}}(t) + \mathbf{K}(\mathbf{q}(t))\mathbf{q}(t) = \mathbf{F}(t) \tag{1}$$

with initial conditions $\mathbf{q}(0) = \mathbf{q}_0$ and $\dot{\mathbf{q}}(0) = \dot{\mathbf{q}}_0$, where $\mathbf{M}$ is the mass matrix, $\mathbf{K}(\mathbf{q}(t))$ is the stiffness matrix, which depends on the vector of generalized coordinates $\mathbf{q}(t)$, $\mathbf{C}$ is the damping matrix, which is usually mass and/or stiffness proportional, and $\mathbf{F}(t)$ is the generalized vector of external forces.
The computational techniques of the NNM and the NFRF can be divided into analytical and numerical. The analytical methods are applicable to a limited number of cases and they are appropriate to small systems. The most common ones are the multiple scales method, the invariant manifold approach and the method of normal

forms. The numerical methods, used to compute the NNM and the NFRF, are employed in two steps: (i) computation of the periodic response, and (ii) continuation of the periodic solution.
The initial value problem (1) is converted into a two point boundary value problem by employing the periodicity condition $\mathbf{q}(T) = \mathbf{q}_0$ and $\dot{\mathbf{q}}(T) = \dot{\mathbf{q}}_0$, where T is the period of vibration. Some of the common methods used to solve the boundary value problem are the finite difference method or the shooting method. The shooting method finds iteratively the initial conditions $\mathbf{q}_0$ and $\dot{\mathbf{q}}_0$ which perform a periodic motion. The collocation method and the PoincarÃĭ map method can also be used to construct the periodic solutions. Another popular approach, is to express the solution by finite Fourier series, this method is known as harmonic balance method and it is considered to be semi-analytical. Finally, the brute force approach is also listed here. It integrates the system of ODE for a long time interval. Eventually, the systems converges to an attractor.
Once a periodic solution is obtained, a scheme which computes the continuum of the periodic response is required. Usually, the additional parameter used in the structural vibration problems, is the frequency of vibration. There are three commonly used continuation schemes. The sequential continuation method uses the frequency of vibration for continuation parameter. This method is not able to pass turning points (also known as folds or saddle nodes), but it is simple for implementation. The arc-length continuation and the pseudo arc-length continuation methods are able to pass turning points. The former method uses the arc-length as a continuation parameter and the additional constraint is the length of the arc. The last method imposes as a constraint an orthogonality condition, i.e. the solution is forced to be orthogonal to the predictor step.

3 Numerical examples

An aluminum beam ($E = 70\,GPa$, $\nu = 0.3$, $\rho = 2778\,kg\,m^{-3}$) with dimensions 0.02 m x 0.002 m x 0.58 m, and with clamped-clamped boundary conditions is considered for the numerical example. A harmonic point force, $\mathrm{F}(t) = \mathrm{A}\,\cos(\omega t)$, is applied on the middle of the beam. The equation of motion is derived by the principle of virtual work and it is discretized by the p-FEM. The vector of generalized coordinates is expressed in Fourier series by assuming harmonics up to third order and the harmonic balance method is applied. The resulting nonlinear algebraic system is solved by the arc-length continuation method [4]. The NFRFs, for different amplitudes of the external force, and the NNM, that starts from the fundamental linear frequency, are presented in Figure 1. It can be seen that the beam has hardening nonlinear effect, which is due to the geometrical nonlinear terms. The results show that the force vibrations, occur in the neighborhood of the free oscillations. The example also demonstrates that the amplitude of vibration depends not only on the amplitude of the external force, but also on the frequency of vibration, in contrast to the linear models, where the frequency of vibration does not depend on the amplitude.
Further examples will demonstrate the effect of the geometrical nonlinear terms on

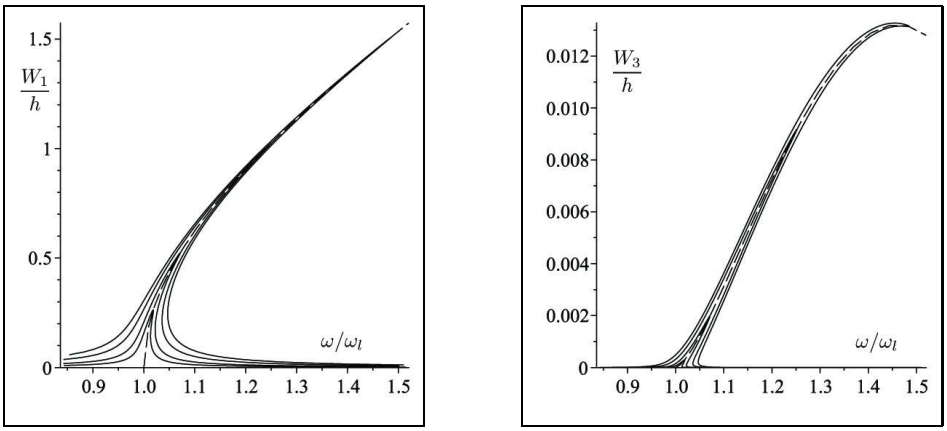

Figure 1: - - - - NNM and —— NFRFs of elastic beam for different force amplitudes. F(t) = A cos(ωt), A = 0.005, 0.01, 0.02 and 0.03 N. W_1 and W_3 - amplitudes of first and third harmonics, h - thickness, ω - excitation frequency, ω_l - first linear frequency.

the stability of the solution. Bifurcation points and the resulting secondary branches with the shapes of vibration will be shown for plate and shell structures.

Acknowledgments

The support of this work through the project AComIn "Advanced Computing for Innovation", grant 316087, funded by the FP7 Capacity Programme and the Bulgarian NSF Grant DCVP 02/1 are gratefully acknowledged.

References

[1] R.M. Rosenberg, On nonlinear vibrations of systems with many degrees of freedom, Adv. Appl. Mech. 9 (1966) 155-242.

[2] S.W. Shaw, C. Pierre, Normal modes for non-linear vibratory systems, J. Sound Vib. 164 (1993) 85-124. 18

[3] G. Kerschen, M. Peeters, J.C. Golinval, A. Vakakis, Nonlinear normal modes, Part I: a useful framework for the structural dynamicist, Mech. Syst. Signal Process. 23 (2009) 170-194.

[4] S. Stoykov, P. Ribeiro, Nonlinear free vibrations of beams in space due to internal resonance, J. Sound Vib. 330 (2011) 4574-4595.

A Multiscale Multigrid Algorithm Applied to Bone Tissue Modeling

Rosangela Sviercoski and Svetozar Margenov

There are two types of osseous tissue that form bones, the cortical and the trabecular bone. The trabecular tissue is an example of deformable medium that has complex hierarchical morphology in the sense that essential features are needed to consider from nanometer to millimeter scales. These features modeled at various scales determine how well the bone tissue meets conflicting mechanical and mass-transport needs. However, the modeling to predict the flow and mechanical behavior in such systems with hierarchical structures and multiple, often poorly separated length-scales, is very computationally demanding, thus making everyday mechanical and flow simulations of bone tissue impractical.

The goal of this study is to propose an efficient numerical tool that reduces significantly the computational resources applicable to this class of problems, which will enable such predictive simulations as an integral part of osteoporosis treatment. To achieve that, highly heterogeneous media are considered that share similarities with trabecular bone tissue's characteristics. The contribution of the fluid phase is interpreted in terms of almost incompressible material. The related linear elasticity problem has coefficients with high contrast and high frequency. The multiple scale system is set up using the displacement decomposition (DD) method, and solved by using a preconditioner given by an upscaled block diagonal form.

The new feature is that a multilevel technique is applied that incorporates an analytical effective tensor of the respective heterogeneous bulk modulus into the upscaled block diagonal, together with the averaging of the spatially variable Poisson ratio at values approaching the incompressibility limit $\nu \to 0.5$. This averaging relates to the approximation of the effective tensor presented in previous work of the author [2]. The efficiency and reliability of the solver will be demonstrated numerically near the incompressibility limit, when compared with other well known upscaled forms, such as the arithmetic and harmonic averages.

Without loss of generality, the problem at the fine-scale is posed in $\Omega \subset R^2$, as a bounded domain, with boundary $\Gamma = \partial\Omega$ and $\mathbf{u} = (u_1, u_2)$, is the displacement in Ω. The pure displacement deformation of a body under the influence of applied forces, $\mathbf{f}$, (and considering only first order terms in the displacement) is described by:

$$\begin{cases} -\nabla \cdot \sigma(x) = \mathbf{f} & x \in \Omega \\ \mathbf{u}(x) = 0 & x \in \partial\Omega \end{cases} \tag{1}$$

where $\sigma(x)$ is the stress tensor, and the notation (x) here and elsewhere, is to identify the variable's spatial variablity, which is the main interest here. The stress tensor has components, $\sigma_{ij}(x)$, given by Hooke's law:

$$\sigma_{ij}(x) = \Sigma_{k,l=1}^{2} c_{ijkl}(x)\varepsilon_{kl}(\mathbf{u}), \quad 1 \leq i, j, \leq 2. \tag{2}$$

The components of the strain-displacement tensor are given by:

$$\varepsilon_{ij}(\mathbf{u}) = \frac{1}{2}\left(\frac{\partial u_i}{\partial x_j} + \frac{\partial u_j}{\partial x_i}\right), \quad 1 \leq i, j, \leq 2, \tag{3}$$

and $c_{ijkl}(x)$ are the spatially dependent properties describing the behavior of the material. These properties are related to Lamé's coefficients $(\lambda(x), \mu(x))$:

$$\lambda(x) = \frac{3K(x)\nu(x)}{(1+\nu(x))} = K(x)\Lambda(x), \quad \mu(x) = \frac{3K(x)(1-2\nu(x))}{2(1+\nu(x))} = K(x)\kappa(x) \tag{4}$$

where it has been used the relationship for the Young's module $E(x) = 3K(x)(1 - 2\nu(x))$, as a function of spatially dependent, bulk modulus $K(x)$, and of the Poisson ratio $\nu(x) \in [0, \frac{1}{2})$. The case when the spatially variable $\nu(x) = \frac{1}{2} - \delta$ ($\delta > 0$ is a small parameter) leads to the notion of *almost incompressible* material. We observe that (1) becomes ill-posed at the incompressibility limit, when $\nu(x) \to \frac{1}{2}$.
For $\mathbf{f} = (f_1, f_2)^T \in (L_2(\Omega))^2$, the weak formulation of (1) reads as finding $\mathbf{u} \in (H_0^1(\Omega))^2 = \{\mathbf{u} \in (H^1(\Omega))^2 | \mathbf{u}_{\partial\Omega} = 0\}$ such that for all $\mathbf{v} \in (H_0^1(\Omega))^2$:

$$A(\mathbf{u}, \mathbf{v}) = \int_\Omega \lambda div(\mathbf{u}) div(\mathbf{v}) + 2\mu\Sigma_{k,l=1}^2 \varepsilon_{ij}(\mathbf{u})\varepsilon_{ij}(\mathbf{v}) = \int_\Omega \mathbf{f}^T\mathbf{v}dx. \tag{5}$$

The bilinear form $A(\mathbf{u}, \mathbf{v})$ can be written as:

$$A(\mathbf{u}, \mathbf{v}) = \int_\Omega < C(x)\mathbf{d}(\mathbf{u}), \mathbf{d}(\mathbf{v}) > dx \tag{6}$$

Where,

$$\mathbf{C}(x) = \mathbf{K}(x) \begin{bmatrix} (\Lambda(x) + 2\kappa(x)) & 0 & 0 & \Lambda(x) \\ 0 & \kappa(x) & \kappa(x) & 0 \\ 0 & \kappa(x) & \kappa(x) & 0 \\ \Lambda(x) & 0 & 0 & (\Lambda(x) + 2\kappa(x)) \end{bmatrix} \tag{7}$$

and $\mathbf{d}(\mathbf{u}) = \left[\frac{\partial u_1}{\partial x_1}, \frac{\partial u_1}{\partial x_2}, \frac{\partial u_2}{\partial x_1}, \frac{\partial u_2}{\partial x_2}\right]$. In the 2-D case, $\mathbf{K}(x)$ is a 4×4 isotropic diagonal tensor. Note also that the formulation of the compliance matrix $\mathbf{C}(x)$ is used in a general setting, unlike the work in [3] where a modified $\mathbf{C}(x)$ was used for the particular case of pure displacement.
In the literature, there are estimates relating the number of V-cycle iterations for resolving the DD system, N_{DD}, with the number of V-cycle iterations for the scalar elliptic equation, N_E. For instance, the inequality $N_{DD} \leq C(1-2\nu)^{-1/2}N_E$ holds true. This result follows from the second Korn's inequality, which concerns the case of isotropic homogeneous media (see, e.g., [1]). However, our results will illustrate that when the coefficients are heterogeneous, the estimate seemed not to be uniform with respect to the coefficient jumps, particularly for contrast higher than one order of magnitude. The numerical results will also demonstrate the reliability of the procedure across geometries and contrast ratios at the incompressibility limit.

Acknowledgments

The authors were fully supported by the European Commission, under FP7 Grant FastMM, No PIIF - 236913.

References

[1] Axelsson, O. and Gustafsson, I. *Iterative Methods for the Navier Equations of Elasticity*, Comp. Meth. Appl. Mech. Engin., 15; pp. 241ï£¡258, (1978).

[2] Sviercoski, R. F. *An Analytical Effective Tensor for Flows through Generalized Composites*. Advances in Water Resources, 33(7), pp. 728-739, (2010).

[3] Sviercoski, R. F., Margenov, S. *Displacement Decomposition ACO based preconditioning of FEM elasticity systems*, in APPLICATION OF MATHEMATICS IN TECHNICAL AND NATURAL SCIENCES.Editor: Michail D. Todorov, AIP Conf. Proc. 1561, 112 (2013); http://dx.doi.org/10.1063/1.4827220.

Estimation of WRF-CMAQ Modeling System Performance Using AQMEII Infrastructure

D. Syrakov, M. Prodanova, E. Georgieva, K. Slavov

1 Introduction

The Air Quality Model Evaluation International Initiative (AQMEII) aims to build a common strategy on model development and establish methodologies for model evaluation as to increase knowledge on processes and to support the use of models for policy development [6]. Long-term air quality simulations for North America and Europe performed by different models used worldwide and the evaluation of results, both individually and as an ensemble, are the basis to achieve these objectives. The ENSEMBLE system, a web-based platform for model inter-comparison and multi-model ensemble analysis, developed by the Joint Research Centre (JRC) [3, 4], has been used to archive and analyze both qualitatively and quantitatively the meteorological and air quality (AQ) modeling results obtained. Bulgarian National Institute of Meteorology and Hydrology (NIMH) took part in this Initiative performing simulations over Europe for 2010.

2 HIMH task settings

2.1 Models used

HIMH AQ modeling group exploits US EPA Models-3 System, consisting of CMAQ (Chemical Transport Model, [1], WRF (Meteorological pre-processor,[7]) and SMOKE (Emission pre-processor, [2]) linked by a set of Linux-scripts and FORTRAN modules in a system.

2.2 Calculation domain

A grid of 201x201 points with resolution of 25 km is set over Europe using Lambert conformal projection with true latitudes 30N and 60N, mean meridian 13E, and center at (13E,53N).

2.3 Emission data and emission processing.

Yearly inventory data for anthropogenic emission prepared by Netherlands's TNO [5] was interpolated to NIMH's grid and processed by AEmis and PEmis routines, which over-posed monthly, weekly and daily profiles on the yearly data producing Area source (AS) and Point source (PS) emission files for each day of 2010 on hourly

basis, profiles provided by TNO as well. The wild fire emissions were downloaded from the Finnish Meteorological Institute database. Respective processing routine was created and the resulting 3D emissions were added to the PEmis output. The biogenic emissions (VOC from vegetation and NO from soil) are prepared by SMOKE on the base of gridded LU data and current meteorology. In addition SMOKE was used to merge the three emission files (AS, PS and BgS) in a common CMAQ emission input. The sea salt and the dust emissions were calculated by modules built in CMAQ v.4.6.

2.4 Chemical boundary conditions

The CMAQ chemical boundary conditions (BC) are prepared from ECMWF MACC-II project data. After re-mapping of MACC pollutants to CMAQ ones, horizontal, vertical and time interpolation, BC-files for each day of 2010 on hourly basis were created.

2.5 Calculations, data archiving, post-processing

The WRF-CMAQ modeling system was run on a 32-core server day by day, initial condition for each day being last hour of the previous day. Simultaneous archiving of the needed by AQMEII parameters took place extracting them from the CMAQ output. Intensive post-processing was necessary as to convert this data to a format perceivable for ENSEMBLE.

3 Results and Discussion

In this study we focused on the surface values of Europe's most problematic pollutants - O3, NO2, PM10 and PM2.5. The observation sites included in the analysis belong to an EuropeanâĂŞwide rectangular domain. Due to the coarse model grid resolution only background stations were used, classified as rural, urban and suburban ones.
On the Figure 3, examples of different estimates for ozone are presented, charts produced by ENSEMBLE. These are: Box-Whisker plots (a), Taylor diagrams (b), mean diurnal variations (c) and yearly variations of monthly means (d) for rural (left column), urban (centre) and suburban (right) stations. Analyzing model performance based on comparison of modeling results to surface observations in European wide domain the following main conclusions can be drawn:

- The model performs better at rural than at urban stations. The model system hardy sees differences between urban and rural type of stations, predicting very similar results at both types. This is not surprisingly in view of the coarse model grid resolution and lack of particular urban parameterizations in the model;
- Ozone concentrations are in general overestimated while concentrations of nitrogen dioxide and particulate matter are underestimated. Best statistical indicators refer to ozone during summer, and annual NO2 and particulate matter

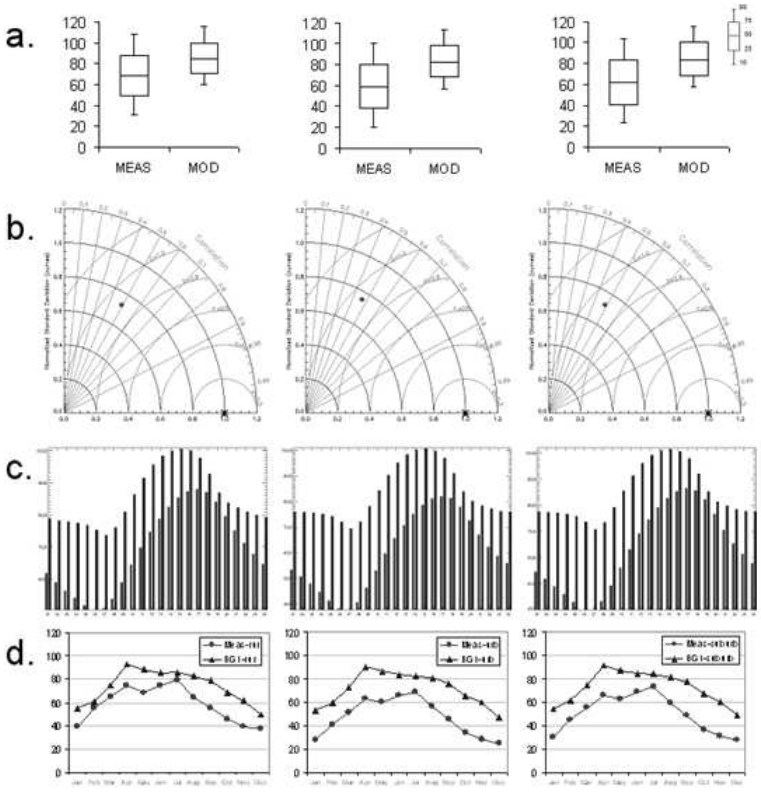

at rural sites. Ozone overestimation is especially pronounced during nighttime. Preliminary analysis points out that some deficiency in NOx emission might have contributed to this;

- PM performance is rather poor, with large negative bias. Also the spread of modeled data is much smaller than the spread of observed values;
- The statistical indicators have values within the limits, proposed in the recent literature as performance criteria, which take observation uncertainty into account.

As the shown model performance is related only to operational model evaluation, further investigation including diagnostic evaluations and model inter-comparison could reveal advantages and shortcomings of the NIMH air quality modeling system.

Aknowledgements

This work is based on the results obtained within the ENSEMBLE Consortium which is acknowledged. Deep gratitude is due to JRC, Ispra, Italy, for supporting the AQMEII and ENSEMBLE activities. Thanks go to US EPA and to US NCEP for providing free-of-charge AQ models and meteorological data.

References

[1] Byun D. and K.L. Schere (2006) Review of the Governing Equations, Computational Algorithms, and Other Components of the Models-3 Community Multiscale Air Quality (CMAQ) Modeling System, Applied Mechanics Reviews, 59, 51-77.

[2] CEP (2003): Sparse Matrix Operator Kernel Emission (SMOKE) Modeling System, University of North Carolina, Carolina Environmental Programs - CEP, Research Triangle Park, North Carolina.

[3] Galmarini, S., et al. (2004a): Ensemble dispersion forecasting, part 1: concept, approach and indicators. Atmospheric Environment 38 (28), 4607-4617.

[4] Galmarini, S., et al. (2004b): Ensemble dispersion forecasting, part II: application and evaluation. Atmospheric Environment 38 (28), 4619-4632.

[5] Kuenen J.J.P., A.J.H. Visschedijk, M. Jozwicka and H.A.C. Denier van der Gon (2013) TNO-MACC-II, A multi-year consistent high-resolution European emission inventory 2003-2009 for air quality modelling, in: Special Issue on "Monitoring atmospheric composition and climate, research in support of the Copernicus/GMES atmosphere service" (in publication).

[6] Rao, S.T., Galmarini, S., Puckett, K. (2011) Air Quality Model Evaluation International Initiative (AQMEII): advancing the state of the science in regional photochemical modeling and its applications, Bulletin of the Amer. Meteor. Society, 92, 23-30.

[7] Skamarock, W.C., Klemp, J.B., Dudhia, J., Gill, D.O., Barker, D.M., Duda, M.G., Huang, X.-Y., Wang, W., Powers, J.G., 2008. A Description of the Advanced Research WRF Version 3, NCAR Tech Note NCAR/TN 475 STR, 125 pp.

A Numerical Procedure for Computation of the Upper Bound of the Throughput of a Crossbar Switch Node

Tasho D. Tashev, Vladimir V. Monov

1. Introduction. Crossbar switch node is a device which maximizes the speed of data transfer using parallel existing flows between the nodes of a communication network. In the ideal case the switch sends packets with a speed corresponding to the speed with which nodes produce these packets, without delay and without losses [1]. This is obtained by means of a non-conflict commutation schedule calculated by the control block of the switch node.

From a mathematical point of view the calculation of such a schedule is NP-complete [2]. The existing solutions partly solve the problem, using different formalisms [3]. Constantly increasing volumes of the communication traffic requires new more effective algorithms, which have to be checked for efficiency. The efficiency of the switch performance is firstly evaluated by the throughput (THR) provided by the node. The next important characteristic is the average time for waiting (average cell delay), before the packet is send for commutation.

At the stages of design of switches, it is firstly assessed the THR of algorithms for non-conflict schedule. For a given algorithm, its THR will depend on the type of incoming traffic. The incoming traffic in real conditions is greatly variable. In order to evaluate the properties of the suggested algorithms, they should be compared by using strictly defined properties of the incoming traffic [3]. For a chosen traffic model, THR of a switch depends on the load intensity ρ of its input lines.

For a chosen algorithm, traffic model and load intensity ρ of the input lines, THR depends on the dimension of its commutation field $n \times n$ (n input lines, n output lines) and the dimension of the input buffer i. In our computer simulations of THR, we shall denote this dependence by a function f i.e.:

$$0 \leq THR(n,i) = f(n,i) \leq 1, \text{ where } n = 2,3,\ldots \; i = 1,2,\ldots$$

Here, THR with value 1 corresponds to 100% - normalized throughput with respect to the maximum throughput of the output lines of the switch.

During the simulations as well as in analytic investigations we shall look for an answer of the questions:

$$\lim_{\substack{i\to\infty,\\ n=const}} f(n,i) =? \qquad \lim_{\substack{i\to\infty,\\ n\to\infty}} f(n,i) =?$$

where $i \to \infty$ means infinitely large input buffer and $n \to \infty$ means infinitely large commutation field.

In the present paper, a numerical procedure for computation of the upper bound of the THR is described, which allows for a calculation of the first limit mentioned above. If it exists then the solution is unique. In this procedure we use the results from a computer simulation of the THR performed on the grid-structure BG01-IPP of the Institute of information and communication technologies IICT-BAS. Our modeling

of the THR utilizes PIM-algorithm [4], Chao-model for "hotspot" load traffic [5] and $\rho = 100\%$ load intensity of each input (i.i.d. Bernoulli). The obtained results give an upper bound of the THR for $n \in [3, 100]$ which enables us to estimate the limit of the THR for $n \to \infty$. This estimate is obtained to be 0.775.

2. Numerical procedure for computation of upper bound. We shall perform simulations for a specific algorithm for non-conflict schedule, a model for incoming traffic and a load intensity. We choose the interval for values of n and i, where i will define the increase in the size of the input buffer. As a result, we will have a set of curves for selected values of $n \in [n1, n2]$, and $i \in [1, 1000]$. Let us chose values âĂŃâĂŃfor i :

$$i = 1, m_1, m_2, m_3, ..., m_p, \text{ where } 1 = m_0 < m_1 < m_2 < m_3 < \cdots < m_p.$$

We shall perform $p + 1$ simulations in order to obtain $p + 1$ curves for THR. The obtained curves will be denoted as follows:

$$f_1(n, i) = f(n, m_0),\ f_2(n, i) = f(n, m_1),\ \ldots, f_{p+1}(n, i) = f(n, m_p)$$

Denote the difference between two consecutive curves f_j and f_{j+1} by res_j:

$$res_1(n, i) = f_2(n, i) - f_1(n, i) = f(n, m_1) - f(n, m_0)$$
$$res_2(n, i) = f_3(n, i) - f_2(n, i) = f(n, m_2) - f(n, m_1)$$
$$\ldots$$
$$res_p(n, i) = f_{p+1}(n, i) f_p(n, i) = f(n, m_p) f(n, m_{p-1})$$

Denote the ratio of the values âĂŃâĂŃof two successive curves res_j and res_{j+1} through δ_j:

$$\delta_1(n, i) = res_2(n, i)/res_1(n, i) = (f(n, m_2) - f(n, m_1))/(f(n, m_1) - f(n, m_0))$$
$$\delta_2(n, i) = res_3(n, i)/res_2(n, i) = (f(n, m_3) - f(n, m_2))/(f(n, m_2) - f(n, m_1))$$
$$\ldots$$
$$\delta_{p-1}(n, i) =$$
$$= res_p(n, i)/res_{p-1}(n, i) = (f(n, m_p) - f(n, m_{p-1}))/(f(n, m_{p-1}) - f(n, m_{p-2}))$$

Simulation data allow us to calculate $\delta_1, \delta_2, \ldots, \delta_{p-1}$. If we can find a dependency $\delta_{j+1} = \phi(\delta_j)$ for $\delta_1, \delta_2, \ldots, \delta_{p-1}$ in the case $j \to \infty$, then we can determine the expected upper bound.

From the last formula we obtain:

$$f_{p+1}(n, i) = f(n, m_{p-1}) + \delta_{p-1}(n, i).(f(n, m_{p-1}) - f(n, m_{p-2}))$$

and for a known dependency $\delta_{j+1} = \phi(\delta_j)$, we can write

$$f_{p+2}(n, i) = f(n, m_{p-1}) + [1 + \phi(\delta_{p-1}(n, i))].\delta_{p-1}(n, i).(f(n, m_{p-1}) - f(n, m_{p-2}))$$
$$\ldots$$
$$f_{p+q}(n, i) = f(n, m_{p-1}) + [1 + \phi(\delta_{p-1}(n, i)) + \phi(\delta_{p-1}(n, i)).\phi(\delta_p(n, i)) + \ldots$$
$$\cdots + \phi(\delta_{p-1}(n, i)).\phi(\delta_p(n, i)). \ldots \phi(\delta_{p+q-3}(n, i))].\delta_{p-1}(n, i).(f(n, m_{p-1}) - f(n, m_{p-2}))$$

When $q \to \infty$ then $f_{(p+q\to\infty)}(n, i)$ is the necessary bound $\lim_{\substack{i\to\infty, \\ n=const}} f(n, i)$.

If there is an upper bound of the throughput of a switch node, it is clear that the dependency $\delta_{j+1} = \phi(\delta_j)$ exists. Then the sum

$$[1 + \phi(\delta_{p-1}(n, i) + \cdots + \phi(\delta_{p-1}(n, i)).\phi(\delta_p(n, i)). \ldots \phi(\delta_{p+q-3}(n, i))]$$

for $q \to \infty$ is convergent and has a boundary.

3. Finding dependencies $\delta_{j+1} = \phi(\delta_j)$. We have found one such relation for our model of PIM-algorithm, specified by means of Generalized nets [6], with Chao-model for "hotspot" load traffic, for which we defined the family of patterns $Chao_i$ for traffic matrices [7]. For a simulation with this family of patterns we have chosen

the sequences for $i:\ i = 1, m^1, m^2, m^3, ..., m^p, \ldots$. Here, we present the result for simulations with $m = 2$. This is the minimal value of m in its definition area $m \in [2, 3, 4, \ldots)$.
When $m = 2$, then $i = 1, 2, 4, 8, 16, 32, 64, \ldots, 2^p, \ldots$. The initial evaluation of the required number of curves for THR is at least 4 (from Pattern $Chao_1$). In our example, we have seven curves (patterns). In the figures below, $Chao_i$ is denoted as Ci for $i = 1, 2, \ldots$ We get results for $C1, C2, C4, C8, C16, C32, C64$ - which are shown in Figure 1a. The dimension n varies from 3×3 to 100×100 and 10 000 simulations for each pattern. Then we calculate the difference between throughput for neighboring patterns. The obtained curves for the differences are shown in Figure 1b.

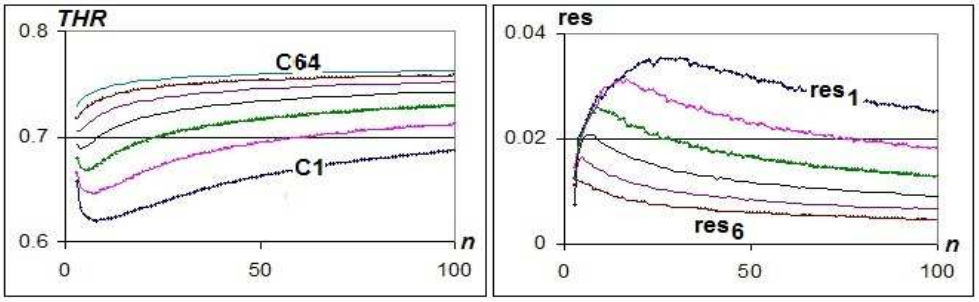

Figure 1: a) Throughput for $Chao_1, \ldots, Chao_{64}$ b) Differences between throughput

Then we calculate the convergence parameter δ_j which is the ratio of the differences and the obtained curves are shown in Figure 2a. The values of δ_j tend to $(1,41 \pm 0,05)^{-1}$.
From our simulations in the case $m = 2$, we have drawn the following conclusion:
Conclusion: The dependence $\delta_{j+1} = \phi(\delta_j)$ is a constant, i.e. $\delta_{j+1} = \delta_j = 2^{-1/2}$ with an accuracy depending on the error of simulations. Thus, $\delta_j(n, i) = const$ when $i \in [1, \infty),\ n \in [n1, n2],\ m = const\ \ (i = 1, m^1, \ldots, m^p, \ldots)$, with an accuracy within the error of simulations.
As a consequence, the upper boundary in case $m = const$ can be calculated as:

$$f_{p+1}(n, i) = f(n, m^{p-1}) + \delta(m).(f(n, m^{p-1}) - f(n, m^{p-2}))$$
$$f_{p+2}(n, i) = f(n, m^{p-1}) + (\delta(m) + \delta^2(m)).(f(n, m^{p-1}) - f(n, m^{p-2}))$$
$$\ldots$$
$$f_{p\to\infty}(n, i) = f(n, m^{p-1}) + [\delta(m) + \delta^2(m) + \cdots + \delta^p(m) + \ldots](f(n, m^{p-1}) - f(n, m^{p-2})) =$$
$$= f(n, m^{p-1}) + [m^{-1/2} + (m^{-1/2})^2 + \cdots + (m^{-1/2})^p + \ldots].(f(n, m^{p-1}) - f(n, m^{p-2})) =$$
$$= f(n, m^{p-1}) + [m^{-1/2} + [(m^{1/2} - 1)^{-1}].(f(n, m^{p-1}) - f(n, m^{p-2}))$$

In this simulation $m = 2$ and we calculate the boundary by

$$f_{p\to\infty}(n, i) = f(n, 64) + [(2^{1/2} - 1)^{-1}].(f(n, 64) - f(n, 32))$$

The result is shown in Figure 2b. Thus we conclude that $\lim_{\substack{i\to\infty,\\ n\to\infty}} f(n, i) = 0,775 \pm 0,001$.
The differences between the values of δ_j obtained in the simulations and the value $\delta(m) = m^{-1/2}$ are equal to the absolute error of the simulations.

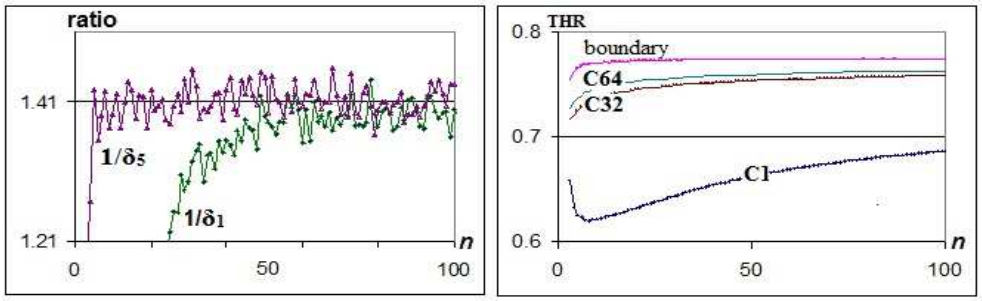

Figure 2: a) Ratio $1/\delta_1$, $1/\delta_5$ between differences b) Upper boundary of throughput

4. Conclusion. Our computer simulation confirms applicability of the suggested numerical procedure. The obtained results give an upper bound of the THR for $n \in [3, 100]$ which enables us to estimate the limit of the THR for $n \to \infty$. This estimate is obtained to be 0.775.

In a future study, the suggested procedure will be tested using other models of the incoming traffic, for example uniform and unbalanced traffic models.

Acknowledgments. The research work reported in the paper is partly supported by the project AComIn "Advanced Computing for Innovation", grant 316087, funded by the FP7 Capacity Programme (Research Potential of Convergence Regions).

References

1. Kang K., Park K., Sha L., Wang Q. Design of a crossbar VOQ real-time switch with clock-driven scheduling for a guaranteed delay bound. Real-Time Systems, January 2013, V. 49, Issue 1, pp. 117-135.

2. Chen T, Mavor J, Denyer Ph, Renshaw D. Traffic routing algorithm for serial superchip system customisation. IEE Proc., Jan 1990, Vol. 137, No.1. pp.65-73.

3. Chao H.J, Lui B. High performance switches and routers. John Wiley & Sons, 2007.

4. T.Anderson, S.Owicki, J.Saxe, and C.Thacker. High speed switch scheduling for local area networks. ACM Trans. Comput. Syst., 1993, vol. 11, no.4, pp.319-352.

5. Chao-Lin Yu; Cheng-Shang Chang; Duan-Shin Lee; CR Switch: A Load-Balanced Switch With Contention and Reservation. IEEE/ACM Transactions on Networking, vol. 17 no.5, P. 1659âĂŞ1671, October 2007.

6. Atanassov K. Generalized Nets and System Theory. Akad. Press "Prof.M. Drinov", Sofia, Bulgaria, 1997.

7. Tashev, T., Modelling throughput crossbar switch node with nonuniform load traffic. Proc. of the International Conference DCCN 2011, Oct. 26-28, 2011 , Moscow, Russia. Moscow, R& D Company "INT", 2011. pp.96-102, (in Russian).

Renormalization Plus Convolution Method Applied to the Analysis of AC Resonant States in Aperiodic Nanowires

Chumin Wang, Vicenta Sanchez

1 Introduction

Nanowires with axial and/or core-shell heterostructures possess fascinating structure-property relationships derived from quantum confinement and interface effects. For example, their unique density of states in the limit of small diameters, can manifest in many electronic and optical properties such as diameter dependent thermal conductivity [1], that are quite different from their macroscopic solid. Nanowires can also act as sensing probes for chemical and biochemical substances as they can offer smaller, more sensitive, less power consuming, and faster reacting sensors. Their sensor operation involves the reversible change in the conductance of the nano-structure upon absorption of the agent to be detected. As nanowires have large surface to volume ratio and small cross-section available for conduction channels, they show increased sensitivity and faster response time. Traditionally, the nanowires with diameters of few nanometers and high aspect ratio are studied by using the supercell model in the reciprocal space. However, their axial heterostructures as well as their zigzag geometry are frequently non-periodic and then, the reciprocal-space approach is inadequate or useless. In this paper, we study the ac conductivity of aperiodic nanowires by using the Kubo-Greenwood formalism and taking the advantage of a previously developed renormalization plus convolution method [2].

2 Formalism

Core-shell nanowire heterostructures have been widely studied in the last years [3]. One example of them is shown in Figure 1, where two types of blocks with 89 hopping integrals, t_A or t_B, are alternated following periodic or Fibonacci sequences along the nanowire. On each cross-section plane there are 25 core atoms with site energy ε_c (blue balls) and 24 shell ones with ε_s (red balls).
In the linear response theory, the electrical conductivity (σ) can be analyzed by using the Kubo-Greenwood formula given by [4]

$$\sigma(\mu,\omega,T)=\frac{2e^2\hbar}{\pi\Omega m^2}\int_{-\infty}^{\infty}dE\frac{f(E)-f(E+\hbar\omega)}{\hbar\omega}Tr[p_xImG^+(E+\hbar\omega)p_xImG^+(E)] \tag{1}$$

where Ω is the system volume, $p_x=(im/\hbar)[H,x]$ is the projection of the momentum operator along the applied electrical field with frequency ω, G^+ is the one-particle re-

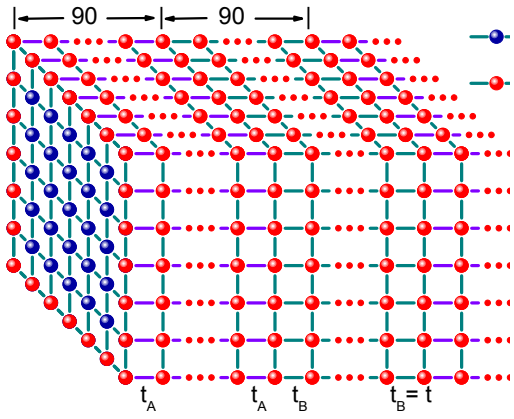

Figure 1: (Color online) Schematic representation of a core-shell heterostructure nanowire with 25 core and 24 shell atoms on each plane.

tarded Green's function, and $f(E) = [\exp(\frac{E-\mu}{k_B T})+1]^{-1}$ is the Fermi-Dirac distribution with the Fermi energy μ and temperature T.
In order to isolate quasicrystalline effects on the conductivity, we consider a simple s-band tight-binding Hamiltonian given by $H = \sum_j \{\varepsilon_j |j\rangle \langle j| + t_{j,j+1} |j\rangle \langle j+1| + t_{j,j-1} |j\rangle \langle j-1|\}$, where $\varepsilon_j = \varepsilon_c$ or ε_s and $t_{i,j} = t_A$ or t_B between nearest-neighbor atoms. To study nanowires, the real-space renormalization method is combined with the convolution theorem, which leads to [2]

$$\sigma(\mu, \omega, T) = \frac{1}{\Omega_\perp} \sum_\beta \sigma^\parallel(\mu - E_\beta, \omega, T) \tag{2}$$

where E_β are eigenenergies of the perpendicular subspace Hamiltonian for the cross-section planes and $\sigma^\parallel(E, \omega, T)$ is calculated by using the one-dimensional renormalization method. The electrical conductance (g) of nanowires are calculated by means of $g(\mu, \omega, T) = \sigma(\mu, \omega, T)\Omega_\perp/\Omega_\parallel$, where $\Omega_\perp$ and $\Omega_\parallel$ are the cross-section area and the nanowire length along the applied electric field, respectively.

3 Results

In Figure 2, the dc electrical conductance $g(\mu, 0, 0)$ of (a) periodic, (b) periodic core-shell with $\Delta\varepsilon = \varepsilon_c - \varepsilon_s = 2|t|$, (c) periodic core-shell with $\Delta\varepsilon = 10|t|$ nanowire heterostructures of 832040 A-type blocks and 832040 B-type ones are shown for $t_A = t_B$ (gray lines) and $t_A = 0.9t_B$ (pink lines). These nanowires are connected to two semi-infinite periodic leads with null site energies and hopping integrals t.

The calculation includes an imaginary part of the energy of $10^{-13}|t|$. Notice that for the single-type-block periodic nanowires, $t_A = t_B$, there are perfect quantum steps in units of $g_0 = 2e^2/h$ and g diminishes in two-type-block heterostructures. When $\Delta\varepsilon = 10|t|$, two separated conducting bands are observed. Each of these bands are centered on the site energies of $\pm 5|t|$. In Figures 2(a'-c') the corresponding dc electrical conductance of heterostructures with 832040 A-type and 514229 B-type blocks ordered following the Fibonacci sequence are illustrated (violet lines). Note the highly oscillating spectra originated from a densely distributed band-gap structure.

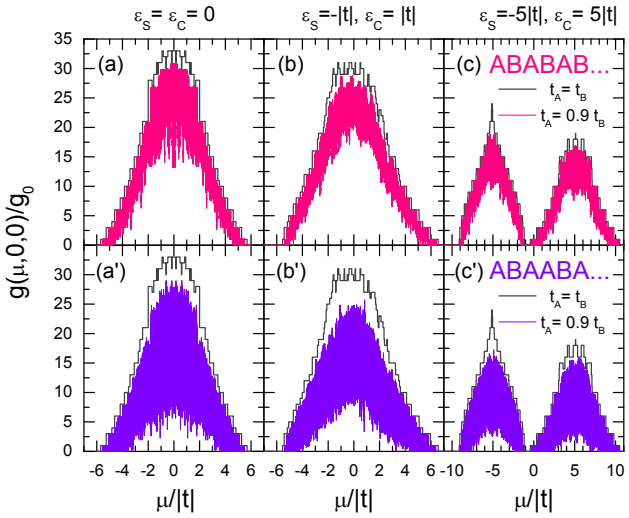

Figure 2: (Color online) Electrical conductance (g) of (a-c) periodic and (a'-c') quasiperiodic core-shell nanowire heterostructures.

The ac conductance spectra $g(\mu, \omega, 0)$ are presented in Figure 3 for (a) a periodic nanowire and (b) a core-shell quasiperiodic nanowire as in Figure 2(b') with 21 A-type and 13 B-type blocks. Observe in (a) the Drude-decay behavior of $g(\mu, \omega, 0)$ as ω increases for the periodic case. However, for the quasiperiodic core-shell nanowire $g(\mu, \omega, 0)$ can significantly improve the ballistic conductance given in Figure 3(a) at the conducting band edges. This phenomenon is due to the resonant scattering process in quasiperiodic heterostructures. The spectrum averaged values of $g(\mu, \omega, 0)$ (open circles), as well as their maximum and minimum values (error bars) are summarized in Figure 3 for quasiperiodic nanowires as in Figure 2(b') with the numbers of A-type and B-type blocks of (2,1), (3,2), (5,3), (8,5), (13,8) and (21,13), respectively.

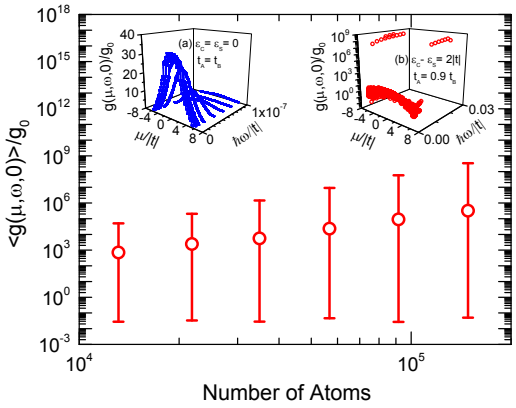

Figure 3: (Color online) AC conductance spectra $g(\mu, \omega, 0)$ of (a) periodic and (b) quasiperiodic core-shell nanowire heterostructures. The spectrum averaged ac conductance (open circles), as well as the corresponding maximum and minimum values (error bars) are shown for the quasiperiodic case.

4 Conclusions

The real-space renormalization method seems to be a very efficient manner to address aperiodic systems, such as interfaces in electronic devices. Moreover, combining with the convolution theorem, the Kubo-Greenwood formula can be evaluated in an exact way for multidimensional lattices. The results show ac resonance peaks significantly larger than the ballistic ones for several μ and $\hbar\omega$. The resonance frequencies ($\hbar\omega$) are determined by the difference of eigenenergies, which can be explained by the Fermiï£¡s golden rule [5]. On the other hand, the core-shell and segmented heterostructures diminish the dc conductivity, but can cause truly high resonant ac conduction at the band edges.

Acknowledgements This work has been partially supported by UNAM-IN113813, UNAM-IN113714 and CONACyT-131596. Computations were performed at Miztli of DGTIC, UNAM.

References

[1] D. Li, T. Wu, P. Kim, L. Shi, P. Yang and A. Majumdar, *Appl. Phys. Lett.* **83**, 2934 (2003); Z. Wang and N. Mingo, *Appl. Phys. Lett.* **97**, 101903 (2010).
[2] V. Sanchez and C. Wang, *Phys. Rev. B* **70**, 144207 (2004).
[3] J.K. Hyun, S. Zhang and L.J. Lauhon, *Annu. Rev. Mater. Res.* **43**, 451 (2013).
[4] E.N. Economou, *Green's functions in quantum physics*, 3rd ed. (Springer, Berlin, 2006) pp 184.
[5] V. Sanchez and C. Wang, *Int. J. Comput. Mater. Sci. Eng.* **1**, 1250003 (2012).

Multicriteria Analysis of Ontologically Represented Information

Katarzyna Wasielewska, Maria Ganzha, Marcin Paprzycki, Ivan Lirkov

The presented work is another attempt to achieve and extend goals presented in [4, 1], i.e. to design a decision support system for the software selection problem. The main idea is to utilize expert knowledge, to help the user in selecting the best method / software / computer resource to solve a computational problem, e.g. from the domain of numerical linear algebra. To achieve that: (1) expert knowledge has to be captured and represented, and (2) an efficient method for utilization of this knowledge has to be proposed. In [4] author suggested that domain experts could express functional relations between properties of the mathematical problem and the performance of the software. Moreover, he considered the problem of knowledge acquisition, i.e. how to construct a knowledge base that can be easily extended and handled. Practical aspects of software selection were discussed in [1]. There, authors proposed a problem solving environment (named EPODE), focused on the initial value problems for ordinary differential equations. Matchmaking in EPODE is based on decision trees, while an expert system with a knowledge base is prepared by the domain experts. Other software selection systems, in the area of differential equations (described in [11, 2]), include decision mechanisms based on decision trees or data mining of the performance history. Unfortunately, neither of these systems is "continued" today.

In this context, we hope that application of modern tools, such as ontological representation of domain knowledge and semantic data processing supported by multicriterial analysis will allows us to develop a system that will efficiently support users. Here, note that, the crucial aspect of designing a knowledge representation scheme is its transparency and ease of use. We believe that expressiveness of ontological languages will allow to capture and represent expert knowledge in an intuitive and user-friendly way.

The context of the work is provided by the Agents in Grid project (AiG [8]), which aims at development of an agent-semantic infrastructure for efficient resource management in the Grid. Decision support within the system should help the user to choose an optimal algorithm and/or resource to solve a problem from a given domain, and later to choose the best contract defining terms of collaboration with the provider of computer resource. The system should assist users with no in-depth knowledge of "computing" by selecting the method and the resource that (together) best fit the problem to be solved (and then find the needed resources). The best contract to be selected is a result of autonomous multi-round negotiations. As a starting point, the domain of linear algebra was modeled. While the decision to use ontologies throughout the system was made (e.g. for storage of expert knowledge / opinions), another crucial step is to select and apply multicriterial decision making method. To choose the best method, the following premises have to be considered:

1. knowledge is captured from multiple experts (decision-makers) and can have different weights (priorities), depending on how a given expert is confident in the selected domain,
2. multiple criteria can have different priorities, e.g. the price may be regarded as more important than time of completion when specifying terms of collaboration,
3. criteria are multi-dimensional, both quantitative and qualitative,
4. advantageous would be the possibility to model the decision problem as a tree, where the root is the problem and subsequent levels represent criteria, further decomposed into subcriteria,
5. another advantage would be to be able to check consistency of data provided by the user.

Here, note that during method and/or resource selection the system should consider aggregated recommendation of many experts, i.e. the system should "develop" one opinion from the set of expert opinions that is "closest" to all of them with regard to a given topic.
The first method evaluated in the context of the AiG project was the Analytical Hierarchy Process (AHP; [6]). This is a well known and widely applied method to approach complex problems, taking into account subjective assessment by multiple decision-makers. The AHP allows to perform aggregation on two levels: (i) preferences regarding criteria, (ii) assessment of alternatives. Moreover, the decision problem can be structured as a tree with root being the problem itself. The importance of a given criteria is assessed with respect to the parent criteria. Crucial for calculating priorities of the criteria is the construction of the comparison matrices, in which the user (or the expert) expresses preferences regarding pairs of criteria from a given level. These preferences are later weighted to obtain global priorities. There is also a possibility to check the consistency of specified preferences and thus to validate user's input. This approach is more user-friendly and transparent than analyzing and assigning weights directly to all criteria. In the AiG, both the requirements and the alternatives are represented with ontology class expressions and ontology instances. Since ontology can be depicted as a directed graph (in our case, acyclic), requirements and alternatives can be easily transformed into problem trees, where the root is the class expression or the instance, edges are properties and children are values of properties. Detailed descripiton of AHP utilization in the AiG can be found in [9, 10].
Besides the AHP, other decision making methods were researched in order to assess them in the context of the AiG scenario and use with ontologies. We have considered an extension of the AiG decision support module with the implementation of the TOPSIS method (Technique for order preference by similarity to ideal solution; [7]) supported by the ontological matchmaking [5]. The TOPSIS method is based on the idea of *ideal* and *negative ideal* alternatives that represent best and worst possible "offers." The goal is to choose an alternative that is the closest to the ideal and the

furthest from the negative ideal. In case of the AiG, construction of ideal and negative ideal is quite intuitive for the contract selection (with one expert), since the alternatives are composed of respectively best and worst values received in offers. In the case of expert recommendations, the ideal alternative for an expert is the one that she specified, while negative ideal should be provided separately by each expert. In our case mutltiple decision-makers have to be considered, so the global ideal and the negative ideal can be estimated as an average of experts preferences. The next step is to determine the separation from the ideal and the negative ideal. Here, ontological matchmaking can be utilized. It allows to measure semantic distance between ontology instances, where the ontology is represented as a graph. Additionally, this method seamlessly fits multiple experts recommendations and user requirements. The calculation of the distance is divided into two phases: (i) semantic distance between concepts in the conceptual model, and (ii) semantic relevance between instances. The first phase is prepared by experts who assign distances between concepts, that are later aggregated (corresponds to preparation of expert opinions and comparison matrices in the AHP). The second phase is analogous to scaling expert distances by priorities assigned by the user. It should be noted that this approach nicely fits with ontologies. However, to handle multiple experts it requires additional step of the specification of a negative ideal alternative, and analyzing the whole conceptual model to assign distances.

Moreover, we inspected the PROMETHEE method [3] that does not in any way take advantage of ontological representation of data. However, it was designed as a group decision support method, i.e. it supports multiple decision-makers, and involves sensitivity analysis and conflict resolution. Here, the first step is the selection of the evaluation criteria (common and individual to the expert) as well as the preference functions. In the AiG this can be done by analyzing the ontology class expression, with requirements provided by the user and expert opinions. Afterwards, each decision-maker evaluates alternatives (all registered opinions, or contract offers) and obtains alternative ranking, by calculating the net flow value for each of them. The last step is to find the global consensus solution, by analyzing the global evaluation matrix, where the alternative net flows are aggregated and scaled by the expert weight. Even though, the PROMETHEE is designed for group decision making, it does not allow to structure the problem hierarchically and each expert has to select the preference functions for all criteria directly, which is not as intuitive as pairwise comparisons with the verbal scale.

While, above, we have described three methods, during the presentation we will briefly analyze also other possible methods, e.g. linear additive model, multi-attribute utility theory.

References

[1] D.Petcu and V.Negru. Interactive system for stiff computations and distributed computing. In *Proceedings of IMACS'98: International Conference on Scientific Computing and Mathematical Modelling*, pages 126–129. IMACS, June 1998.

[2] M.S. Kamel, W.H. Enright, and K.S. Ma. Odexpert: an expert system to select numerical solvers for initial value ode systems. *ACM Trans. Math. Softw.*, 19(1):44–62, 1993.

[3] Bertrand Mareschal, Jean Pierre Brans, and Cathy Macharis. The GDSS PROMETHEE procedure: a PROMETHEE-GAIA based procedure for group decision support. ULB Institutional Repository 2013/9373, ULB – Universite Libre de Bruxelles, 1998.

[4] M.Lucks. *A Knowledge-Based Framework for the Selection of Mathematical Software*. PhD thesis, Southern Methodist University, 1990.

[5] Sang Keun Rhee, Jihye Lee, Myon-Woong Park, MichałSzymczak, Grzegorz Frąckowiak, Maria Ganzha, and Marcin Paprzycki. Measuring semantic closeness of ontologically demarcated resources. *Fundam. Inf.*, 96(4):395–418, December 2009.

[6] T.L. Saaty. *The Analytic Hierarchy Process*. RWS Publications, Pittsburg, 1990.

[7] Hsu-Shih Shih, Huan-Jyh Shyur, and E. Stanley Lee. An extension of {TOPSIS} for group decision making. *Mathematical and Computer Modelling*, 45(7âĂŞ8):801 – 813, 2007.

[8] Katarzyna Wasielewska, Michał Drozdowicz, Maria Ganzha, Marcin Paprzycki, Naoual Attaui, Dana Petcu, Costin Badica, Richard Olejnik, and Ivan Lirkov. Trends in Parallel, Distributed, Grid and Cloud Computing for engineering. chapter Negotiations in an Agent-based Grid Resource Brokering Systems. Saxe-Coburg Publications, Stirlingshire, UK, 2011.

[9] Katarzyna Wasielewska and Maria Ganzha. Using analytic hierarchy process approach in ontological multicriterial decision making - Preliminary considerations. In *AIP Conference Proceedings*, volume 1487, pages 95–103. American Institute of Physics, 2012.

[10] Katarzyna Wasielewska, Maria Ganzha, Marcin Paprzycki, Paweł Szmeja, Michał Drozdowicz, Ivan Lirkov, and Costin Badica. Applying Saaty's Multicriterial Decision Making Approach in Grid Resource Management. In Zoran Budimac, Mirjana Ivanovic, and Milos Radovanovic, editors, *CEUR Workshop Proceedings*, volume 920, page 134, 2012.

[11] Sanjiva Weerawarana, Elias N. Houstis, John R. Rice, Anupam Joshi, and Catherine E. Houstis. Pythia: a knowledge-based system to select scientific algorithms. *ACM Trans. Math. Softw.*, 22(4):447–468, 1996.

Non-linear systems of PDEs arising in large-scale environmental models

Zahari Zlatev, Krassimir Georgiev, Ivan Dimov

1 Introduction of the systems of PDEs arising in large-scale environmental models

We shall restrict ourselves to the topic of long-range transport of air pollution and to a particular model (UNI-DEM, the Unified Danish Eulerian Model, [11, 13]), but most of the results can easily be extended to other environmental models. UNI-DEM is described mathematically by the following system of partial differential equations (PDEs):

$$
\begin{aligned}
\frac{\partial c_i}{\partial t} \quad = \quad & -u\frac{\partial c_i}{\partial x} - v\frac{\partial c_i}{\partial y} && \texttt{horizontal transport} \\
& +\frac{\partial}{\partial x}\left(K_x\frac{\partial c_i}{\partial x}\right) + \frac{\partial}{\partial y}\left(K_y\frac{\partial c_i}{\partial y}\right) && \texttt{horizontal diffusion} \\
& +Q_i\left(t,x,y,z,c_1,c_2,\ldots,c_q\right) + E_i(t,x,y,z) && \texttt{chemical reactions +} \\
& && \texttt{emissions} \qquad (1) \\
& +(k_{1i}+k_{2i})c_i && \texttt{dry and wet} \\
& && \texttt{depositions} \\
& -w\frac{\partial c_i}{\partial z} + \frac{\partial}{\partial z}\left(K_z\frac{\partial c_i}{\partial z}\right), && \texttt{vertical transport} \\
& i=1,\ldots,q, \qquad \texttt{number of equations (chemical species).}
\end{aligned}
$$

The different quantities for the chemical species i at point (x,y,z) of the space domain and at time t of the time-interval involved in (1) are briefly described below:

- $c_i = c_i(t,x,y,z)$ is the concentration ,
- $u = u(t,x,y,z), v = v(t,x,y,z)$ and $w = w(t,x,y,z)$ are wind velocities (along the O_x, O_y and O_z directions respectively),
- $K_x = K_x(t,x,y,z), K_y = K_y(t,x,y,z)$ and $K_z = K_z(t,x,y,z)$ are diffusivity coefficients (it is often assumed that K_x and K_y are non-negative constants, while the calculation of K_z is normally rather complicated),
- $k_{i1} = k_{1i}(t,x,y,z)$ and $k_{2i} = k_{2i}(t,x,y,z)$ are deposition coefficients (dry and wet deposition respectively).
- $E_i = E_i(t,x,y,z)$ is an emission source.

2 Applying splitting techniques

The system of partial differential equations (1) can be split ([13]) into the following three sub-systems:

$$\frac{\partial c_i^{(1)}}{\partial t} = -w\frac{\partial c_i^{(1)}}{\partial z} + \frac{\partial}{\partial z}\left(K_z\frac{\partial c_i^{(1)}}{\partial z}\right), \quad (2)$$

$$\frac{\partial c_i^{(2)}}{\partial t} = -u\frac{\partial c_i^{(2)}}{\partial x} - v\frac{\partial c_i^{(2)}}{\partial y} + \frac{\partial}{\partial x}\left(K_x\frac{\partial c_i^{(2)}}{\partial x}\right) + \frac{\partial}{\partial y}\left(K_y\frac{\partial c_i^{(2)}}{\partial y}\right) \quad (3)$$

$$\frac{\partial c_i^{(3)}}{\partial t} = Q_i(t,x,y,z,c_1^{(3)},c_2^{(3)},\ldots,c_q^{(3)}) + E_i(t,x,y,z) + (k_{1i}+k_{2i})\,c_i^{(3)}. \quad (4)$$

The vertical exchange is described by the first of these three sub-systems. The horizontal transport (the advection) and the horizontal diffusion is described by the second sub-system. The last sub-system describes the combination of the chemical reactions, the emission sources and the deposition.
The three sub-systems are fully defined by (2)-(4), but not the splitting procedure, which will be determined only when it is explained how these sub-systems are combined. The simple sequential splitting procedure, which is obtained as explained below, is applied in UNI-DEM. Let us assume that the space domain is discretized by using a grid with $N_{xyz} = N_x \times N_y \times N_z$ grid-points, where N_x, N_y and N_z are the numbers of the grid-points along the grid-lines parallel to the O_x, O_y and O_z axes. Assume also that the number of chemical species involved in the model is $N_s = q$. Finally, assume that approximate values of the concentrations (for all species and at all spatial grid-points) have already been found for $t - t_n$. These values can be considered as components of a vector-function $c(t_n, x_i, y_j, z_k) \in R^{N_x \times N_y \times N_z \times N_s}$. The next time-step, time-step $n+1$ ($t_{n+1} = t_n + \Delta t$ where Δt is some increment), can be performed by solving successively the three sub-systems. The approximations $c(t_n, x_i, y_j, z_k)$ are used as initial conditions in the solution of (2). The solution of (2) is used as an initial condition of (3). Finally, the solution of (3) is accepted as an initial condition of (4). Then the solution of (4) is considered as an approximation to $c(t_{n+1}, x_i, y_j, z_k)$. When these calculations are completed, everything is prepared for the calculations in the next time-step, step $n+2$.
The great advantage of any splitting procedure that is based on the above three sub-systems is due to the fact that no extra boundary conditions are needed when (2)-(4) are used. This is true not only for the sequential splitting procedure sketched above, but also for any other splitting procedure based on the sub-systems defined by (2)-(4).

3 Selection of numerical methods

First and foremost it must be mentioned here that different numerical algorithms can be applied in the different sub-systems and this is one of the big advantages of

using splitting techniques. This means that for each sub-system one can select the most suitable of the available algorithms. Assume that the spatial derivatives are discretized by the selected numerical algorithm. Then the three systems of PDEs represented by (2) - (4) will be transformed into three systems of ODEs (ordinary differential equations):

$$\frac{dg^{(1)}}{dt} = f^{(1)}\left(t, g^{(1)}\right), \qquad \frac{dg^{(2)}}{dt} = f^{(2)}\left(t, g^{(2)}\right), \qquad \frac{dg^{(3)}}{dt} = f^{(3)}\left(t, g^{(3)}\right). \quad (5)$$

Each component of the functions $g^{(m)}(t) \in R^{N_{xyz} \times N_s}, m = 1, 2, 3$ is an approximation at time t of the concentration at one of spatial grid-points and for one of the chemical species. The components of right-hand-side functions $f^{(m)}(t) \in R^{N_{xyz} \times N_s}, m = 1, 2, 3$ depend both on quantities involved in the right-hand-side of (1) and on the particular numerical algorithms that are used in the discretization of the spatial derivatives.
A linear finite element method is used to discretize the spatial derivatives in (2) and (3). The spatial derivatives can also be discretized by selecting other numerical methods as, for example, finite differences, a pseudo-spectral discretization, a semi-Lagrangian discretization, etc, see .g. [13].
The first system of ODEs in (5) can be solved by using many classical time-integration methods. The well-known $\Theta-$ method with $\Theta = 0.75$ is currently used in UNI-DEM. Several predictor-corrector (PC) methods with several different correctors, which are discussed in [10], are used in the solution of the second system of ODEs in (5). The correctors are carefully chosen so that the absolute stability properties of the method are considerably improved. More details can be found in [10, 13, 12].
The treatment of the third system in (5) is more complicated, because it is both time-consuming and very stiff. Often the QSSA (Quasi-Steady-State-Approximation) method, which is very simple and relatively stable but not very accurate (and has to be run with a small time-stepsize), is selected for the solution of this system. An improved version of the QSSA method was implemented in UNI-DEM. Classical numerical methods for stiff systems of ODEs (the Backward Euler Method, the Trapezoidal Rule and Runge-Kutta algorithms) lead to the solution of non-linear systems of algebraic equations (which have to be handled by some quasi-Newton iterative method) and, therefore, they are normally more expensive. On the other hand, these methods can be incorporated with an error control and normally with considerably larger time-steps. Partitioning can also be used. Some convergence problems related to the implementation of partitioning have been studied in [12]. For more details see [1, 2, 10, 11, 12, 13].

4 Parallelization techniques

The greatest advantage of using splitting procedures is the appearance in a quite natural way of many parallel tasks. It is easy to see that (**a**) the first system of ODEs in (5) contains $N_x \times N_y \times N_s$ independent tasks (for each chemical compound, each system along a vertical grid-line can be treated independently), (**b**) the second system

of ODEs in (5) contains $N_z \times N_s$ independent tasks (for each chemical compound the system along a horizontal grid-plane can be treated independently) and (**c**) the third system of ODEs in (5) contains N_{xyz} independent tasks (the chemical compounds at each grid-point can be treated independently of the chemical compounds at the other grid-points). Standard parallel tools, OpenNP and MPI, are used in parallel version of UNI-DEM. More details in [1, 11, 13]. Results from many tests indicate that the algorithm based on the MPI technique is performing better than the algorithm exploiting the OpenMP tools when UNI-DEM is run on parallel computers (see e.g. [1, 13].

5 Some important applications

UNI-DEM has been used in many different studies (many of them are reported in [3, 4, 5, 6, 7, 8, 9, 12, 14, 15]. Investigations of the influence of the climate changes on pollution levels in (*a*) Europe [5, 9], (*b*) Denmark [16], (*c*) the Balkan Peninsula [14][15] and (*d*) Hungary with its surroundings ([15] have recently been carried out.

6 Concluding remarks

If we assume that $N_x = N_y = 480, N_z = 10, N_s = 480$ are used (as in [5, 6, 9, 14, 15, 16]), then the total number of equations is **80 640 000** and **213 120** time-steps are needed to perform calculations with meteorological and emission data covering a whole year. Moreover, calculations over a long time-period (sixteen years) were needed in [5, 6, 9, 14, 15, 16]. It is clear that it was possible to resolve the enormous computational problems only if (*a*) efficient splitting procedures are used, (*b*) suitable numerical methods are selected for each sub-model and (*c*) parallel computations are applied. It should nevertheless be emphasized that **further improvements** in connection with the tasks related to (*a*)–(*c*) are highly desirable.

Acknowledgments

Krassimir Georgiev was supported by Grants DFNI I01/5 and DCVP-02/1 from the Bulgarian NSF .

References

[1] V. Alexandrov, W. Owczarz, P. G. Thomsen and Z. Zlatev: *Parallel runs of large air pollution models on a grid of SUN computers*, Mathematics&Computers in Simulations, Vol. 65 (2004), pp. 557-577.

[2] V. Alexandrov, A. Sameh, Y. Siddique and Z. Zlatev: *Numerical integration of chemical ODE problems arising in air pollution models*, Environmental Modelling and Assessment, Vol. 2 (1997), pp. 365-377.

[3] C. Ambelas Skjth, A. Bastrup-Birk, J. Brandt and Z. Zlatev: *Studying variations of pollution levels in a given region of Europe during a long time-period*, Systems Analysis Modelling Simulation Vol. 37 (2000), pp. 297-311.

[4] A. Bastrup-Birk, J. Brandt, I. Uria and Z. Zlatev: *Studying cumulative ozone exposures in Europe during a 7-year period*, Journal of Geophysical Research, Vol. 102 (1997), pp. 23917-23035.

[5] P. Csomós, et al: *Impact of Climate Changes on Pollution Levels in Europe*, Final report for a NATO Linkage Project (Grant 980505),2006: available e.g. at http://www.meteo.bg/bulair/NATO.pdf .

[6] I. Dimov, G. Geernaert and Z. Zlatev: *Impact of future climate changes on high pollution levels*, Int. J. of Environment and Pollution Vol. 32, Issue 2 (2008), pp. 200-230.

[7] G. Geernaert and Z. Zlatev: *Studying the influence of the biogenic emissions on the AOT40 levels in Europe*. Int. J. of Environment and Pollution, Vol. 23, Issues 1-2, (2004), pp. 29-41.

[8] Á. Havasi and Z. Zlatev: *Trends of Hungarian air pollution levels on a long time-scale*, Atmospheric Environment, Vol. 36 2002, pp. 4145-4156.

[9] Z. Zlatev: *Impact of future climate changes on high ozone levels in European suburban areas*, Climatic Change, Vol. 101 (2010), pp. 447-483.

[10] Z. Zlatev: *Application of predictor-corrector schemes with several correctors in solving air pollution problems*, BIT, Vol. 24 (1984), pp. 700-715.

[11] Z. Zlatev: *Computer treatment of large air pollution models*, Kluwer, Academic Publishers: Dordrecht-Boston-London, 1995

[12] Z. Zlatev: *Partitioning ODE systems with an application to air pollution models*, Computers&Mathematics with Applications, Vol. 42 (2001), pp. 817-832.

[13] Z. Zlatev and I. Dimov: *Computational and numerical challenges in environmental modelling*, Elsevier, Amsterdam, 2006.

[14] Z. Zlatev, K. Georgiev and I. Dimov: *Influence of climatic changes on air pollution levels in the Balkan Peninsula*. Computers&Mathematics with Applications, Vol. 65, No. 3 (2013), pp. 544-562.

[15] Z. Zlatev, Á. Havasi and I. Faragó: *Influence of climatic changes on pollution levels in Hungary and its surrounding countries*. Atmosphere, Vol. 2 (2011), pp. 201-221.

[16] Z. Zlatev, L. Moseholm: *Impact of climate changes on pollution levels in Denmark*, Environmental Modelling, Vol. 217 (2008), pp. 305-319.

Part B

List of participants

James Adler,
Tufts University,
503 Boston Ave.,
02155 Medford, USA
james.adler@tufts.edu

Vassil Alexandrov,
Barcelona Supercomputing Center,
C/ Jordi Girona 29,
08034 Barcelona, Spain
vassil.alexandrov@bsc.es

Said Al-Garni,
King Fahd University of
Petroleum & Minerals,
P.O. Box 873,
31261 Dhahran, Saudi Arabia
garnis@kfupm.edu.sa

Sebastian Aniţa,
University Al. Ioan Cuza,
Carol I Bd. nr. 11,
700506 Iasi, Romania
sanita@uaic.ro

Peter Arbenz,
ETH Zürich,
UniversitÃďtsstrasse 6,
CH-8092 Zürich, Switzerland
arbenz@inf.ethz.ch

Emanouil Atanassov,
Institute of Information and
Communication Technologies,
Bulgarian Academy of Sciences,
Acad. G. Bonchev Str., bl. 25A,
1113 Sofia, Bulgaria
emanouil@parallel.bas.bg

Owe Axelsson,
Institute of Geonics,
Academy of Sciences of the
Czech Republic,
Studentska 1768,
70800 Ostrava-Poruba, Czech Republic
owe.axelsson@it.uu.se

Radim Blaheta,
Institute of Geonics,
Academy of Sciences of the
Czech Republic,
Studentska 1768,
70800 Ostrava-Poruba, Czech Republic
blaheta@ugn.cas.cz

James Brannick,
Pennsylvania State University,
16802 University Park, PA, USA
brannick@psu.edu

Gabriel Dimitriu,
University of Medicine and Pharmacy,
16 Universitatii street,
700115 Iasi, Romania
dimitriu.gabriel@gmail.com

Ivan Dimov,
Institute of Information and
Communication Technologies,
Bulgarian Academy of Sciences,
Acad. G. Bonchev Str., bl. 25A,
1113 Sofia, Bulgaria
ivdimov@bas.bg

Stefka Dimova,
Faculty of Mathematics and Informatics,
Sofia University "St. Kl. Ohridski",
5 James Bourchier Blvd.,
1164 Sofia, Bulgaria
dimova@fmi.uni-sofia.bg

Nina Dobrinkova,
Institute of Information and
Communication Technologies,
Bulgarian Academy of Sciences,
Acad. G. Bonchev Str., bl. 2,
1113 Sofia, Bulgaria
ninabox2002@gmail.com

Mariana Durcheva,
Technical University of Sofia,
8, Kliment Ohridski St.,
1756 Sofia, Bulgaria
mdurcheva66@gmail.com

Stefka Fidanova,
Institute of Information and
Communication Technologies,
Bulgarian Academy of Sciences,
Acad. G. Bonchev Str., bl. 25A,
1113 Sofia, Bulgaria
stefka@parallel.bas.bg

Mihail Galabov,
Institute of Information and
Communication Technologies,
Bulgarian Academy of Sciences,
Acad. G. Bonchev Str., bl. 25A,
1113 Sofia, Bulgaria
mishogal@gmail.com

Kostadin Ganev,
National Institute of Geophysics,
Geodesy and Geography,
Bulgarian Academy of Sciences,
Acad. G. Bonchev str. bl. 3,
1113 Sofia, Bulgaria
kganev@geophys.bas.bg

Ivan Georgiev,
Institute of Information and
Communication Technologies,
Bulgarian Academy of Sciences,
Acad. G. Bonchev Str., bl. 25A,
1113 Sofia, Bulgaria
ivan.georgiev@parallel.bas.bg

Krassimir Georgiev,
Institute of Information and
Communication Technologies,
Bulgarian Academy of Sciences,
Acad. G. Bonchev Str., bl. 25A,
1113 Sofia, Bulgaria
georgiev@parallel.bas.bg

Ivelina Georgieva,
National Institute of Geophysics,
Geodesy and Geography,
Bulgarian Academy of Sciences,
Acad. G. Bonchev str. bl. 3,
1113 Sofia, Bulgaria
iivanova@geophys.bas.bg

Damyan Grancharov,
Faculty of Physics,
Sofia University "St. Kl. Ohridski",
5 James Bourchier Blvd.,
1164 Sofia, Bulgaria
dgrancharov@phys.uni-sofia.bg

Silvia Grozdanova,
Institute of Information and
Communication Technologies,
Bulgarian Academy of Sciences,
Acad. G. Bonchev Str., bl. 25A,
1113 Sofia, Bulgaria
silvia@parallel.bas.bg

Todor Gurov,
Institute of Information and
Communication Technologies,
Bulgarian Academy of Sciences,
Acad. G. Bonchev Str., bl. 25A,
1113 Sofia, Bulgaria
gurov@parallel.bas.bg

Martin Hasal,
Institute of Geonics,
Academy of Sciences of the
Czech Republic,
Studentska 1768,
70800 Ostrava-Poruba, Czech Republic
martin.hasal@vsb.cz

Oleg Iliev,
Fraunhofer ITWM,
Fraunhofer Platz 1,
67663 Kaiserslautern, Germany
iliev@itwm.fraunhofer.de

Nevena Ilieva-Litova,
Institute for Nuclear Research
and Nuclear Energy,
Bulgarian Academy of Sciences,
Tzarigradsko Shose 72 Blvd,
1784 Sofia, Bulgaria
nilieval@mail.cern.ch

Mariya Ishteva,
Vrije Universiteit Brussel,
Building K, Pleinlaan 2,
1050 Brussels, Belgium
mariya.ishteva@vub.ac.be

Kab Seok Kang,
Max-Planck Institute for Plasma Physics,
Boltzmannstrasse 2,
D-85748 Garching, Germany
kskang@ipp.mpg.de

Nedu Karaivanov,
Institute of Information and
Communication Technologies,
Bulgarian Academy of Sciences,
Acad. G. Bonchev Str., bl. 25A,
1113 Sofia, Bulgaria
nedu@parallel.bas.bg

Aneta Karaivanova,
Institute of Information and
Communication Technologies,
Bulgarian Academy of Sciences,
Acad. G. Bonchev Str., bl. 25A,
1113 Sofia, Bulgaria
anet@parallel.bas.bg

Adem Kaya,
Izmir Institute of Technology,
Gülbahçe Mh.,
35430 Izmir, Turkey
ademkaya@iyte.edu.tr

Nikola Kosturski,
Institute of Information and
Communication Technologies,
Bulgarian Academy of Sciences,
Acad. G. Bonchev Str., bl. 25A,
1113 Sofia, Bulgaria
kosturski@parallel.bas.bg

Johannes Kraus,
University of Duisburg-Essen,
AThea-Leymann Str. 9,
45141 Essen, Germany
johannes.kraus@uni-due.de

Raytcho Lazarov,
Texas A&M University,
University Drive,
College Station, TX, USA
lazarov@math.tamu.edu

Elena Lilkova,
Faculty of Physics,
Sofia University "St. Kl. Ohridski",
5 James Bourchier Blvd.,
1164 Sofia, Bulgaria
elilkova@phys.uni-sofia.bg

Angelos Liolios,
Civil Engineering Dept.
Democritus University of Thrace,
L. Pyrgou 35 B,
GR-67100 Xanthi, Greece
aliolios@civil.duth.gr

Konstantinos Liolios,
Environmental Engineering Dept.,
Democritus University of Thrace,
L. Pyrgou 35 B,
GR-67100 Xanthi, Greece
kliolios@envil.duth.gr

Ivan Lirkov,
Institute of Information and
Communication Technologies,
Bulgarian Academy of Sciences,
Acad. G. Bonchev Str., bl. 25A,
1113 Sofia, Bulgaria
ivan@parallel.bas.bg

Leandar Litov,
Faculty of Physics,
Sofia University "St. Kl. Ohridski",
5 James Bourchier Blvd.,
1164 Sofia, Bulgaria
Leandar.Litov@cern.ch

Maria Lymbery,
Institute of Information and
Communication Technologies,
Bulgarian Academy of Sciences,
Acad. G. Bonchev Str., bl. 25A,
1113 Sofia, Bulgaria
mariq@parallel.bas.bg

Emil Manoach,
Institute of Mechanics,
Bulgarian Academy of Sciences,
Acad. G. Bonchev Str., bl. 4,
1113 Sofia, Bulgaria
e.manoach@imbm.bas.bg

Svetozar Margenov,
Institute of Information and
Communication Technologies,
Bulgarian Academy of Sciences,
Acad. G. Bonchev Str., bl. 25A,
1113 Sofia, Bulgaria
margenov@parallel.bas.bg

Rositsa Marinova,
Faculty of Physics,
Sofia University "St. Kl. Ohridski",
5 James Bourchier Blvd.,
1164 Sofia, Bulgaria
rosie.marinova@gmail.com

Stoyan Markov,
Institute of Information and
Communication Technologies,
Bulgarian Academy of Sciences,
Acad. G. Bonchev Str., bl. 25A,
1113 Sofia, Bulgaria
markov@acad.bg

Ivan Markovsky,
Vrije Universiteit Brussel,
Building K, Pleinlaan 2,
1050 Brussels, Belgium
imarkovs@vub.ac.be

Peter Minev,
Dept. of Math. & Stat. Sciences,
University of Alberta,
T6G 2G1 Edmonton, Canada
minev@ualberta.ca

Dalah Mohamed,
Faculty of Sciences,
Constantine University,
25000 Constantine, Algeria
dalah.mohamed@yahoo.fr

Costică Moroşanu,
University Al. Ioan Cuza,
Carol I Bd. nr. 11,
700506 Iasi, Romania
costica.morosanu@uaic.ro

Askin Mutlu,
Faculty of Engineering.,
Istanbul University,
34320 Istanbul, Turkey
askin@istanbul.edu.tr

Helmut Neunzert,
International Affairs,
Scientific Exchange
Fraunhofer-Institut fuer Techno-
und Wirtschaftsmathematik (ITWM)
Fraunhofer-Platz 1
D-67663 Kaiserslautern
neunzert@itwm.fraunhofer.de

Tzvetan Ostromsky,
Institute of Information and
Communication Technologies,
Bulgarian Academy of Sciences,
Acad. G. Bonchev Str., bl. 25A,
1113 Sofia, Bulgaria
ceco@parallel.bas.bg

Ketty Peeva,
Technical University of Sofia,
8, Kliment Ohridski St.,
1756 Sofia, Bulgaria
kgp@tu-sofia.bg

Peicho Petkov,
Faculty of Physics,
Sofia University "St. Kl. Ohridski",
5 James Bourchier Blvd.,
1164 Sofia, Bulgaria
peicho@phys.uni-sofia.bg

Nedyu Popivanov,
Faculty of Mathematics and Informatics,
Sofia University "St. Kl. Ohridski",
5 James Bourchier Blvd.,
1164 Sofia, Bulgaria
nedyu@fmi.uni-sofia.bg

Vicenta Sanchez,
Universidad Nacional
Autonoma de Mexico,
Av. Universidad No. 3000,
4510 Distrito Federal, Mexico
vicenta@unam.mx

Blagovest Sendov,
Institute of Information and
Communication Technologies,
Bulgarian Academy of Sciences,
Acad. G. Bonchev Str., bl. 25A,
1113 Sofia, Bulgaria
sendov2003@yahoo.com

Ruslan Serbezov,
National Nature Protection Service,
Ministry of Environment and Water,
Bulgaria
serbezov@moew.government.bg

Kiril Shterev,
Institute of Mechanics,
Bulgarian Academy of Sciences,
Acad. G. Bonchev Str., bl. 4,
1113 Sofia, Bulgaria
kshterev@imbm.bas.bg

Jian-Jun Shu,
Nanyang Technological University,
50 Nanyang Avenue,
639798 Singapore, Singapore
mjjshu@ntu.edu.sg

Nikolai Spassov,
National Museum of National History,
Bulgarian Academy of Sciences
nspassov@nmnh.bas.bg

Stanislav Stoykov,
Institute of Information and
Communication Technologies,
Bulgarian Academy of Sciences,
Acad. G. Bonchev Str., bl. 25A,
1113 Sofia, Bulgaria
stoykov@parallel.bas.bg

Rosangela Sviercoski,
Institute of Information and
Communication Technologies,
Bulgarian Academy of Sciences,
Acad. G. Bonchev Str., bl. 25A,
1113 Sofia, Bulgaria
rosviercoski@msn.com

Muhammed Syam,
Dept. of Math. Sciences,
UAE University,
P.O.Box 15551, Al-Ain,
United Arab Emirates
m.syam@uaeu.ac.ae

Dimiter Syrakov,
National Institute of
Meteorology and Hydrology,
Bulgarian Academy of Sciences,
Tzarigradsko Shose 66 Blvd,
1784 Sofia, Bulgaria
dimiter.syrakov@meteo.bg

Tasho Tashev,
Institute of Information and
Communication Technologies,
Bulgarian Academy of Sciences,
Acad. G. Bonchev Str., bl. 2,
1113 Sofia, Bulgaria
ttashev@iit.bas.bg

Panayot Vassilevski,
Lawrence Livermore
National Laboratory,
7000 East Avenue, L-560,
94550 Livermore, CA, USA
panayot@llnl.gov

Vladimir Veliov,
Vienna University of Technology,
Argentinierstrasse 8,
W-1040 Vienna, Austria
veliov@tuwien.ac.at

Yavor Vutov,
Institute of Information and
Communication Technologies,
Bulgarian Academy of Sciences,
Acad. G. Bonchev Str., bl. 25A,
1113 Sofia, Bulgaria
yavor@parallel.bas.bg

Chumin Wang,
Universidad Nacional
Autonoma de Mexico,
Av. Universidad No. 3000,
4510 Distrito Federal, Mexico
chuminS@unam.mx

Huseyin Yildiz,
Dept. of Machinery,
Voc. School of Tech. Sciences,
Istanbul University,
34320 Istanbul, Turkey
huseyin.yildiz@istanbul.edu.tr

Ludmil Zikatanov,
Pennsylvania State University,
16802 University Park, PA, USA
luso@psu.edu

Zahari Zlatev,
Asrhus University,
Frederiksborgveh 399,
Dk-4000 Roskilde, Denmark
zz@dmu.dk